

**MAGNETOSTRATIGRAPHIC STUDY OF BARAIL GROUP IN  
CHAMPHAI DISTRICT, MIZORAM**

**C. LALREMRUATFELA**

**DEPARTMENT OF GEOLOGY  
MIZORAM UNIVERSITY**

**MAGNETOSTRATIGRAPHIC STUDY OF BARAIL GROUP IN CHAMPHAI  
DISTRICT, MIZORAM**

**By**

**C. LALREMRUATFELA  
DEPARTMENT OF GEOLOGY**

**Submitted in partial fulfilment of the requirement of the Degree of Doctor of  
Philosophy in Geology of Mizoram University, Aizawl**

DEPARTMENT OF GEOLOGY

MIZORAM UNIVERSITY

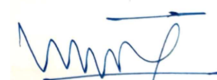
AIZAWL- 796004

**CERTIFICATE**

Certify that Mr. C. Lalremruatfela has carried out research under our supervision and guidance in the Dept. of Geology, Mizoram University. The results of the research work by Mr. C. Lalremruatfela have been presented in this thesis entitled 'Magnetostratigraphic study of Barail group in Champhai District, Mizoram' and the same has been submitted to Mizoram University, Aizawl, Mizoram for the degree of Doctor of Philosophy.

Mr. C. Lalremruatfela has fulfilled all the requirements under the Ph.D. regulations of the Mizoram University. To the best of my knowledge, this thesis as a whole or any part thereof has not been submitted to this University or any other Institution for any degree.

Dr. J. Malsawma  
Asst. Professor  
Dept. of Geology  
Mizoram University  
(Supervisor)



Prof. R.P Tiwari  
Vice Chancellor  
Dr. Harisingh Gour University  
(Joint-Supervisor)

**MIZORAM UNIVERSITY**

**DECLARATION**

**Month: December**

**Year: 2019**

I, C. Lalremruatfela, hereby declare that the subject matter of this thesis is the record of work done by me, that the contents of this thesis did not form basis of the award of any previous degree to me or to the best of my knowledge to anybody else, and that the thesis has not been submitted by me for any research degree in any other University/Institute.

This is being submitted to Mizoram University for the degree of Doctor of Philosophy in Geology.

Date : 20.12.2019  
Place : Aizawl

(C. LALREMRUATFELA)  
Research Scholar

Prof. Shiva Kumar  
(Head of Department)

Dr. J. Malsawma  
Asst. Professor  
Dept. of Geology  
Mizoram University  
(Supervisor)



## ACKNOWLEDGEMENTS

Foremost, I wish to acknowledge my supervisor Dr. J. Malsawma, Department of Geology, Mizoram University and joint supervisor Prof. R.P. Tiwari, Vice Chancellor, Dr. Harisingh Gour University whose expertise were invaluable for the completion of my thesis. I express my utmost sincere gratitude for their patience, encouragement and immense knowledge they have imparted in me.

Throughout my research work, I have received a great deal of assistance and guidance, on and off the field of research from Dr. Paul Lalnunluanga, Assistant Professor, Department of Geology, Mizoram University, to which I am eternally indebted. I am extremely grateful to Dr. C.Zoramthara, who has assisted me on several field visits and Dr. C. Lalmuankimi and Mr. Laltlankima, my colleagues at Govt. Zirtiri Residential Science College for their support. I wish to thank our Principal, Prof. B. Zoliana for granting me much needed time to pursue my research.

I take this opportunity to thank all my teachers at Mizoram University: Prof. Shiva Kumar, Head of Department, Prof. K.S. Rao, Dr. Jimmy Lalnunmawia and Dr. Kavita Devi for giving me this opportunity and access to all available facilities in the Department. My profound gratitude goes out to Dr. Lalchawimawii and all the staff of Geology Department for their positive attitude and willingness to help me in every step of the way. Remembering the life and legacy of Dr. Victor Zochhuana Ralte (1976-2015), who enlighten me in the world of Geological Sciences. A great teacher and an even better friend, “You’ll never walk alone”.

Completion of my thesis would not be possible without the help of great friends, colleagues and fellow research scholars. I express my gratitude to Mr. C.

Lalchhanhima for accompanying me in my field work, Miss Cory Lalbiakzuali for preparing maps for my study area, Mr. Benjamin L, Chhange for his fruitful contributions and Dr. P.C Rohmingliana for taking my place on several college duties. I truly appreciate the contributions and work done by P.C Lalfakzuala, Lawrence Laldinthara, Lalmalsawma, Lallenpuui, Mary Lalruatpuui, R. Lalduhawmi and Malsawmtluangi Pachuau, former students of Geology Department, MZU. I thank my friends Lalrinchhana, Lalhlimpuia and Dr. C. Lalrammawia for helping me on several occasions regarding field visit, sample collection and many more.

I would like to dedicate this thesis to my family who, no doubt is the main reason behind my accomplishment. My parents, C. Laltlanmawia and Liansailovi who supports me in everything I do, spiritually and emotionally. I express my profound gratitude to my big brother Dr. C. Laldinpuia, for his financial support and encouraging words. I thank my brother C. Lalrinnunga and sister Miriam Lalnunhlui for motivating me to be strong and to move forward in various aspects of life. Last but not least, I thank my lovely wife C. Vanlalmuanpuui and my two boys; Mayson and Jovan for believing in me and making each day better and brighter.

Above all, I thank Almighty God for the love and blessings He has bestowed upon me and my family, and his guidance for future endeavors.

Date: 20<sup>th</sup> December 2019

Place: Aizawl

(C. LALREMRUATFELA)

## CONTENTS

| CHAPTER         | PAGE    |
|-----------------|---------|
| Certificate     | i       |
| Declaration     | ii      |
| Acknowledgement | iii-iv  |
| Contents        | v-x     |
| List of Figures | x-xiv   |
| List of Tables  | xiv- xv |

|            |                                 |             |
|------------|---------------------------------|-------------|
| <b>1</b>   | <b>INTRODUCTION</b>             | <b>1</b>    |
| <b>1.1</b> | <b>RATIONALE OF THE STUDY</b>   | <b>1-2</b>  |
| <b>1.2</b> | <b>ABOUT THE STUDY AREA</b>     | <b>2-3</b>  |
| <b>1.3</b> | <b>PHYSIOGRAPHY AND CLIMATE</b> | <b>3-4</b>  |
| <b>1.4</b> | <b>VEGETATION AND WILDLIFE</b>  | <b>4-5</b>  |
| <b>1.5</b> | <b>REVIEW OF LITERATURE</b>     | <b>5-9</b>  |
| <b>1.6</b> | <b>SCOPE OF PRESENT WORK</b>    | <b>9-10</b> |
| <b>1.7</b> | <b>OBJECTIVES</b>               | <b>10</b>   |

|            |  |              |
|------------|--|--------------|
| <b>2</b>   | <b>REGIONAL GEOLOGY AND GEOLOGY OF THE STUDY AREA</b>    | <b>11</b>    |
| <b>2.1</b> | <b>GEOLOGICAL SETUP</b>                                  | <b>11</b>    |
| <b>2.2</b> | <b>INDIAN CRATON</b>                                     | <b>11-12</b> |
| <b>2.3</b> | <b>SHILLONG PLATEAU</b>                                  | <b>13</b>    |
| <b>2.4</b> | <b>BENGAL BASIN</b>                                      | <b>14-16</b> |
| <b>2.5</b> | <b>INDO-BURMAN RANGES (IBR)</b>                          | <b>17</b>    |
| <b>2.6</b> | <b>SURMA BASIN</b>                                       | <b>17-18</b> |
| <b>2.7</b> | <b>STRATIGRAPHIC FRAMEWORK OF MIZORAM</b>                | <b>18-19</b> |
| <b>2.8</b> | <b>LITHOSTRATIGRAPHY OF THE STUDY AREA</b>               | <b>20-37</b> |
|            | <b>2.8.1 Lithostratigraphy of Ruantlang section (RT)</b> | <b>20-21</b> |
|            | <b>2.8.1.1 Litho-units of Ruantlang (RT) section</b>     | <b>21-26</b> |
|            | <b>2.8.2 Lithostratigraphy of Zote section (ZT)</b>      | <b>27</b>    |
|            | <b>2.8.2.1 Litho-units of Zote (ZT) section</b>          | <b>28-32</b> |
|            | <b>2.8.3 Lithostratigraphy of Ngur section (NG)</b>      | <b>33</b>    |
|            | <b>2.8.3.1 Litho-units of Ngur (NG) section</b>          | <b>34-37</b> |
| <b>3</b>   | <b>METHODOLOGY</b>                                       | <b>38-59</b> |
| <b>3.1</b> | <b>INTRODUCTION</b>                                      | <b>38-42</b> |

|            |  |               |
|------------|--|---------------|
| <b>3.2</b> | <b>LITERATURE SURVEY</b>   | <b>43</b>     |
| <b>3.3</b> | <b>PRELIMINARY SURVEY</b>  | <b>43</b>     |
| <b>3.4</b> | <b>FIELD WORK</b>  | <b>43-47</b>  |
|            | <b>3.4.1 Preparation of Litholog</b>   | <b>44</b>     |
|            | <b>3.4.2 Collection of Samples</b>   | <b>45-47</b>  |
| <b>3.5</b> | <b>LABORATORY WORK</b>   | <b>48-50</b>  |
|            | <b>3.5.1 Cutting and marking of samples</b>  | <b>48</b>     |
|            | <b>3.5.2 Demagnetization</b>   | <b>48-50</b>  |
|            | <b>3.5.2.1 Alternating field demagnetization</b>                                       | <b>49</b>     |
|            | <b>3.5.2.2 Thermal Demagnetization</b>   | <b>49-50</b>  |
| <b>3.6</b> | <b>GRAPHICAL REPRESENTATION AND<br/>CALCULATION</b>                                    | <b>50-52</b>  |
| <b>3.7</b> | <b>GEOMAGNETIC POLARITY TIME SCALE (GPTS)<br/>AND SEDIMENT ACCUMULATION RATE (SAR)</b> | <b>52-53</b>  |
| <b>3.8</b> | <b>SAMPLING AND LABORATORY TECHNIQUES OF<br/>ROCK MAGNETISM</b>                        | <b>53-56</b>  |
| <b>4</b>   | <b>RESULTS</b>   | <b>60-108</b> |

|            |  |               |
|------------|--|---------------|
| <b>4.1</b> | <b>MAGNETIC MINERALOGY</b>   | <b>60-66</b>  |
|            | <b>4.1.1 Ruantlang section</b>                                       | <b>60-63</b>  |
|            | <b>4.1.2 Zote-Ngur section</b>                                       | <b>63-66</b>  |
| <b>4.2</b> | <b>MAGNETOSTRATIGRAPHIC RESULTS</b>                                  | <b>67-108</b> |
|            | <b>4.2.1 Ruantlang Section (RT)</b>                                  | <b>67-80</b>  |
|            | <b>4.2.1.1 Thermal Demagnetization</b>                               | <b>67-70</b>  |
|            | <b>4.2.1.2 Alternating Field Demagnetization</b>                     | <b>71-73</b>  |
|            | <b>4.2.1.3 Magnetic Polarity reconstruction of Ruantlang section</b> | <b>79-80</b>  |
|            | <b>4.3.2 ZOTE SECTION (ZT)</b>                                       | <b>81-86</b>  |
|            | <b>4.3.2.1 Thermal Demagnetization</b>                               | <b>81-83</b>  |
|            | <b>4.3.2.2 Alternating Field Demagnetization</b>                     | <b>84-86</b>  |
|            | <b>4.3.3 ZOTE-NGUR SECTION (ZN)</b>                                  | <b>86-89</b>  |
|            | <b>4.3.3.1 Thermal Demagnetization</b>                               | <b>86-88</b>  |
|            | <b>4.3.3.2 Alternating Field Demagnetization</b>                     | <b>88-89</b>  |
|            | <b>4.3.3.3 Magnetic Polarity reconstruction of Zote section</b>      | <b>97-98</b>  |
|            | <b>4.3.4 Ngur Section (NG)</b>                                       | <b>99-108</b> |
|            | <b>4.3.4.1 Thermal Demagnetization</b>                               | <b>99-100</b> |

|  |   |                |
|--|---|----------------|
|  | <b>4.3.4.2 Alternating Field Demagnetization</b>                | <b>101-102</b> |
|  | <b>4.3.4.3 Magnetic Polarity reconstruction of Ngur section</b> | <b>106-108</b> |

|            |   |                |
|------------|---|----------------|
| <b>5</b>   | <b>RATE OF SEDIMENTATION AND STRATIGRAPHIC CORRELATION OF MIZORAM</b> | <b>109-118</b> |
| <b>5.1</b> | <b>INTRODUCTION</b>   | <b>109</b>     |
| <b>5.2</b> | <b>SEDIMENT ACCUMULATION RATE (SAR) OF RUANTLANG SECTION (RT)</b>     | <b>109-110</b> |
| <b>5.3</b> | <b>SEDIMENT ACCUMULATION RATE (SAR) OF ZOTE SECTION (ZT)</b>          | <b>111-112</b> |
| <b>5.4</b> | <b>SEDIMENT ACCUMULATION RATE (SAR) OF NGUR SECTION (NG)</b>          | <b>112-113</b> |
| <b>5.5</b> | <b>SEDIMENT ACCUMULATION RATE (SAR) SUMMARY FOR ALL SECTIONS</b>      | <b>113-114</b> |
| <b>5.6</b> | <b>STRATIGRAPHIC CORRELATION FOR MIZORAM</b>                          | <b>114-118</b> |

|          |                                |                |
|----------|--------------------------------|----------------|
| <b>7</b> | <b>SUMMARY AND CONCLUSIONS</b> | <b>119-127</b> |
|----------|--------------------------------|----------------|

|                   |                |
|-------------------|----------------|
| <b>REFERENCES</b> | <b>128-142</b> |
|-------------------|----------------|

**BRIEF BIO-DATA OF THE CANDIDATE****PARTICULARS OF THE CANDIDATE****LIST OF FIGURES**

| <b>SL.NO</b> | <b>FIG.NO</b> | <b>DESCRIPTION</b>   | <b>PAGE</b> |
|--------------|---------------|--|-------------|
| <b>1.</b>    | <b>1.1</b>    | Location map of the study area   | <b>3</b>    |
| <b>2.</b>    | <b>2.1</b>    | Map of the Bengal basin with the Dauki Fault separating the Sylhet trough from the uplifted Shillong Plateau (after Uddin and Lundberg, 1998).   | <b>12</b>   |
| <b>3.</b>    | <b>2.2</b>    | Cross-sectional profile through the Chittagong– Tripura Fold Belt Province showing the structural elements and development of Neogene accretionary prism complex (after Sikder and Alam, 2003).              | <b>16</b>   |
| <b>4.</b>    | <b>2.3</b>    | Location map of Ruantlang section  | <b>21</b>   |
| <b>5.</b>    | <b>2.4</b>    | Panoramic view of Ruantlang section (RT).  | <b>22</b>   |
| <b>6.</b>    | <b>2.5</b>    | Field Photographs of Ruantlang section A) Fissile olive green shales B) Trace fossil C) Brown sandstone bed with load cast D) Spheroidal weathering in shales E) Shale bed overlain by brown sandstone beds. | <b>26</b>   |
| <b>7.</b>    | <b>2.6</b>    | Location map of Zote section   | <b>27</b>   |
| <b>8.</b>    | <b>2.7</b>    | Panoramic view of Zote section (ZT).   | <b>28</b>   |
| <b>9.</b>    | <b>2.8</b>    | Field Photographs of Zote section A) Tidal bundles. B) Spheroidal weathering in shale. C) Ball and pillow structure D) Trace fossil. E)  | <b>32</b>   |



|            |             |  |           |
|------------|-------------|--|-----------|
|            |             | Bedded brown sandstones. F) Fissility and laminations in shale bed.  |           |
| <b>10.</b> | <b>2.9</b>  | Location map of Ngur section.  | <b>33</b> |
| <b>11.</b> | <b>2.10</b> | Panoramic view of Ngur section.  | <b>34</b> |
| <b>12.</b> | <b>2.11</b> | Field Photographs of Ngur section A) Bedded brown sandstones with ripple marks. B) Sandstone beds alternating with thin shale beds. C) Intra formational conglomerate. D) Ngur quarry. E) Heterolithic bedding in grey sandstones.F) Outcrop view of Ngur section.                                       | <b>37</b> |
| <b>13.</b> | <b>3.1</b>  | Graphical presentation of the magnetic, geomagnetic, and geographic poles and equators. (Mc Elhinny and McFadden, 2000).   | <b>39</b> |
| <b>14.</b> | <b>3.2</b>  | Magnetic material moments under applied and zero field. Hollow arrow in the right-hand side of the diagrams show the magnetization acquires when in an applied magnetic field (solid arrow).   | <b>40</b> |
| <b>15.</b> | <b>3.3</b>  | Generalized paleomagnetic sampling scheme. Multiple samples are collected from different sites and individually marked (Butler, 1998).   | <b>45</b> |
| <b>16.</b> | <b>3.4.</b> | Orientation system for sample collected by portable core drill. Left is a schematic representation of core sample in situ. The z axis points into outcrop; the x axis is in the vertical plane; the y axis is horizontal. Diagram on the right shows orientation angles for core samples (Butler, 1998). | <b>47</b> |

|            |                 |  |           |
|------------|-----------------|--|-----------|
|            |                 |  |           |
| <b>17.</b> | <b>3.5</b>      | Demagnetization plots shown using Stereonet, Zijderveld diagram (Zijderveld 1967) and intensity decay curves for a specimen.   | <b>51</b> |
| <b>18.</b> | <b>3.6. (a)</b> | Field work photographs A) Measuring thickness of beds using bamboo scale. B) Measuring attitude and recording sedimentary structures. C) Drilling with portable handheld driller connected with water pump. D) Refueling driller. E) Cleaning, marking and packing of samples. F) Orientation fixture. | <b>57</b> |
| <b>19.</b> | <b>3.6. (b)</b> | Laboratory photographs A) Dual-blade cutter. B) Marked samples for magnetostratigraphy and magnetic minerals study. C) Samples for demagnetization process. D) Alternating field demagnetizer (AFD). E) Thermal demagnetizer. F) JR6 dual spinner magnetometer.  | <b>58</b> |
| <b>20.</b> | <b>3.6. (c)</b> | Laboratory photographs A) Bartington MS2 Magnetic susceptibility meter. B) ASC Scientific Impulse magnetizer. C) Panoramic view of laboratory. D) Paleomagnetic lab building, Dept of geology, MZU.  | <b>59</b> |
| <b>21.</b> | <b>4.1</b>      | The Isothermal Remanent Magnetization curves for representative samples of varied lithology within Ruantlang section.  | <b>61</b> |
| <b>22.</b> | <b>4.2</b>      | Temporal distribution of the representative mineral magnetic parameters for Ruantlang section  | <b>63</b> |
| <b>23.</b> | <b>4.3</b>      | The Isothermal Remanent Magnetization curves   | <b>66</b> |

|            |                  |  |                |
|------------|------------------|--|----------------|
|            |                  | for representative samples of varied lithology within Zote-Ngur section.   |                |
| <b>24.</b> | <b>4.4</b>       | Temporal distribution of the representative mineral magnetic parameters for Zote-Ngur section.   | <b>66</b>      |
| <b>25.</b> | <b>4.5 (A-D)</b> | Demagnetization plots [Stereonet, Zijderveld diagram (Zijderveld 1967) and intensity decay curve] for representative samples from Ruantlang Section. | <b>74-77</b>   |
| <b>26.</b> | <b>4.6</b>       | Magnetic polarity reconstruction of Ruantlang Section.   | <b>80</b>      |
| <b>27.</b> | <b>4.7 (A-F)</b> | Demagnetization plots [Stereonet, Zijderveld diagram (Zijderveld 1967) and intensity decay curve] for representative samples from Zote Section.      | <b>90-95</b>   |
| <b>28.</b> | <b>4.8</b>       | Magnetic polarity reconstruction of Zote (ZT) Section.   | <b>97</b>      |
| <b>29.</b> | <b>4.9 (A-C)</b> | Demagnetization plots [Stereonet, Zijderveld diagram (Zijderveld 1967) and intensity decay curve] for representative samples from Ngur Section.      | <b>103-105</b> |
| <b>30.</b> | <b>4.10</b>      | Magnetic polarity reconstruction of Ngur (NG) Section  | <b>107</b>     |
| <b>31.</b> | <b>5.1</b>       | Sediment Accumulation Rate (SAR) of Ruantlang Section.   | <b>110</b>     |
| <b>32.</b> | <b>5.2</b>       | Sediment Accumulation Rate (SAR) of Zote (ZT) Section  | <b>111</b>     |
| <b>33.</b> | <b>5.3</b>       | Sediment Accumulation Rate (SAR) of Ngur (NG) Section  | <b>112</b>     |

|            |            |   |            |
|------------|------------|---|------------|
| <b>34.</b> | <b>5.4</b> | Correlation of established Magnetic Polarity Scales from various sections within Mizoram and Hari river section (Worm et al.,1998, Tiwari et al., 2007; Malsawma et al., 2010, Malsawma, 2011; Paul, 2013; Paul et al., 2014. | <b>118</b> |
|------------|------------|---|------------|

#### LIST OF TABLES

| <b>SL.NO</b> | <b>TABLE.NO</b>  | <b>DESCRIPTION</b>  | <b>PAGE</b>  |
|--------------|------------------|---|--------------|
| <b>35.</b>   | <b>2.1</b>       | Stratigraphic framework of Mizoram after Karunakaran, 1974 and Ganju 1975.  | <b>19</b>    |
| <b>36.</b>   | <b>2.2 (a-c)</b> | Litholog and description Ruantlang section.   | <b>23-25</b> |
| <b>37.</b>   | <b>2.3 (a-c)</b> | Litholog and description of Zote section.   | <b>29-31</b> |
| <b>38.</b>   | <b>2.4 (a-b)</b> | Litholog and description of Ngur section.   | <b>35-36</b> |
| <b>39.</b>   | <b>3.1</b>       | Types of Remanent Magnetization and their magnetization process.  | <b>41</b>    |
| <b>40.</b>   | <b>3.2</b>       | Types of magnetic minerals, their composition and magnetic properties responsible for magnetization (Collinson, 1983).  | <b>42</b>    |
| <b>41.</b>   | <b>3.3</b>       | Summary of the rock magnetic parameters (after Thompson and Oldfield, 1986; Maher, 1988; Oldfield, 1991).   | <b>56</b>    |
| <b>42.</b>   | <b>4.1</b>       | The average detrital components and various parameters calculated for Ruantlang Section:<br>Units: BOCR = mT, $\chi_{ARM} = 10^{-8} m^3 kg^{-1}$ , SIRM = $10^{-5} Am^3 kg^{-1}$ , SIRM/ $\chi_{lf} = 10^3 Am$ and Soft-IRM = $10^{-2} A/m^2$ . | <b>62</b>    |
| <b>43.</b>   | <b>4.2</b>       | The average detrital components and various parameters calculated for Zote-Ngur section.<br>Units: BOCR = mT, $\chi_{ARM} = 10^{-8} m^3 kg^{-1}$ , SIRM = $10^{-5} Am^3 kg^{-1}$ , SIRM/ $\chi_{lf} = 10^3 Am$ and Soft-IRM                     | <b>65</b>    |

|            |            |   |            |
|------------|------------|---|------------|
|            |            | = $10^{-2}$ A/m <sup>2</sup> .  |            |
| <b>44.</b> | <b>4.3</b> | Number of samples and name, declination and inclination mean, sample height, $k\alpha 95$ (Fisher statistical parameters; concentration parameter and 95% cone of confidence, VAP latitude (normal and reversal) of Ruantlang section (RT). | <b>78</b>  |
| <b>45.</b> | <b>4.4</b> | Normal polarity events of Ruantlang Section   | <b>80</b>  |
| <b>46.</b> | <b>4.5</b> | Number of samples and name, declination and inclination mean, sample height, $k\alpha 95$ (Fisher statistical parameters; concentration parameter and 95% cone of confidence, VGP latitude (normal and reversal) of Zote Section (ZT).      | <b>96</b>  |
| <b>47.</b> | <b>4.6</b> | Normal polarity events of Zote (ZT) and Zote-Ngur (ZN) Section  | <b>98</b>  |
| <b>48.</b> | <b>4.7</b> | Number of samples and name, declination and inclination mean, sample height, $k\alpha 95$ (Fisher statistical parameters; concentration parameter and 95% cone of confidence, VGP latitude (normal and reversal) for Ngur Section (NG).     | <b>106</b> |
| <b>49.</b> | <b>4.8</b> | Normal polarity events of Ngur Section  | <b>108</b> |
| <b>50.</b> | <b>5.1</b> | Estimation of SAR using magnetostratigraphic ages from Ruantlang section.   | <b>110</b> |
| <b>51.</b> | <b>5.2</b> | Estimation of SAR using magnetostratigraphic ages from Zote section.  | <b>112</b> |
| <b>52.</b> | <b>5.3</b> | Estimation of SAR using magnetostratigraphic ages from Ngur section.  | <b>113</b> |
| <b>53.</b> | <b>5.4</b> | Comparison and summary of SAR for Ruantlang, Zote and Ngur sections.  | <b>114</b> |

## CHAPTER I

### INTRODUCTION

#### 1.1 RATIONALE OF THE STUDY

The Surma Basin which makes part of the Greater Bengal Basin (Sarkar and Nandy, 1977; Ferdous and Renault, 1996; Mannan, 2002) and is one the thickest sedimentary basins in the world with ongoing sedimentation till date due to the continuation of tectonic processes operating in the North. Establishment of a well deciphered stratigraphic framework is necessary since the area is well known for its hydrocarbon deposits and susceptibility to natural disasters especially earthquakes and landslides. Furthermore, since the area makes part of the accretionary prism between the Indian plate and its neighboring plates, understanding the geology of the area will greatly contribute to advancement in the knowledge of tectonic evolution of the Indian sub continent. The basin is divided into two main facies, the shelf facies which, due to the presence of distinctive age markers in the form of micro and mega fossils, hence resulting in a well established stratigraphy. The basinal facies representing the study area shows limited lithological variations and devoid of chronostratigraphic markers.

Stratigraphic correlation of parts of Mizoram have been carried out over the years using Magnetostratigraphy covering the Northern (Kolasib District) and Central (Aizawl District) part of Mizoram where Tipam and Bhuban formations of the Mio-Pliocene periods were analyzed leading to a well established stratigraphic framework (Tiwari *et al.*, 2007; Malsawma *et al.*, 2010; Malsawma, 2011; Paul, 2013; Paul *et al.*, 2014). The present study covers the Eastern part of Mizoram which

report rocks of the Oligocene age (Barail group). Since the area lacks various biological and lithological chronostratigraphic constraints, magnetostratigraphic correlation will serve as the main tool for establishment of a detailed chronostratigraphy of the Barail in Mizoram.

## **1.2 ABOUT THE STUDY AREA**

Mizoram is a North-eastern State of India which stretches over an area of 21,081 square kilometers lying between 21°56'N – 24°31'N latitudes and 92°16'E – 93°26'E longitudes with the Tropic of Cancer dividing it into almost two equal parts. The maximum aerial dimension from North to South is 289 km and 115 km running from East to West (Pachau, 1994).

As a part of one of the thickest sedimentary basin in the world, it serves as a significant setting for scientific discourse due to its Geo tectonic evolution as well as prospects in petroleum resources. The sedimentary column of the area is constituted by sandstone, shale, siltstones, mudstones and rare pockets of shell limestone which is divided into 3 major stratigraphic units based on their lithological characteristics (Karunakaran, 1974; Ganju, 1975).

The study area is around Champhai town which is one of the district capitals of Mizoram situated to the Eastern part of the state and about 190 km from Aizawl city, the capital of Mizoram State. It consists of roadside sections along Ruantlang, South of Champhai town and Zote Village running North-east towards Ngur Village which is located at about 5 km from Champhai town. It is covered by the Survey of India topographic sheet Nos. 84 E/7 and 84 E/8 and lies between the coordinates

23°26'26.38" N to 23°27'01.71" N latitudes and 93° 20'24.21" E to 93°15'36.43" E longitudes.

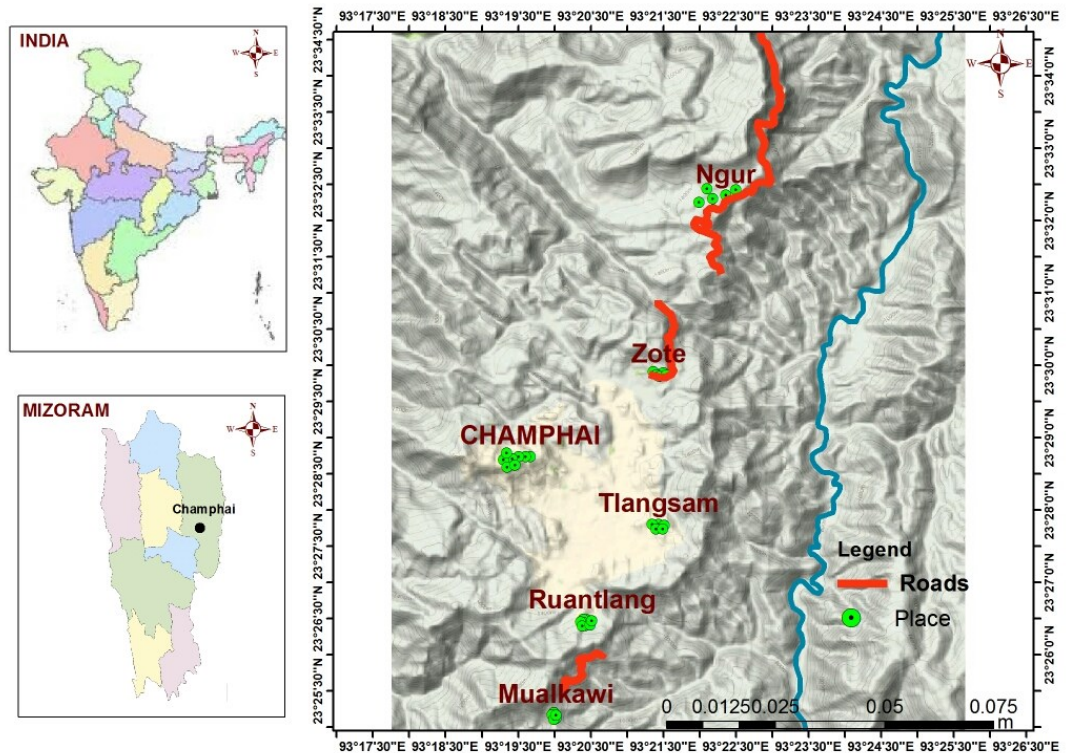


**Fig.1.1:** Location map of the study area

### 1.3 PHYSIOGRAPHY AND CLIMATE

The geomorphology of Mizoram is strongly influenced by tectonics as well as denudation processes in the form of mass wasting, monsoon driven streams and human activities. The mountainous setting consists of rugged terrain consisting of alternating ridges and valleys. Mizoram exhibits a very young topography in terms of geological evolution. The topography is represented by N-S trending anticlines with alternating synclines plunging either in the North or South directions. The bedding



generally dips west or east direction where the western limbs are generally represented by cut slopes and eastern limb by dip slopes. The area is represented by highly dissected ridges with deep gorges, spurs and cols as a result of intense weathering and erosion. The difference in elevation of valleys and ridges increases from west to east varying between 200 and 600m (GSI report, 2011).

The drainage pattern is mostly dendritic with large number of low order streams drained into the adjacent valleys consisting of meandering rivers. Due to the prominent relief and steep topography, the tributaries are mostly angular with parallel to sub parallel pattern following gorges and other fault related structures. The drainage is characterized by high to moderate gradient as it moves from steep upstream to gentler valley floors. The hill ranges are separated by rivers flowing either towards North or South directions.

Mizoram is governed by pleasant climate due to its tropical location and altitude. Durable summers are followed by short winters with the temperature varying between 11°C to 24°C during the winter and 18°C to 30°C during the summer. The periodic arrival of southwest monsoons strongly influences the climate of Mizoram. The state experience heavy rainfall from May to September bringing an average precipitation of 250cm. December and January are the dry months and marks the onset of winter season.

#### **1.4 VEGETATION AND WILDLIFE**

The state of Mizoram is part of a biodiversity hotspot supported by its ideal climatic condition and topographic set up. It has an abundant floral assemblage with plenty of trees, plants, bushes and different varieties of bamboo. The rich assemblage

of vegetation holds refuge to a large variety of wildlife including several species of the feline family like tiger and leopard, clouded leopard, wild cats etc. and grazing animals like sambar, deer, etc. Bear, wild pigs, rodents, reptiles and several species of goats residing in this mountainous terrain.

## **1.5 REVIEW OF LITERATURE**

Evans in 1932 established the first works regarding the stratigraphic set up of the Surma basin and in 1964 he described its tectonic evolution with reference to the Bengal basin followed by Sengupta, (1966) and Raju, (1968). The depositional history, stratigraphic set up and tectonic evolution of the Bengal basin was describe by Alam (1971; 1989; 1991; 1995; 1995a; 1995b; 1997 and 2003) where the depositional environment and facies of the basin was established. Since the Stratigraphy of Bengal Basin established by Evans, (1932) was based on correlation based on lithographic similarities and macro fossil assemblages with exposures from Assam, they were not considered reliable. To establish more reliable framework, Micro fossil studies were carried out by Ahmed in 1968 followed by Chowdury, (1982); Uddin and Ahmed, (1989) and Reimenn, (1993) discourse on trace fossils by Johnson and Alam, (1991); Khan, (1991).

Karunakaran, (1974) and Ganju, (1975) grouped the sedimentary sequence of Mizoram into 3 distinct groups which are Barail, Surma and Tipam. Over the years with more geological information as a result of advancement in science and technologies revisions have been made by Tiwari and Kachhara, (2003); Mandaokar, (2000) and Tiwari *et al.*, 2011). Biostratigraphy and paleontological studies of the Surma succession in Mizoram had been done by a number of researchers including,

La Touche, (1891); Chatterjee, (1972); Dasgupta, (1982); Sinha *et al.*, (1982); Patil, (1990, 1991); Tiwari, (1992, 2001); Tiwari and Satsangi, (1998); Tiwari *et al.*, (1997, 1998, 2011); Mehrotra *et al.*, (2001,2003); Tiwari and Bannikov, (2001); Tiwari and Kachhara, (2000, 2003); Jauhri *et al.*, 2003; Srivastava *et al.*, 2008; Victor *et al.*, 2009); Lalmuankimi *et al.*, (2010); Victor *et al.*, (2011); Lokho and Singh, (2013), Rajkonwar *et al.*, (2013,2014); Rai *et al.*, 2014.

Magnetostratigraphic study was initiated in 1970 on the fossil bearing Himalayan Siwalik sediments of Neogene age covering parts of India and Pakistan [Opdyke *et al.*, 1982; Johnson *et al.*, 1983; Tandon *et al.*, 1984; Ranga Rao *et al.*, 1998; Ranga Rao, 1993; Opdyke and Channel, 1996; Sangode *et al.*, 1996, 1997, 1999, 2001, 2003, and Sangode and Bloemendal, 2004]. The highly fossiliferous rocks are well suited for magnetostratigraphic discourse with the presence of continuous rock exposures. Time history of the sequence was also worked out by, Keller *et al.*, 1977; Opdyke *et al.*, (1979, 1982); Tauxe *et al.*, 1980; Johnson *et al.*, (1982, 1985) and Tauxe and Opdyke, 1982).

Worm *et al.*, (1998) initiated the first work on magnetostratigraphy of Tertiary rocks in North-eastern India where he uncovered a 3500m thick succession of Cenozoic sediments ranging over a period of 30Ma along the Hari River section in Meghalaya. Magnetostratigraphic study in Mizoram was done for the first time in a 560m thick succession of middle Bhuban Formation (Surma Group) exposed between Bawngkawn and Durtlang section of Aizawl (Tiwari *et al.*, 2007). Seven normal and seven reverse magneto-zones were recorded in this section. The corresponding ages delineated were ~21.77 Ma at the bottom and ~15.16 Ma at the

top with a total duration of ~ 6.6 Ma having an average sediment accumulation rate (SAR) of 8.48cm/Ka. Malsawma *et al.*, 2010, delineated 7 normal and 6 reversal magneto-zones in a 1355m thick Bhuban unit (Surma Group) Tuirial section. On correlation with the GPTS the ages ranges from ~12.5 to ~8Ma from base to top. In 2011, Malsawma carried out magnetostratigraphic study for Sairang section where a total of 4 normal and 4 reversal magneto zones were delineated ranging from ~9.8 at the base to ~8.3 at the top section. The average SAR was calculated at 30.17cm/ka thereby having duration of ~1.5 Ma for accumulation of 460m thick Bhuban successions. Paul, (2013) carried out magnetostratigraphy for two sections viz. Zero point-Saihapui and Thuchhuahen section in Kolasib District. The sections expose Tipam sandstones which overlies the Bokalbil, the upper part of the Surma group of rocks. Due to the fragile nature of Tipam sandstones, sampling was done by block method and 3 normal and 3 reversals (Zero point-Saihapui) and 1 normal and 1 reversal (Tuichhuahen) were recorded. The time period for the accumulation of sediments 1279m and 345m thick was ~2.05 Ma having an average SAR of 82.49 cm/ka. Paul *et al.*, 2014 delineated 3 normal and 4 reversals in a 445m thick succession belonging to the Upper and Middle Bhuban formation of the Surma group of rocks exposed in Kolasib-Rengtekawn section of Kolasib district in the northern part of Mizoram. The age of the succession ranges between ~17.2Ma to ~14.9Ma with a total duration of ~2.3 Ma for the accumulation of sediments. A stratigraphic level of 220m in this section records fossils dating back to Burdigalian (Mazumder, 2004) which gives a suitable datum line for correlation.

The proposed area of study belongs to Barail succession which is the only Paleogene rocks reported in Mizoram till date. The existence of Barial group in

Mizoram was debatable as some of the earlier geological and stratigraphic work does not acknowledge its presence, Ganju, (1975); Ganguly, (1975); Shrivasta *et al.*, 1979 and Jokhanram and Venkataraman, (1984). Nandy *et al.*, (1972) described the different structural forms of the Barail and Surma and map the Barial group of rocks in the eastern part of Mizoram. Karunakaran, (1974) and Ganju, (1975) grouped the sedimentary sequence of Mizoram into 3 distinct groups which consists of the Barail group forming the lowest part of the succession. Nandy *et al.*, (1983) reported a 3000m thick succession of Barail rock of the Oligocene period which was composed of sandstones and shales. The Geological Survey of India (GSI) in 2011 reported that from reconnaissance traverse study of Aizawl to Champhai proving the existence of Barail in Champhai area which consist of a monotonous sequence of shales interbedded with siltstone and fine grained sandstones (GSI report, 2011). The most recent report regarding the existence of Barail in Mizoram was given by Betka *et al.*, (2018) through geologic field mapping, detrital thermochronology and structural analysis of eight antiforms in the Indo-Burman Ranges (IBR).

No detailed magnetostratigraphic or paleomagnetic work is available for the Barail succession of Mizoram except for the study of petromineralogic and mineral magnetic carried out by Badekar *et al.*, (2013). In this study he compared 5 sections representing the Barail group, Middle and Upper Bhuban, Bokabil formation and Tipam group where he concluded that the Barail group consists of thin to thinly bedded, compact, fine grained buff colored sandstones with high ferrimagnetic concentrations. Mehrotra *et al.*, (2002a); described ichnogenus *Palaeophycus* from the Barail succession exposed about 8.7km from Champhai on the Champhai- Tuipui road. This was considered the first report of *Palaeophycus* from the Tertiary

succession of north-east India. Extensive investigations were made for recovery of plant impressions from the Paleogene succession of Mizoram for reconstruction of paleoenvironment. Tiwari and Mehrotra, (2002) collected some leaf and fruit/seed impressions from new fossiliferous localities on the Champhai-Tuipui belonging to the Barail Group of Oligocene age. These impressions indicate the occurrence of tropical forest in a nearby area during the time of deposition.

Recently, petrography and geochemistry of the Barial rocks in Champhai was studied by Hauhnaar *et al.*, 2018; Hussain and Bahrali, (2019). Petrographic studies reported that the sandstones were very fine to fine grained sublitharenite to feldspathic litharenite with a mixed provenance of high grade metamorphic to acid to basic igneous with reworked sedimentary rocks derived from the Indo-Burman Ranges. The whole rock geochemistry studies refer the rocks as Quartz arenite to sublithic arenite derived from moderately weathered felsic magmatic source from Rare Earth Element (REE) ratios and chondrite-normalized REE patterns. From the tectonics distribution diagrams the sediment were reported to be deposited in an active continental margin setting or continental island arc setting.

## **1.6 SCOPE OF PRESENT WORK**

Chronostratigraphy of Surma rocks exposed in various parts of Mizoram along with the Tipam sandstone around Kolasib have been established through Magnetostratigraphic correlations by Tiwari *et al.*, 2007; Malsawma *et al.*, 2010, Malsawma, 2011, Paul *et al.*, 2014; Paul, 2013. Since the study area is considered to fall under the regime of the barail group of rocks which lacks any reliable age markers in the form of macro and micro paleontological evidences

Magnetostratigraphy will serve as a robust tool in establishing the chronostratigraphic framework and correlation with already established Surma sequences in various parts of Mizoram.

### **1.7 OBJECTIVES**

The study aims to establish a well defined stratigraphic framework of the area using the methods of Magnetostratigraphy and mineral magnetic through the principles of magnetic polarity magnitude and directions stored within magnetic detrital sediments

1. Work out the Magnetostratigraphy of the Barail succession in Mizoram
2. Estimate the rate of sedimentation and,
3. Establish regional stratigraphic correlation.

## **CHAPTER II**

### **REGIONAL GEOLOGY AND GEOLOGY OF THE STUDY AREA**

#### **2.1 GEOLOGICAL SETUP**

Origin of sediments, the environments where they were collected and their evolution through time provides the much needed knowledge for establishing the geologic setup of a region. The magnetizability of sediments may depend on the fore mentioned factors because provenance control the type of magnetic minerals and depositional environment can have a huge influence on the degree by which they are magnetized and post depositional deformations may control the extent by which various strata may be tilted from their normal orientations. With that being said, the nature of magnetism attained by sediment may vary depending on the depositional settings and by which tectonics may modify the geology of the area. So, to truly understand the magnetism attained in a given area, in depth knowledge on the regional geological settings is necessary.

The Himalayan ranges are the most majestic inland mountain range which forms the main geological framework of the area and stretches over a length of 2500km trending east-west with a width of about 300kms in north-south direction.

#### **2.2 INDIAN CRATON**

The separation of the Indian sub-continent from the mainland of Gondwana is believed to have started around Cretaceous (Curry and Moore, 1974; Acharyya, 1986; Hutchison, (1989); Kent *et al.*, (2002) and Mahoney *et al.*, (1985) reported incidents of basalt lava flows which are Rajmahal consisting of two units (Trap flows and



intertrappean sediments) ~118 Ma and Deccan trap around 70-65Ma. The transition period between the onset of Cretaceous period and starting of the Tertiary was marked by a continuous evolution of high quantities of basaltic magma in small intervals (Mahoney *et al.*, 1985). The breaking up of Gondwana during late Permian to early Triassic led to the formation of rift zones leading to the formation of different continents and widening of the Tethyan Ocean (Curry *et al.*, 1982). The rate at which the Indian sub-continent moves northward dramatically decreases as it collides with the Tibetan plateau thereby marking the start of the Himalayan orogeny (Das Gupta and Nandy, 1995). The Indian craton which consists of Archean gneissic complex (Rahman, 1999) forms the westward boundary of the Bengal basin.

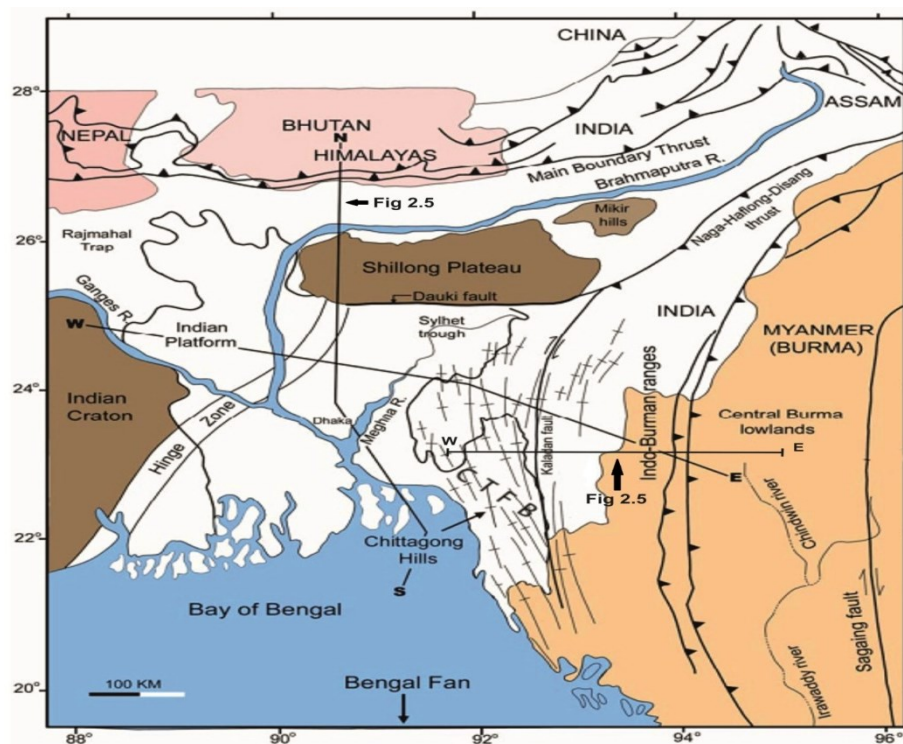


**Fig. 2.1:** Map of the Bengal basin with the Dauki Fault separating the Sylhet trough from the uplifted Shillong Plateau (after Uddin and Lundberg, 1998).

### **2.3 SHILLONG PLATEAU**

This plateau was uplifted to its present height (average 1 km, maximum 2 km) during the Pliocene Epoch. The Shillong plateau is bounded by the Garo-Rajmahal trough fault to the west and the Dauki fault in the south (Johnson and Alam, 1991). “Late Mesozoic and Cenozoic sedimentary rocks drape portions of the southern Shillong plateau and generally dip south in a monocline. “As much as 15-18 km of structural relief between the Shillong plateau and the basement of the Sylhet trough has been postulated” (Hiller and Elahi, 1988). The contact between the Shillong plateau and the Sylhet trough is indicated by the poorly exposed Dauki fault. The 5 km wide Dauki fault has a nearly straight face across the essentially flat topography which is characterized by extensive fracturing (Evans, 1964) and near vertical (85°) dips of Pliocene and Pleistocene strata (Khan, 1978). The Precambrian rocks of the Shillong plateau belong to two groups: (1) an Archean gneissic complex; and (2) the Proterozoic Shillong Group. The gneissic complex, exposed in the northern and western part of the plateau, consists of quartzo-feldspathic gneiss and schists (Rahman, 1999). The boundary between the Gneissic complex and Shillong Group is marked by a lithological as well as structural break. The Proterozoic rocks have undergone regional metamorphism up to garnet-grade prior to the igneous activity in the area. The Shillong Group was overlain by Mesozoic to Miocene rocks prior to the Pliocene uplift of the Shillong plateau (Johnson and Alam, 1991).

## 2.4 BENGAL BASIN

The break-up of eastern Gondwanaland and collision of the Indian plate with the Asian plate are all directly related with the Geologic evolution of the Bengal Basin starting from Upper Palaeozoic. The sedimentary cover of the basin with a maximum thickness of 20 km includes three major lithostratigraphic units separated by three major unconformities. The western part of Bangladesh is the platform shelf, whereas the eastern part of the country is represented by the folded belt (Chittagong-Tripura Fold Belt). The most subsided central part of the basin comprises two major depressions at the north (Sylhet Trough) and south (Patuakhali Depression). The influx of huge amounts of detritus originating from the nearby sources of the basin compensated for the rapid subsidence of the fore-deep of the Bengal Basin. Shallow water conditions and deltaic environment persisted. In addition to the western and northern foreland shelves, which were the earlier source areas, increases erosional rates of the rising chains of the Himalaya and the Indo-Myanmar Ranges provided the much needed sediments in the basinal area since the mid-Miocene (Shamsuddin and Abdullah, 1997).

Plate collision and orogeny along its eastern and northern margins resulted in the gradual closure of the Bengal basin which was formed by rifting from passive continental margin (Rowley, 1996). The basin, which attains a maximum thickness of 20 km in its deeper parts, has been filled by an extremely thick accumulation of sediments, mostly of clastic origin. The Bengal basin has two broad tectonic provinces: (1) the Indian platform, where thin sedimentary strata overlie rocks of the Indian craton in the northwest (in northwestern part of Bangladesh); and (2) a very thick basin-fill that overlies deeply subsided basement of undetermined origin in the

south and east (Bakhtine, 1966; Khandoker, 1989). The two provinces being separated by a northeast-trending hinge zone (Fig. 2.1). Indian continental crust extends beyond the hinge zone toward the southeast (Khandoker, 1989).

The outermost part of the zone of compression between the west Burma block and the Indian plate is marked by the eastern fold belt. The complexity and amplitude of the north-south-trending folds in this belt decreases and broadens westward. Folding intensity rapidly attenuates westwards; the central and western parts of the basin are relatively under-formed. Pliocene to recent being the main age range of the folding and more than one phase of deformation is evident in some structures. The Sylhet trough is a sub-basin of the Bengal basin in north-eastern Bangladesh which is characterized by large, closed, negative gravity anomaly. The Sylhet trough has minimal topography and is actively subsiding (Holtrop and Keizer, 1970) with an estimate sediment thickness range from about 12 to 16 km (Hiller and Elahi, 1984). The eastern part of the Sylhet trough lies in the frontal zone of the Indo-Burman Ranges.

Accretionary prism development is believed to be the main driving force for the structural evolution of Chittagong-Tripura Fold Belt Basin and major east-dipping thrust faults produced by off-scraping of the oceanic sediments as a result of oblique subduction of the Indian plate beneath the Burma plate in an arc-trench setting (Gani and Alam, 1999). Within the individual major thrust sheets, the sediments in the upper part have been deformed by the activity of thin-skinned tectonics giving rise to a series of elongate, north-south trending curvilinear anticlines and synclines in this province; Sikder and Alam, 2003); Lohmann (1995) and Sikder (1998) have pointed out some duplex structures in the western part of Chittagong-Tripura Fold Belt. They

have also suggested thin-skinned detachment and shear-off tectonics to explain the structural style of the region, but did not relate these processes directly to the subduction complex. It is our strong belief that the tectonic and structural development of Chittagong-Tripura Fold Belt may be more readily explained by the accretionary prism formation. Compressive (north–south) wrench tectonics, as a result of convergent-oblique movement of the Indian plate relative to the Burma plate, and the opening of the Andaman Sea during Miocene time has significantly influenced the overall structural architecture of the region (Murphy and Staff BOGMC, 1988; Sikder, 1998). It is anticipated that future identification of the major individual thrust sheets (accretionary wedges) will provide vital information in determining the chronological order of the Tertiary rock succession in the region, since it is well known that the accretionary complex as a whole gets younger and younger towards the west (Dasgupta and Nandy, 1995; Gani and Alam, 1999).

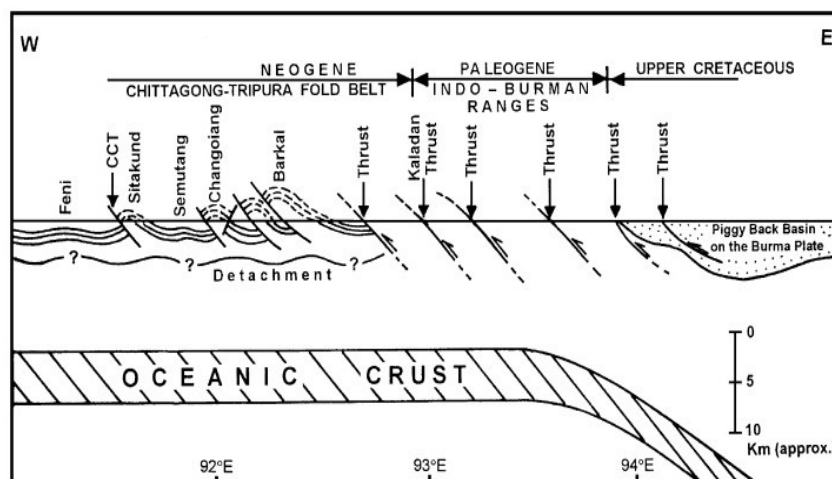


**Fig. 2.2:** Cross-sectional profile through the Chittagong–Tripura Fold Belt Province showing the structural elements and development of Neogene accretionary prism complex (after Sikder and Alam, 2003).

## **2.5 INDO-BURMAN RANGES (IBR)**

The Indo-Burmese Ranges occurring along the eastern margin of the Indian sub-continent, are a clear representation of the collision of the Indian and Eurasian plates. Early Tertiary synorogenic sequences, which have been deformed into imbricate thrust zones are the principal constituent of the Indo-Burmese Range and are prominent geotectonic elements of South Asia. The Indo-Burmese Ranges has a general north-south trend and is an active orogenic belt, comprising of folded, thrust and wrench-faulted outer arc complex, or accretionary prism, that accreted to the edge of the Eurasian Plate beginning the Jurassic (Graham *et al.*, 1975; Rangarao, 1983). With an average width of 230 km., the ranges extend from the southern tip of the Mishmi Hills into southwest China. Mitchell, (1981) divided the ranges into two orogenic belts: the western belt, comprising the Cretaceous to Eocene sedimentary rocks; and the eastern belt, consisting of schist's and turbidites. The eastern belt is locally overthrust by serpentinitized harzburgites with pillow lavas and hornblende gabbros. The Eocene rocks along the west coast of Arakan in the eastern belt of Indo-Burmese Ranges are being unconformably overlain by the Miocene sediments. Several authors (Mitchell, 1993; Das Gupta and Nandy, 1995) have suggested the possibility of the Indo-Burmese Ranges being trench deposits containing ophiolitic mélanges that got scrapped off the Indian plate.

## **2.6 SURMA BASIN**

The Neogene Surma basin is bounded by the post-Barail unconformity, subsequently faulted (Kaladan fault) to the east; the E-W Dauki fault and NE-SW Disang thrust to the north and northeast; the NE-SW Sylhet fault (Nandy *et al.*, 1993),

also term as the 'Hail – Hakula' (Ganguly,1993) lineament and Barisal-Chandpur high concealed below the alluvium of Bangladesh (Sengupta,1966) to the west and north west. To the south, the basin extends upto the Arakan coastal area of Myanmar. Within this vast terrain, the Surma group and the younger sediments occur as westerly convex N-S fold belt for a strike length of about 550 km, having a maximum width of 200 km. The Surma basin covers lower Assam, Tripura, Mizoram, western part of Manipur, Sylhet and Chittagong districts of Bangladesh and Arakan coastal zone of Myanmar. To the east of this basin lies the intricately folded, faulted and thrust Palaeogene outer arc complex of the Indo-Myanmar mobile belt, where as to the west, alluvium covered, gently dipping, homoclinal Tertiary sedimentary succession of Bangladesh (Bengal Basin) occurs. This assumes a 'bell shaped' form having constant southerly and south-westerly palaeo-slope which connected to the open sea in the south.

## **2.7 STRATIGRAPHIC FRAMEWORK OF MIZORAM**

Evans in 1932 established the first works regarding the stratigraphic set up of the Surma basin and in 1964; he described its tectonic evolution with reference to the Bengal basin followed by Sengupta (1966) and Raju (1968). The depositional history, stratigraphic set up and tectonic evolution of the Bengal basin was described by Alam (1989, 1991, 1995, and 1997) where the depositional environment and facies of the basin was established. Since the Stratigraphy of Bengal Basin established by Evans (1932) was based on correlation based on lithographic similarities and macro fossil assemblages with exposures from Assam, they were not considered reliable. To establish more reliable framework, Micro fossil studies were carried out by Ahmed in 1968; followed by Chowdury (1982), Uddin and Ahmed (1989) and Reimenn (1993)

discourse on trace fossils. Johnson and Alam (1991), Khan (1991). Karunakaran (1974) and Ganju (1975) grouped the sedimentary sequence of Mizoram into 3 distinct groups which are Barail, Surma and Tipam. Over the years with more geological information as a result of advancement in science and technologies revisions have been made by Tiwari and Kachhara (2003); Mandaokar, (2000) and Tiwari et al., 2011.

| Age                            | Group                          | Formation | Unit          | Thickness (m) | General Lithology  | Depositional Environment               |
|--------------------------------|--------------------------------|-----------|---------------|---------------|--|--|
| Recent                         | Alluvium                       | -         | -             | -             | Silt, clay & gravel  | River deposits                         |
| Early Pliocene to Late Miocene | Tipam                          | -         | -             | +900          | Friable sandstone with occasional clay bands                         | Stream deposits                        |
| Miocene to Upper Oligocene     | SURMA                          | Bokabil   | -             | +950          | Shales with siltstone and sandstone                                  | Shallow marine                         |
|                                |                                | Bhuban    | Upper Bhuban  | +1100         | Arenaceous with sandstone, shales and siltstone                      | Shallow marine, near shore to lagoonal |
|                                |                                |           | Middle Bhuban | +3000         | Argillaceous with shales, siltstones                                 | Deltaic complex                        |
|                                |                                |           | Lower Bhuban  | +900          | Arenaceous with sandstone, shales and siltstone                      | Shallow marine                         |
| Oligocene                      | Barail                         | -         | -             | +3000         | Shales, siltstone and sandstones                                     | Shallow marine                         |
| Data source                    | Karunakaran, 1974; Ganju, 1975 |           |               |               | Tiwari and Kachhara, 2003; Mandaokar, 2000; Tiwari et al, 2011, 2012 |  |

**Table 2.1:** Stratigraphic framework of Mizoram after Karunakaran, (1974) and Ganju, (1975).



## **2.8 LITHOSTRATIGRAPHY OF THE STUDY AREA**

In the field of magnetostratigraphy, to acquire and record intervals of normal and reversals within a section, a well bedded and continuous exposure of rock succession is required. The area must have minimum vegetation and soil cover. Most often, sections exposed in new road cuttings are preferable along with good exposures of sandstone beds.

Field investigation was carried out on several occasions, the first one for selection of sections. After selection of three sections, a detailed field investigation was conducted where the attitude of beds was recorded and thickness of each bed was measured. The sedimentary structures were carefully noted down for interpretation of deposition and paleoenvironment. After selection and measurement of sections, field data was incorporated into computer for preparation of litholog using surfer software.

Three sections were selected for this study from roadside exposures running along the south to northeast and north-northeast direction from Champhai town. The first section is located to the south of Champhai town and is named Ruantlang section (RT). The second section Zote (ZT) lies to the east of Champhai with plain area lying in between the first two sections. The Ngur section (NG) is the third section and runs along the roadside exposures in the north-northeast direction from Zote.

### **2.8.1 LITHOSTRATIGRAPHY OF RUANGLANG SECTION**

Ruantlang section (RT) is located between N23.430079-23.425748 and E93.337682-93.346024 and constitutes the southern part of this study area selected along a roadside section running from Champhai town to Mualkawi village. The section is named after a small village 'Ruantlang' located on the north-eastern part of

the section. The general dip of the exposure is NNW direction with an average amount of 14°.

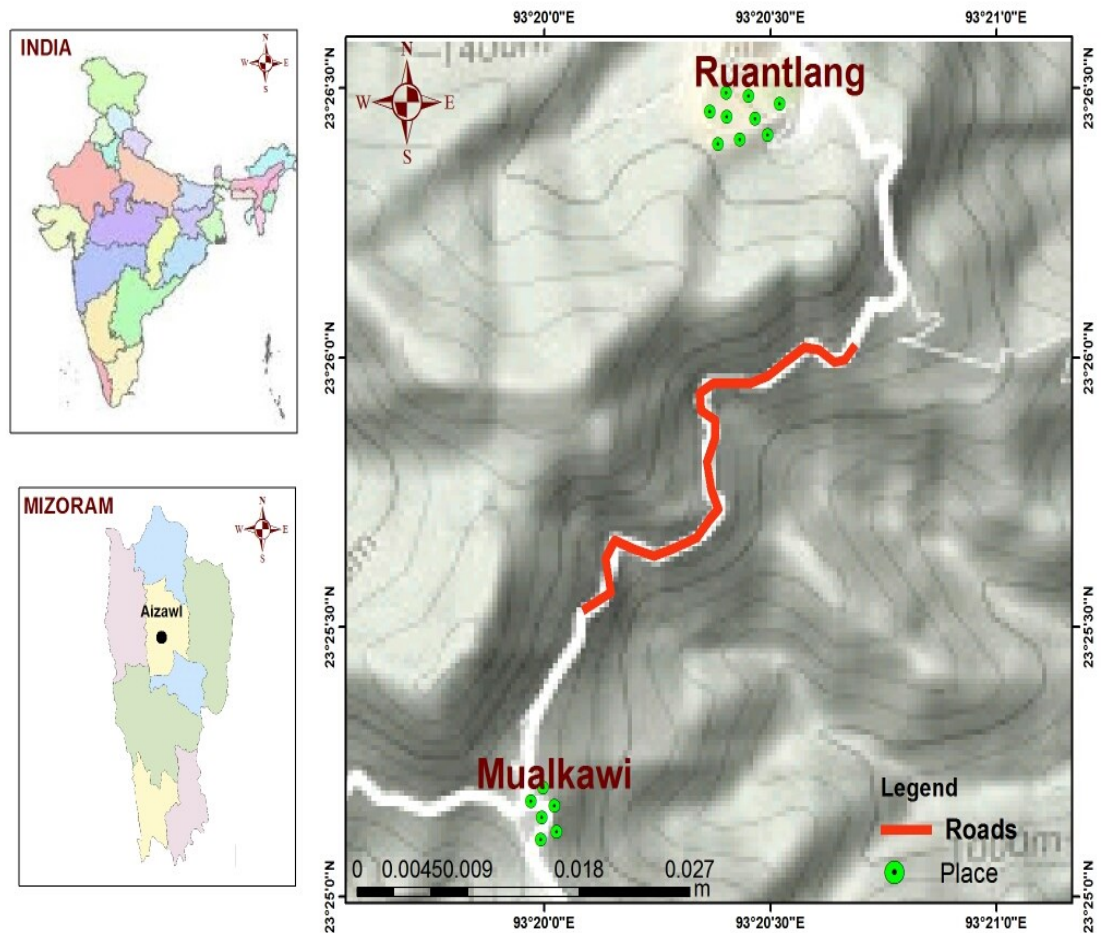


**Fig 2.3:** Location map of Ruantlang section

### 2.8.1.1 Litho-units of Ruantlang (RT) section

The section exposes a 514.3m thick succession of rocks representing the lower part of the Barail exposures in this area. The rocks exposed in Ruantlang section are dominantly argillaceous with occasional sandstone beds. The thickness of sandstone beds vary from a few centimetres to more than a meter and are mostly very fine to fine grained. Sandstone shale alternation is also found in some sections where dominance is shared between the two rock types depending upon the nature of the

facies. Few beds of grey sandstones are also exposed which show lenticular bedding and cross laminations. Shales are dominant throughout the area showing colors ranging from light to dark grey and little pale olive green coloration. The shales are mostly clayey to silty shales and shows different form of weathering patterns like fissility, spheroidal and splintary. The shales are mostly bioturbated with different types of burrows which also protruded in few sandstone beds. Siltstones, silty shales and silty sandstones are also found on numerous occasions, alternating with sandstone and shales. Due to mass wasting and vegetation few sections cannot be analyzed and are represented as slumping in the given litholog. The overall lithology shows a decrease in grain size from top to bottom since sandstones percentage decreases toward the upper part of the exposure. Litholog was prepared for the section where 31 distinct units were recorded as given in table 3.1.



**Fig. 2.4:** Panoramic view of Ruantlang section (RT).

### Ruantlang 1

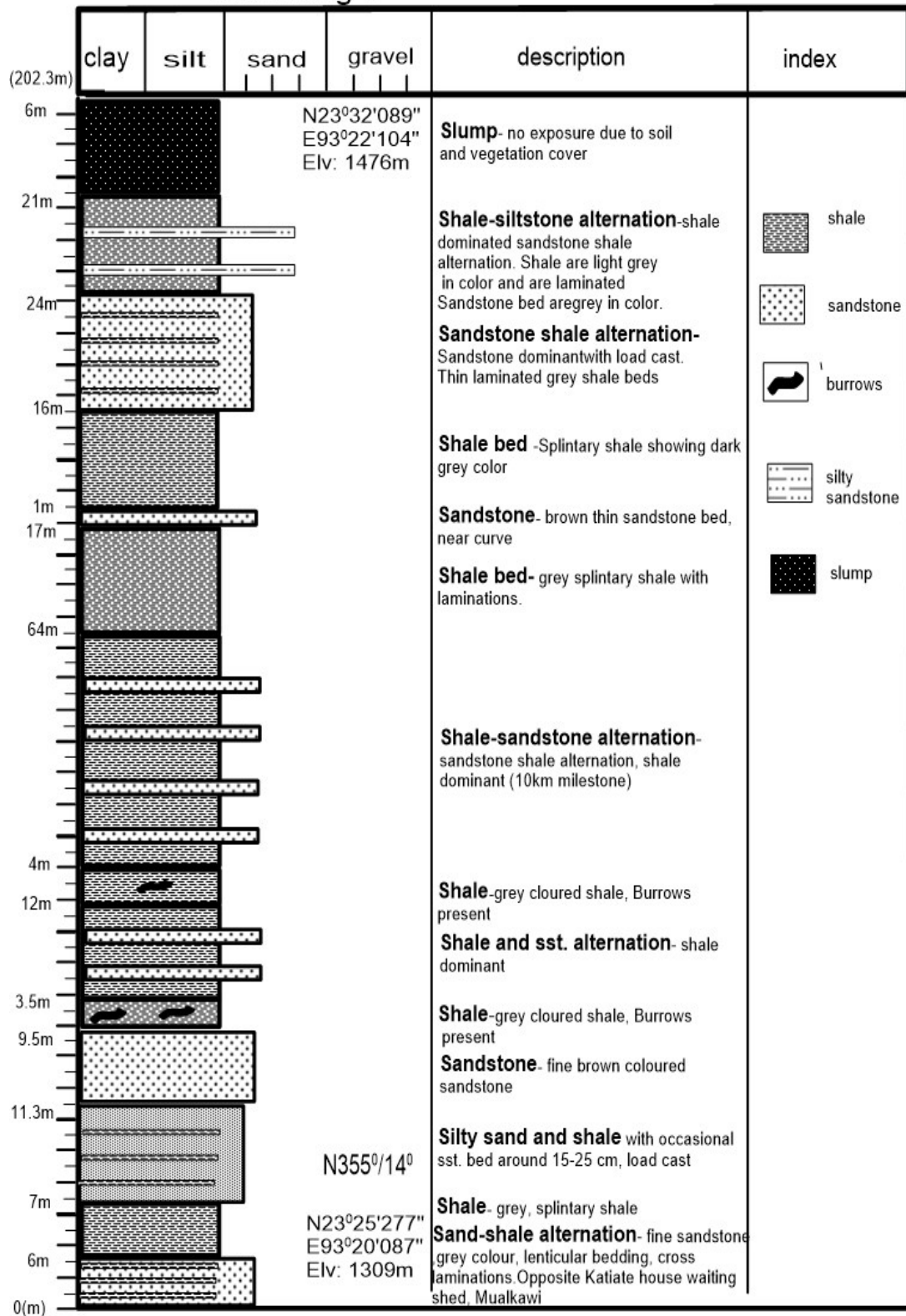


**Table 2.2 (a):** Litholog and description Ruantlang section 1.

### Ruantlang 2

|        | clay | silt | sand                       | gravel | description  | index           |
|--------|------|------|----------------------------|--------|--|-----------------|
| (178m) |      |      |                            |        |  |                 |
| 42m    |      |      | N23°26'109"<br>E93°20'462" |        | <b>Shale bed-</b> grey coloured splintary shale. Borrows found in different sections of the bed. The shales are thinly laminated and show spheroidal weathering patterns | shale           |
| 12m    |      |      |                            |        | <b>Sandstone shale alternation-</b><br>Grey sandstone bed with occasional bed of grey splintary shales   | sandstone       |
| 10m    |      |      |                            |        | <b>Slump-</b> No exposure due to mass wasting  | burrows         |
| 9m     |      |      |                            |        | <b>shale-sandstone transition-</b><br>Grey Splintary shale bed with coarsening upward to grey sandstone bed, bioturbated   | silty sandstone |
| 24m    |      |      |                            |        | <b>Siltysand shale alternation-</b><br>silty shale with occasional bed of sandstone (10-20cm), load cast present in between sand-shale layer                             | slump           |
| 16m    |      |      |                            |        | <b>Silty shale bed-</b> does not show splintary nature due to higher percentage of silt size particles. grey to olive green in color                                     |                 |
| 15m    |      |      | N23°25'573"<br>E93°20'292" |        | <b>Sandstone-shale alternation-</b><br>Olive green shale dominant. Top bioturbated, burrows observed. (Ngiau hmun)   |                 |
| 15m    |      |      |                            |        | <b>Shale bed-</b> grey splintary shale with spheroidal weathering pattern. Thinly laminated  |                 |
| 6m     |      |      |                            |        | <b>Sandstone-shale alternation,</b><br>sst. dominating with thin shale beds (water point)  |                 |
| 18m    |      |      |                            |        | <b>Shale bed-</b> greyish shale with thin laminations. Splintary and show spheroidal weathering patterns(9km milestone)  |                 |
| 11m    |      |      |                            |        | <b>Siltstone-shale alternation-</b><br>siltstone dominant, grey color. Shale thinly bedded, with laminations, grey in color  |                 |
| 0(m)   |      |      |                            |        |  |                 |

**Table 2.2 (b):** Litholog and description Ruantlang section 2.

### Ruantlang 3

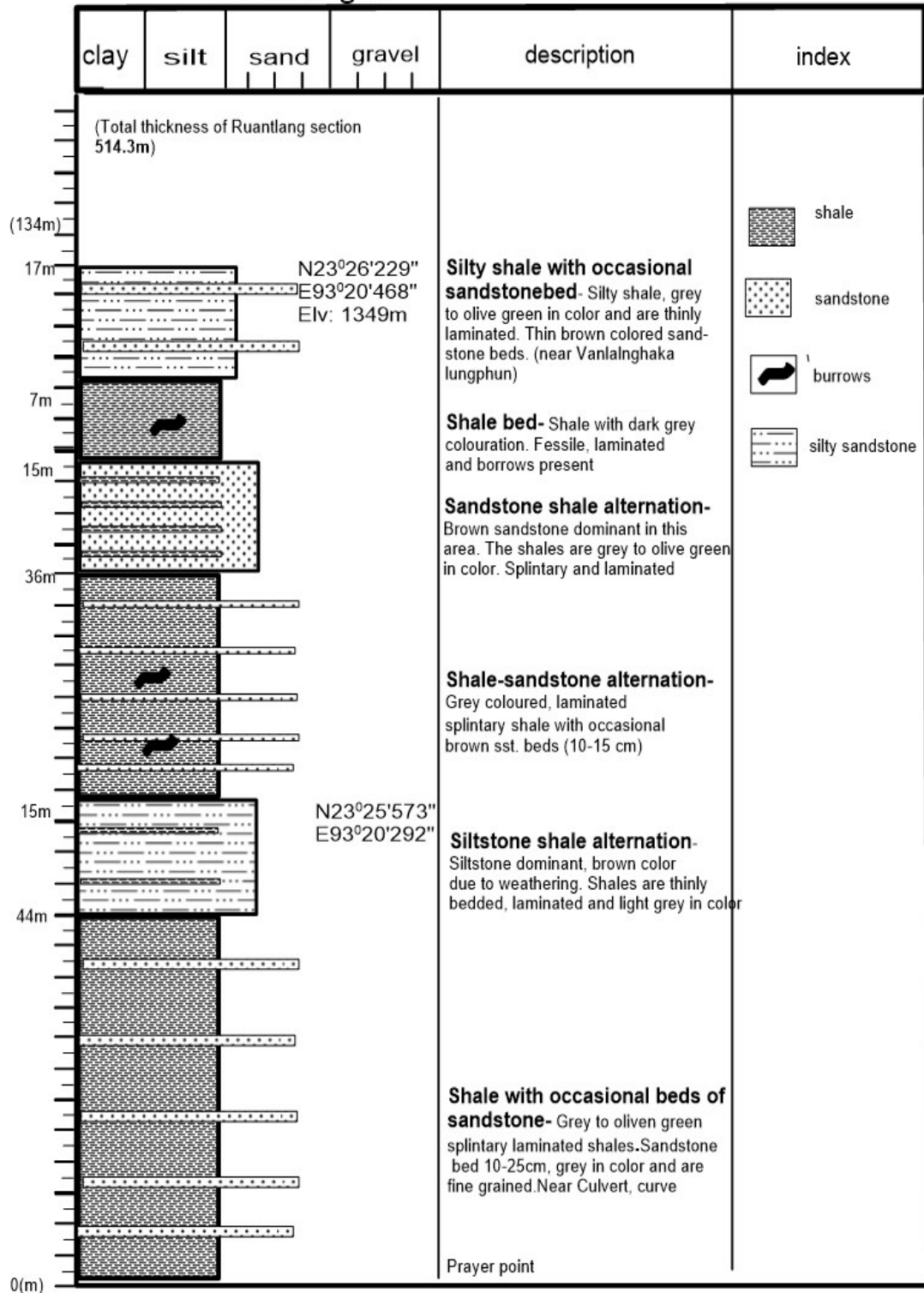


**Table 2.2 (c):** Litholog and description Ruantlang section 3.



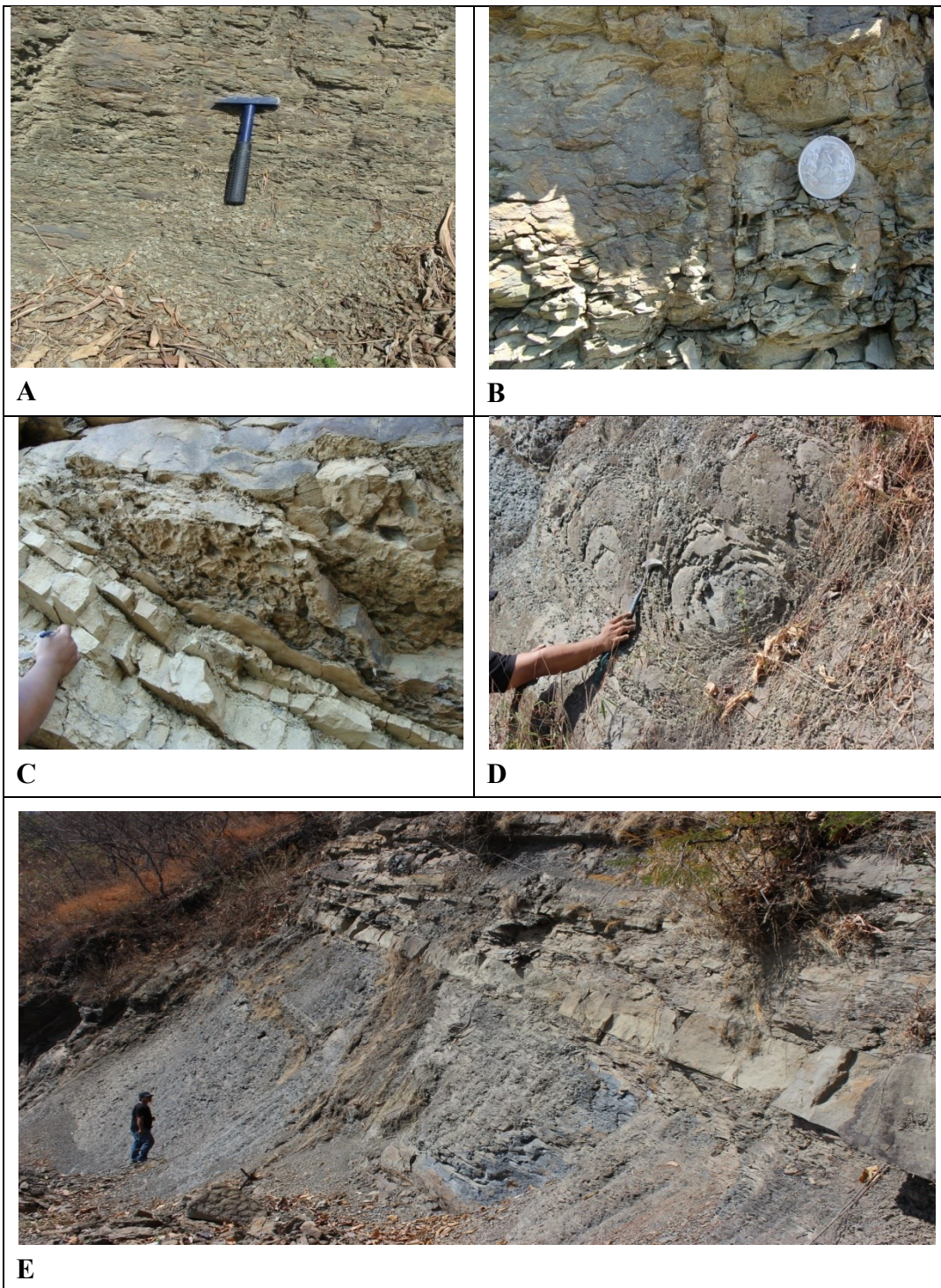


**Fig.2.5.** Field Photograph ; A) Fissile olive green shales B) Trace fossil C) Brown sandstone bed with load cast D) Spheroidal weathering in shales E) Shale bed overlain by brown sandstone beds.

## 2.8.2 LITHOPSTRATIGRAPHY OF ZOTE SECTION (ZT)

Zote section (ZT) is located between N23.507161-23.50470 and E93.356560-93.357204 with an elevation of 1290-1414 m above mean sea level. The section is located to the east of Champhai town and is named after Zote village which is the starting point for this section. Zote section constitutes the middle portion of the study area linking Ruantlang and Ngur sections. The bed dips essentially towards north-northwest direction with a gentle gradient of about 20°.

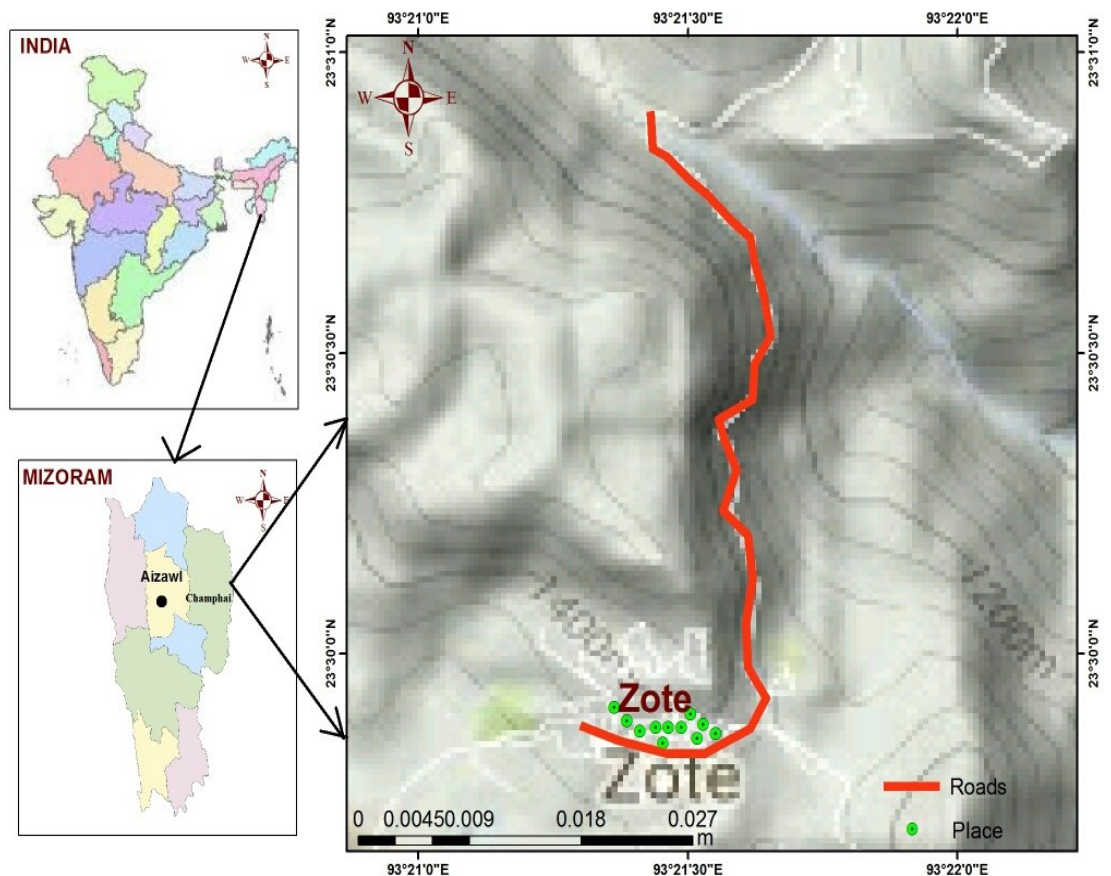


**Fig. 2.6:** Location map of Zote section



### **2.8.2.1 Litho-units of Zote (ZT) section**

The section shows a change in sedimentary facies in comparison with Ruantlang section which is mostly dominated by shales. Zote section exposes a 117.5m thick sedimentary succession which is mainly composed of intermixing and alternation of sandstone and shale. The section can be interpreted as a coarsening upward type of environment since shale is more common in the lower parts with an increasing grain size sequence leading to a more sandy top section. The sandstones are mostly brown in color from massive to thinly bedded in thickness. Mud clast, ball and pillow structure are occasionally found within the sandstone beds. Shale makes up a huge portion of the section. They show different shades of grey color and are thinly laminated and show spheroidal and splintary weathering patterns. Shales are mostly found alternating with sandstone bed and intermixing with sand, forming silty-sandstone formation in some parts of the exposure. A detailed lithological description of the section is given below.



**Fig.2.7:** Panoramic view of Zote section (ZT).

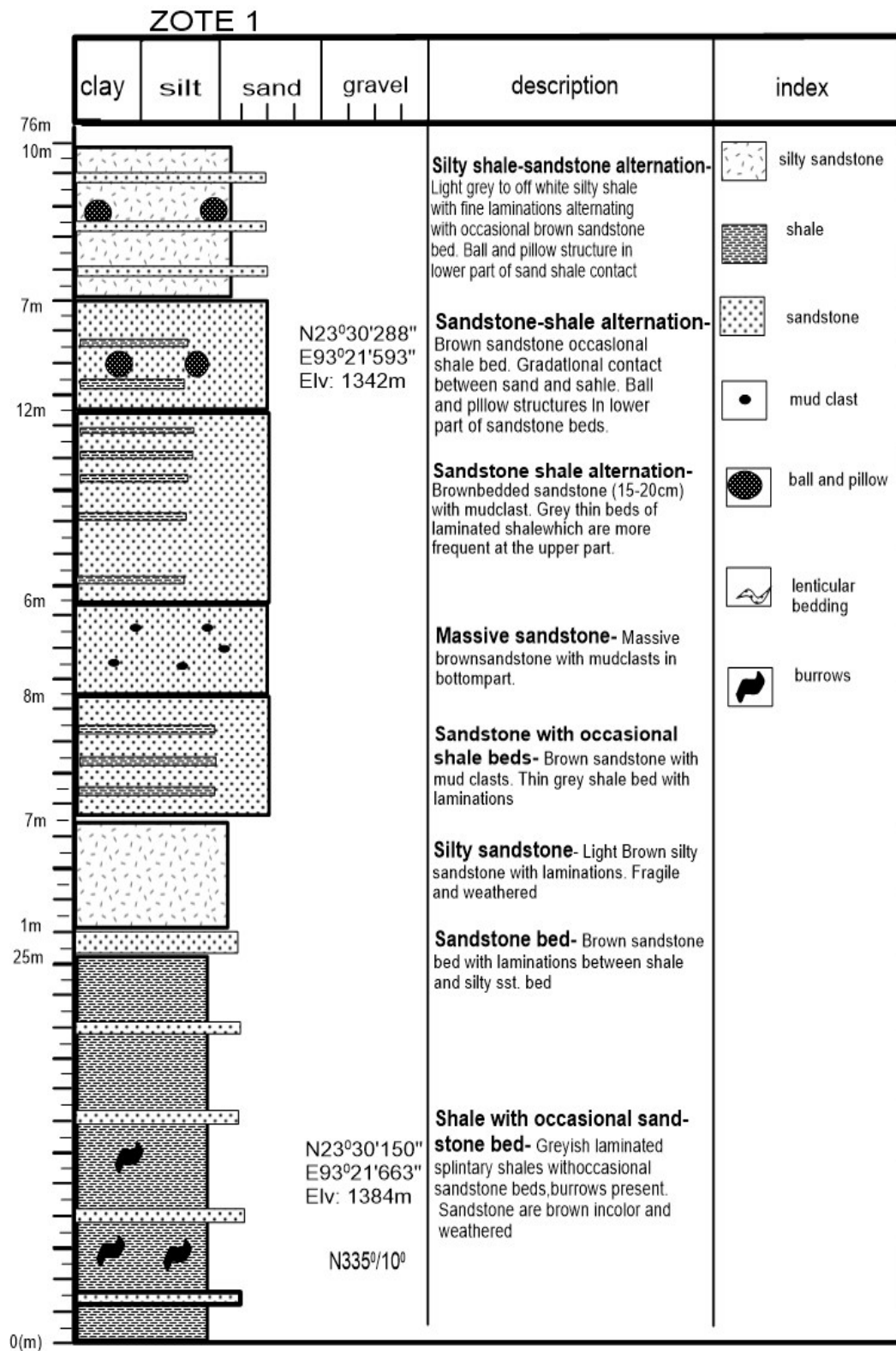


**Table 2.3 (a):** Litholog and description of Zote section 1.

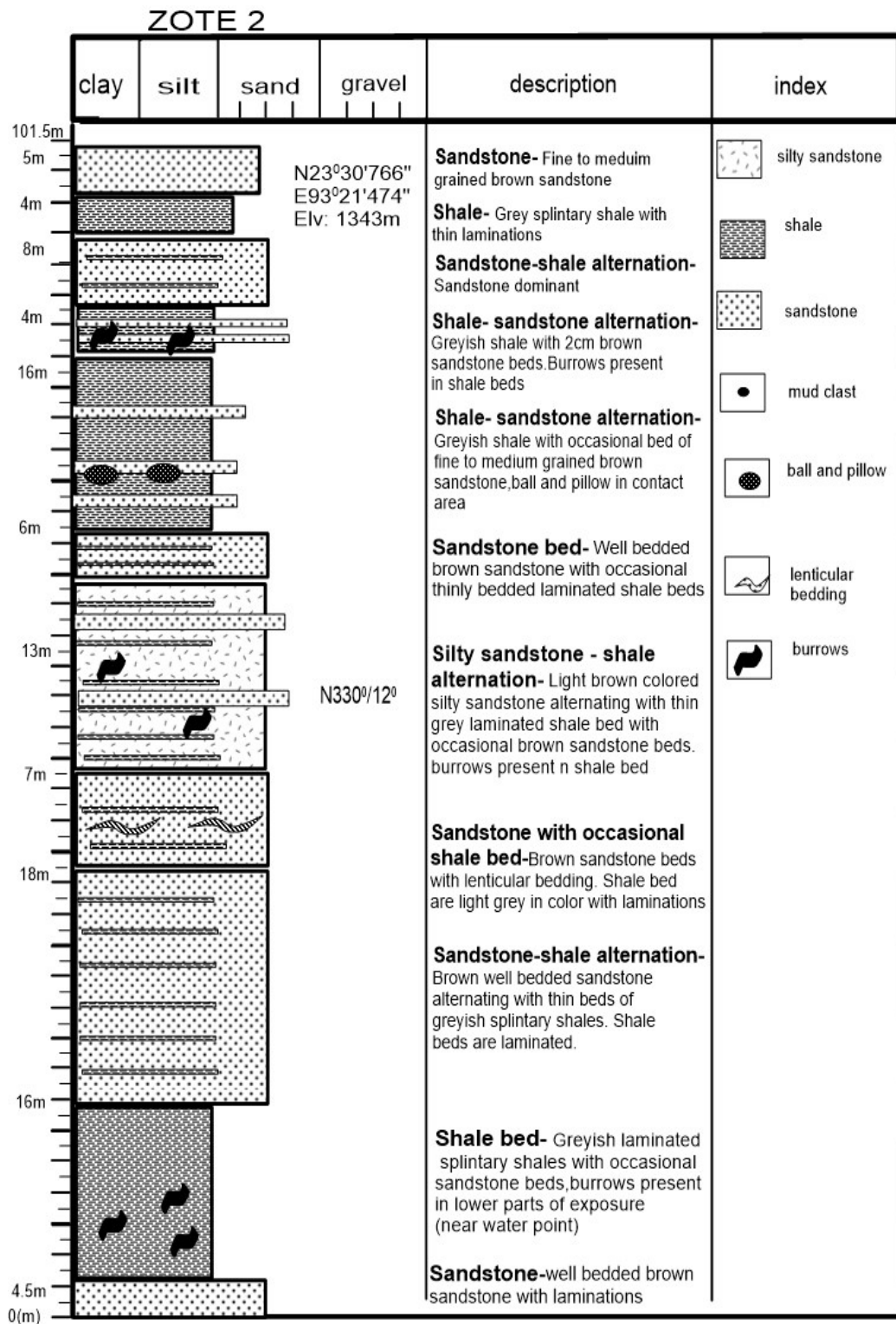


**Table 2.3 (b):** Litholog and description of Zote section 2.

### ZOTE 3

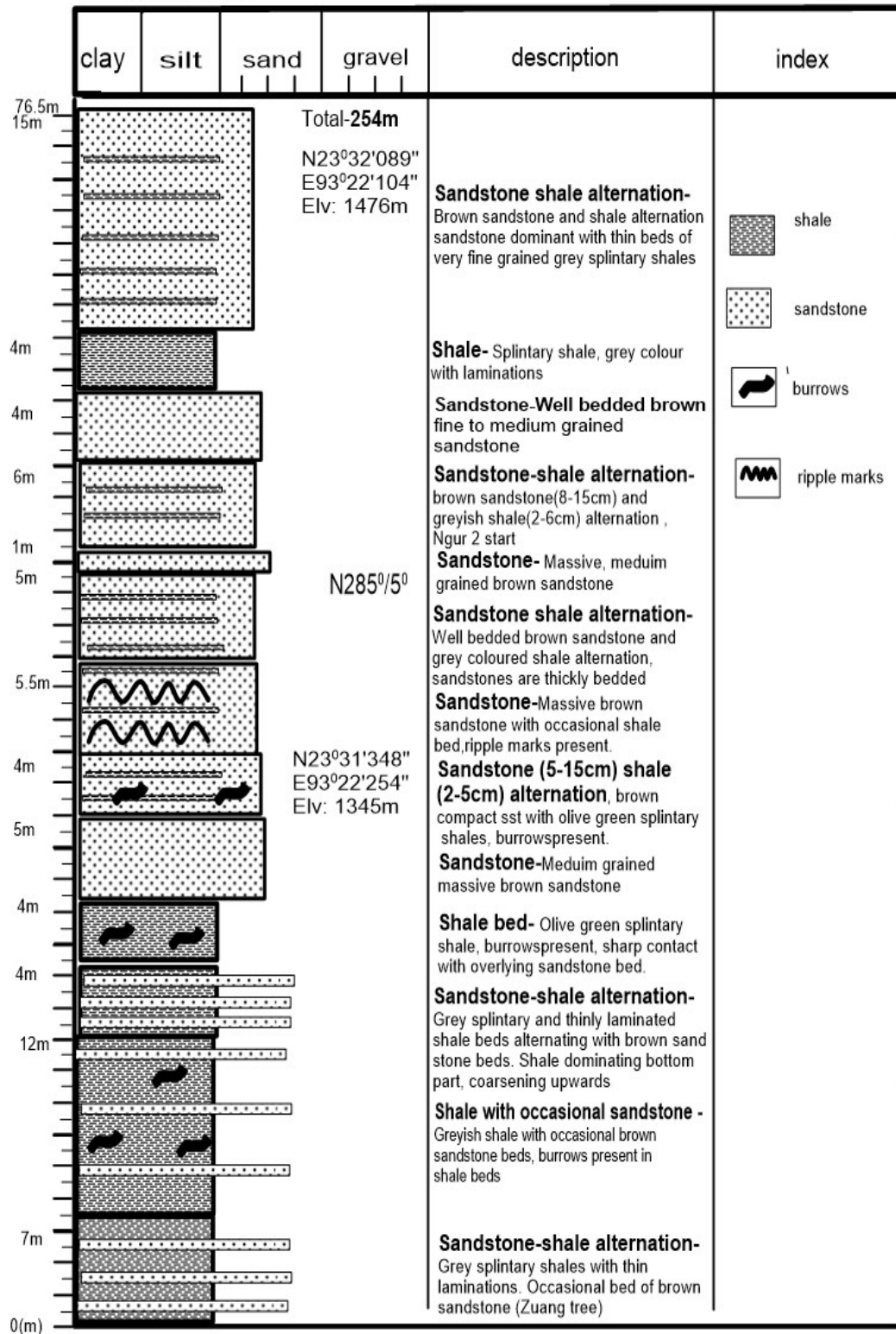
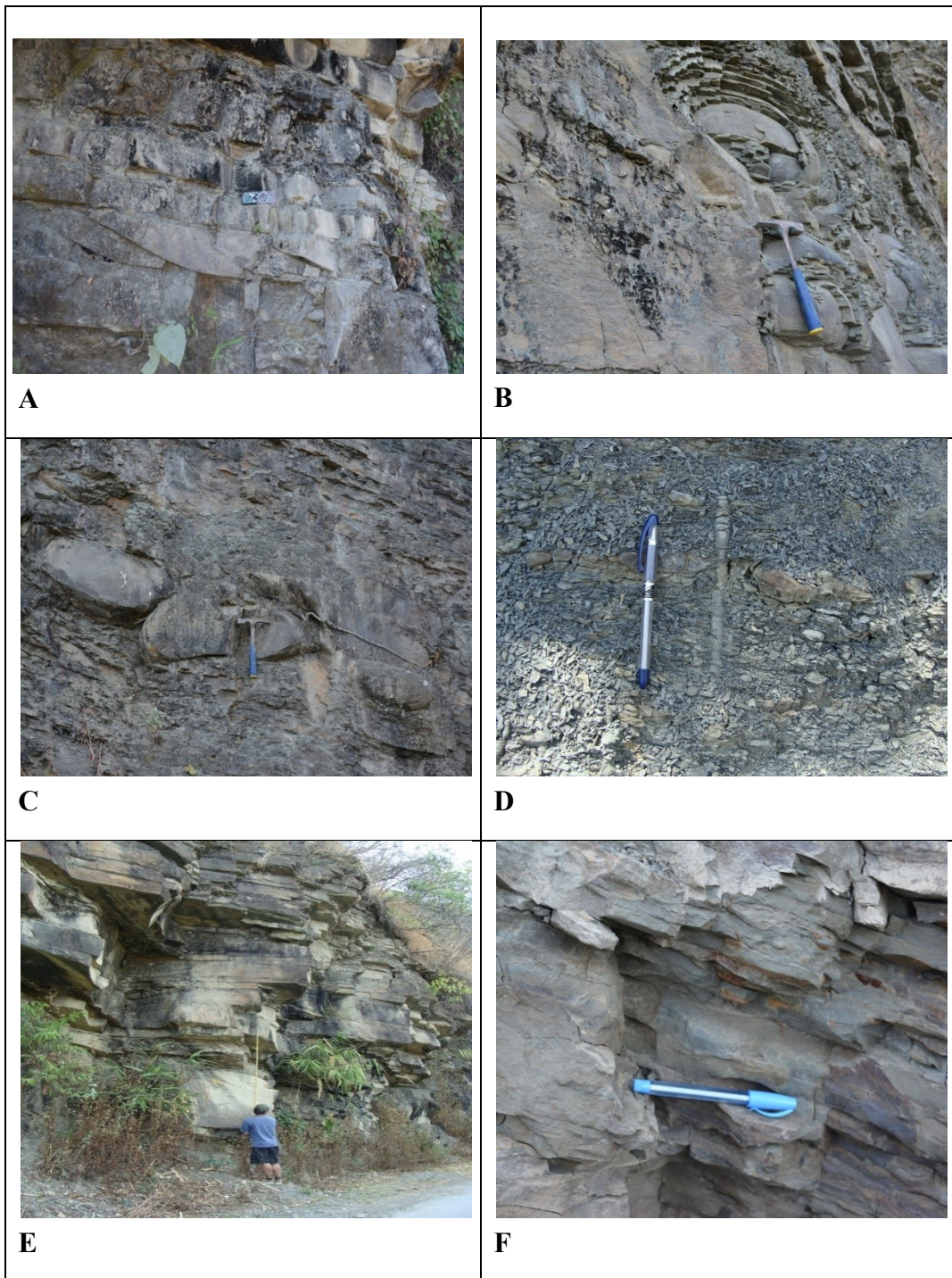


Table 2.3 (c): Litholog and description of Zote section 3.





**Fig.2.8.** Field Photograph A) Tidal bundles. B) Spheroidal weathering in shale. C) Ball and pillow structure D) Trace fossil. E) Bedded brown sandstones. F) Fissility and laminations in shale bed.

### 2.8.3 LITHOSTRATIGRAPHY OF NGUR SECTION

Ngur section (NG) is located between N23.527820-23.571839 and E93.369928-93.386061 with the lowest point at 1340m and highest point with having an elevation of 1603 m above mean sea level. The section is located to the north-east east of Champhai town and constitutes the eastern margin of the study area. The section is named after Ngur village, a small village located in the middle part of the section. The bed dips essentially towards northwest to north-northwest direction with a gentle gradient of about  $5^{\circ}$ - $25^{\circ}$ .

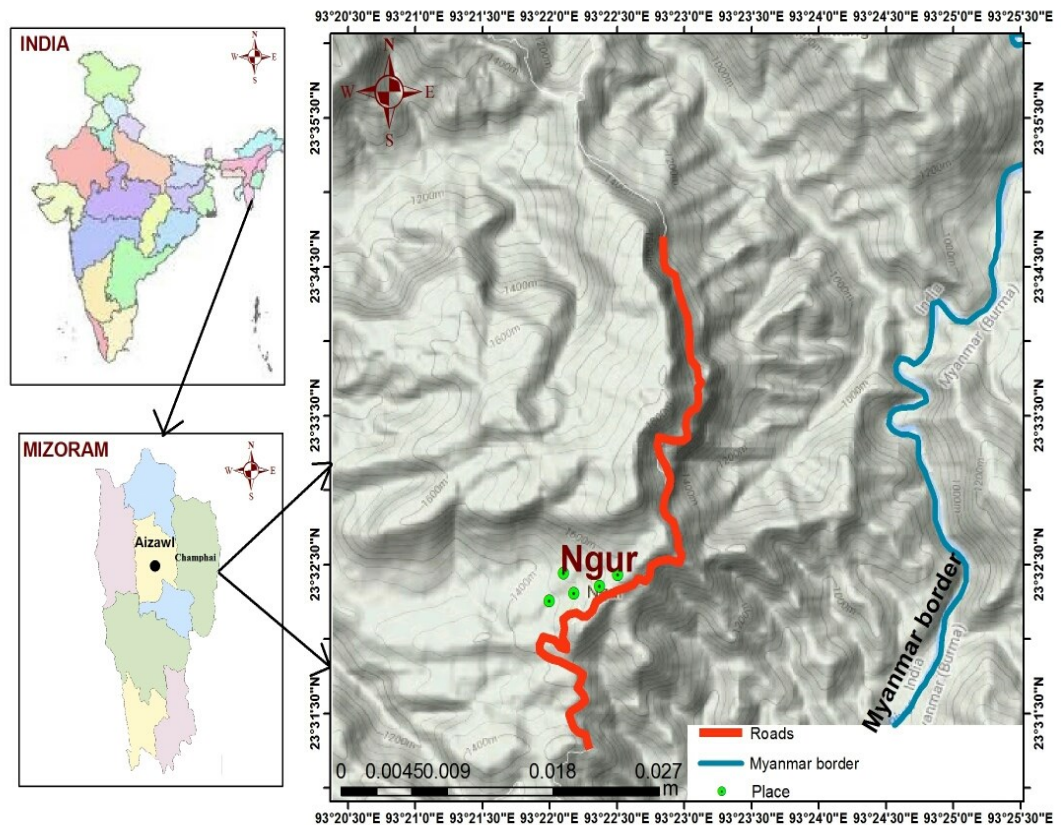


Fig 2.9: Location map of Ngur section



### 2.8.3.1 Litho-units of Ngur (NG) section

Ngur section exposes a 387m thick sedimentary succession which mainly composed of sandstones, shales and sandstone shale alternations. The previous sections show lithological characters that may indicate deeper and low energy environments due to the dominance of shales. However, this section shows a change in sedimentary facies which is represented by large percentage of sandstone exposures and sedimentary structures depicting higher velocity environment as compared with the previous sections. The sandstones show varying colors with brown sandstones dominating the bottom parts and massive bedded grey sandstones making up the upper part of the section. The sandstones show different sedimentary structures like heterolithic bedding, cross lamination and mud-clast which may be interpreted as a shallow marine environment of deposition. The shales are splintary and show spheroidal weathering structures with different shades grey color and are bioturbated.



**Fig. 2.10:** Panoramic view of Ngur section.

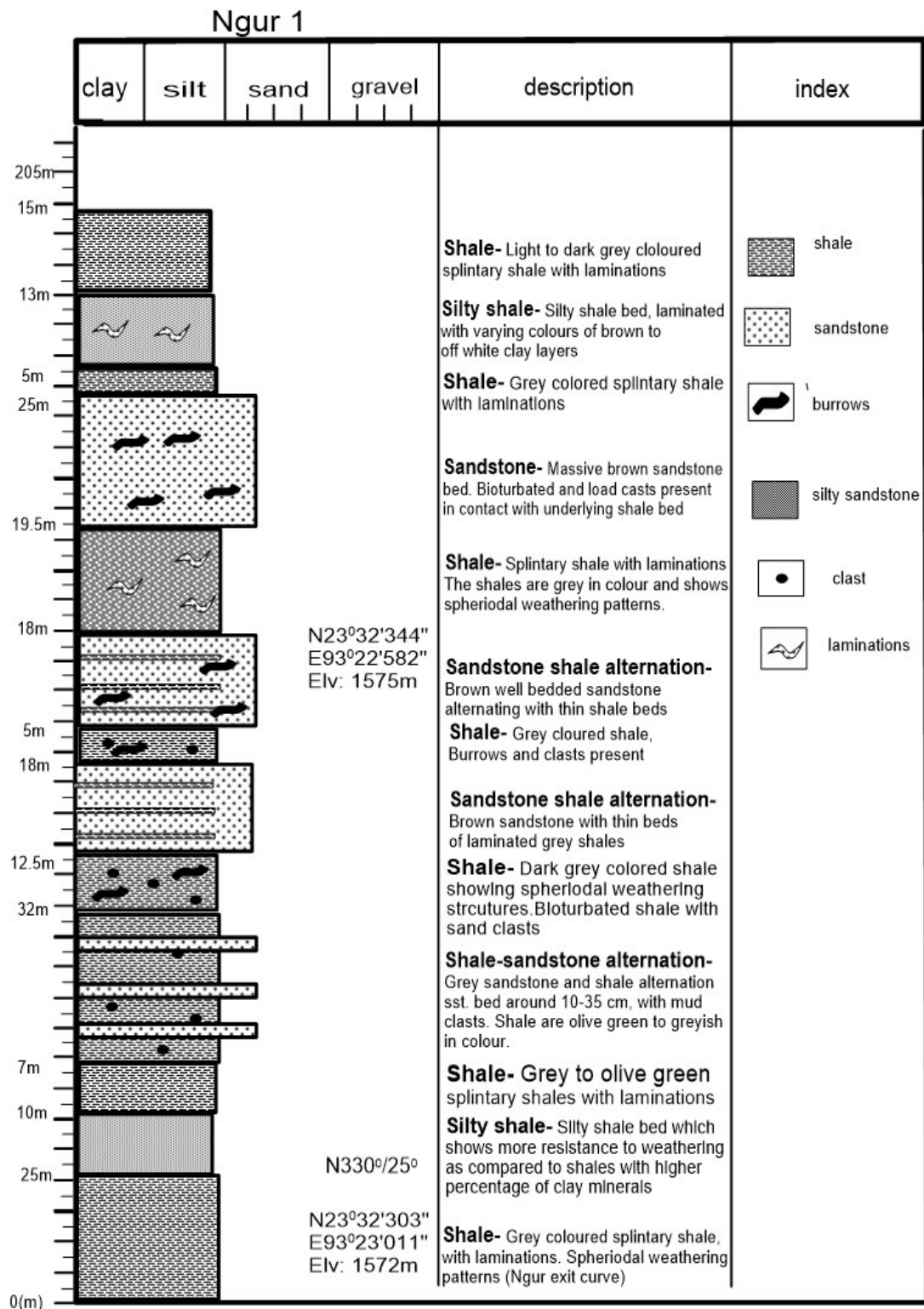


**Table.2.4 (a)** Litholog and description of Ngur section 1.



### Ngur 2

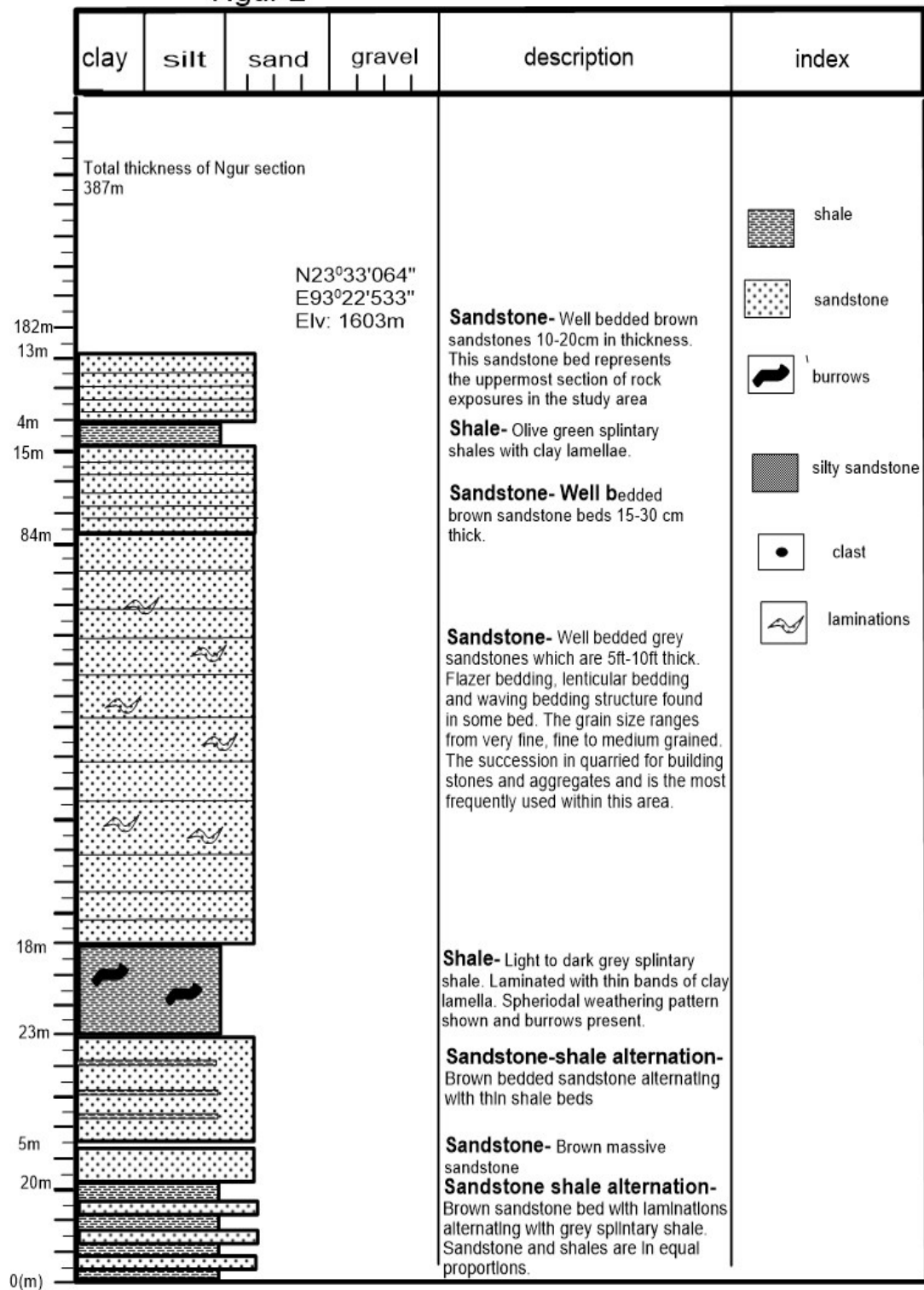


**Table.2.4 (b)** Litholog and description of Ngur section 2.

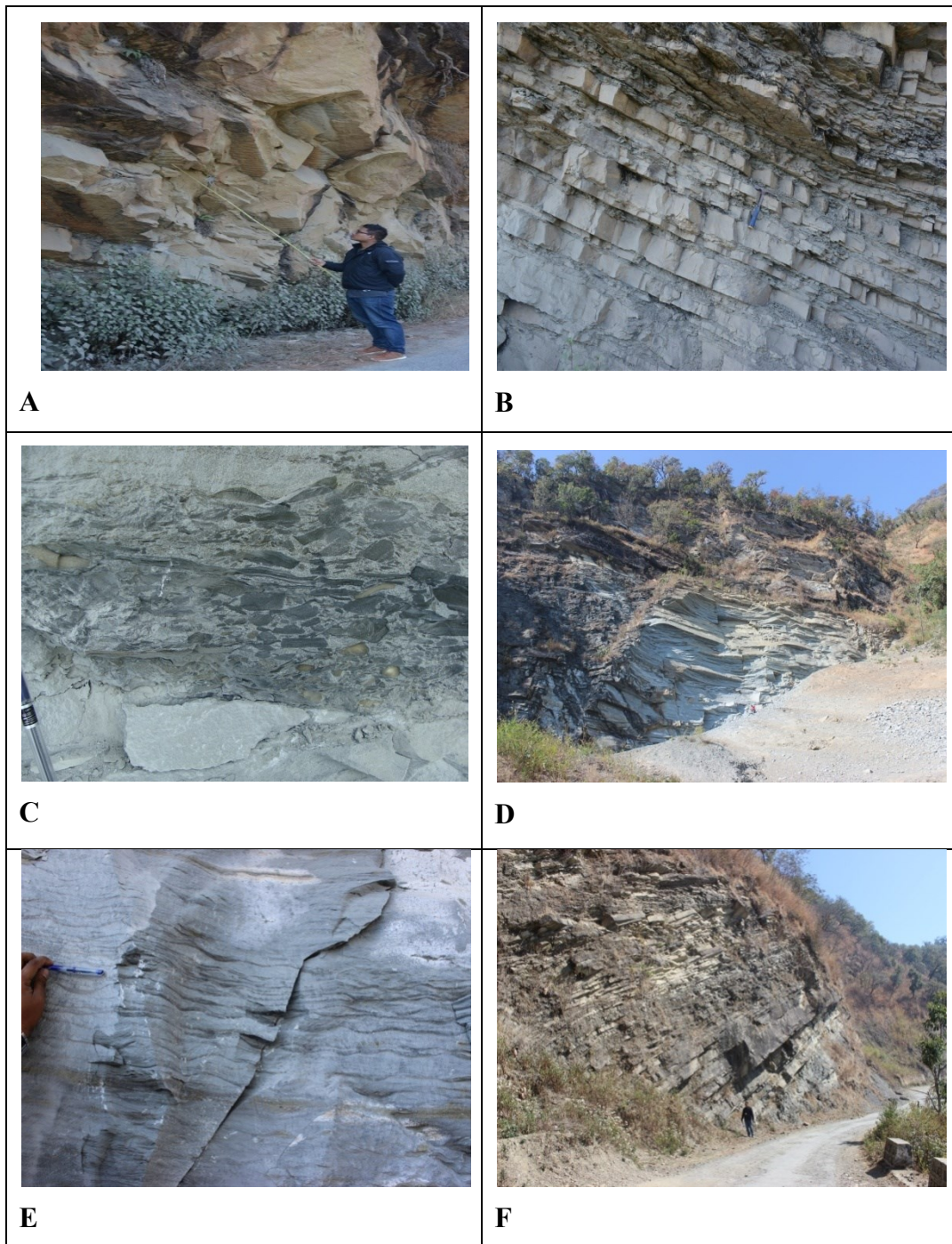


**Fig.2.11:** Field Photograph A) Bedded brown sandstones with ripple marks. B) Sandstone beds alternating with thin shale beds. C) Intra formational conglomerate. D) Ngur quarry. E) Heterolithic bedding in grey sandstones .F) Outcrop view of Ngur section.

## **CHAPTER III**

### **METHODOLOGY**

#### **3.1. INTRODUCTION**

Paleomagnetism is a branch of geology which deals with obtaining past magnetic fields recorded in rocks based on polarity reversals. The direction and magnitude of magnetization is controlled by the different types of magnetic minerals, their properties resulting in different degrees of susceptibility. In the early days, paleomagnetic studies have led to the rise of sea floor spreading (Vine and Matthews, 1963) combined with Hess's, (1962) and rejuvenation of continental drift and ultimately to the formation of plate tectonics theory (Opdyke and Channel, 1996). Because polarity reversals are potentially recorded simultaneously in rocks all over the world, magnetostratigraphic divisions unlike lithostratigraphy and biostratigraphy, are not time transgressive (Jacobs, 1994).

Origin of the Earth's magnetic field is not fully understood till date and our ability to give a plausible explanation is limited by mysteries that scientific knowledge is yet to clarify. All plausible theories involve generation of the geomagnetic field within the fluid outer core of the Earth by some form of magneto-hydrodynamic dynamo (Butler, 1998). Motion produced within the liquid outer core of the earth, which is composed of a mixture of iron and nickel, generate convection currents partially driven by the rotation of Earth creates magnetic field which covers the earth. This self sustaining dynamo produces magnetic field that closely resembles a big bar magnet in the centre of the earth at an angle of about  $11.5^\circ$  to its geographical axis. This angle between the spin axis and the earth's magnetic pole is

called declination (D). The declination is an angle from north measured eastward ranging from  $0^\circ$  to  $360^\circ$ . The inclination (I) is the angle made by the magnetic vector with the horizontal. By convention, it is positive if the north-seeking vector points below the horizontal or negative if it points above.

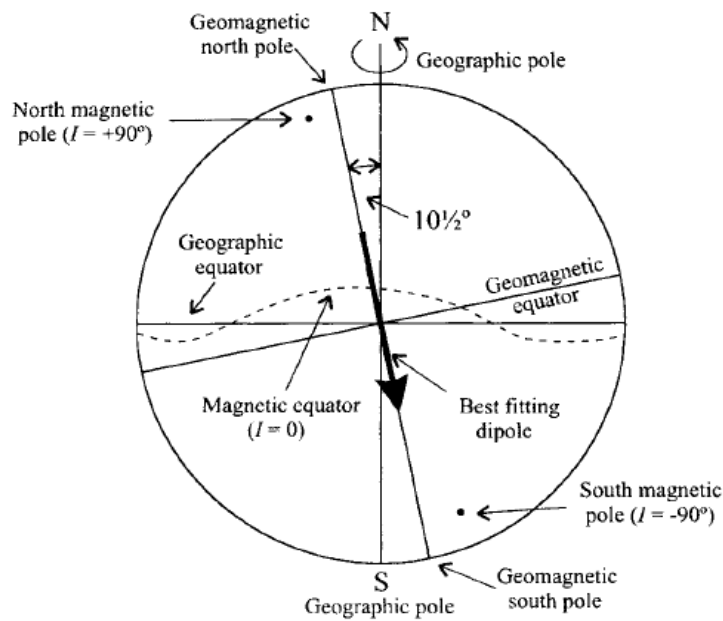


**Fig. 3.1.:** Graphical presentation of the magnetic, geomagnetic, and geographic poles and equators. (McElhinny and McFadden, 2000).

The dipole hypothesis proves that geomagnetic field can be modeled as a geocentric dipole makes it possible to determine the paleolatitude of a site from the mean paleomagnetic direction at any point on the Earth's surface and is of fundamental importance in paleomagnetic studies (Opdyke and Channel, 1996).

The Earth's magnetic field acts like a shield which covers the earth's surface protecting it from cosmic radiations. Rocks formed under the influence of this field may attain magnetization with its magnetic minerals aligning toward the direction of

prevailing polarity directions and magnitude. The degrees by which the minerals are magnetized depends on the susceptibility of each individual grains toward the magnetic field.

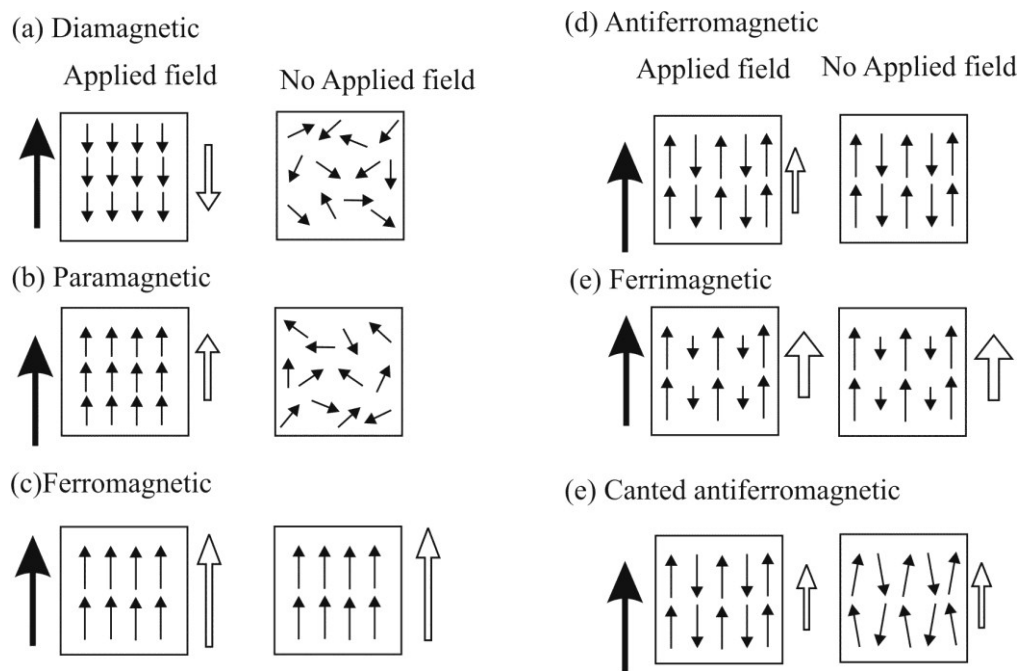


**Fig.3.2:** Magnetic material moments under applied and zero field. Hollow arrow in the right-hand side of the diagrams show the magnetization acquires when in an applied magnetic field (solid arrow).

Rocks owe their magnetic ability due the concentration of magnetic minerals which are mostly in various forms of iron oxide compounds. Magnetization that occurs during the formation of rocks is called the natural remanent magnetization (NRM) or fossil magnetism. Magnetization may be acquired through cooling from the Curie temperatures or due to chemical reactions taking place during crystallization. Other type of remanent magnetization may be induced to magnetic

minerals in its detrital form during deposition or after deposition prior to compaction in the case for sedimentary rocks. Primary magnetization can also be imparted within rocks due to lightning strikes and under induced field in laboratories. Remanance acquired due to long exposures to weak magnetic field is called viscous remanent magnetization (VRM) and Anhysteretic remanent magnetization (ARM) is the magnetization acquired by gradual reduction of strong alternating magnetic field under weak field. Also, due to different processes there can be a series of magnetization after induction of NRM, these are called secondary magnetization. The different types of remanent magnetization are shown in the table below.

| <b>Remanence</b>                                | <b>Acronym</b> | <b>Magnetization Process</b>   |
|---|----------------|--|
| <b>Thermoremanent Magnetization</b>             | <b>TRM</b>     | <b>Magnetization acquired during cooling from a temperature above the Curie Temperature in an external field</b> |
| <b>Chemical Remanent Magnetization</b>          | <b>CRM</b>     | <b>Magnetization acquired during chemical changes in an external field</b>                                       |
| <b>Viscous Remanent magnetization</b>           | <b>VRM</b>     | <b>Magnetization acquired over time in an external field</b>   |
| <b>Isothermal Remanent Magnetization</b>        | <b>IRM</b>     | <b>Magnetization acquired instantaneously in an external field</b>   |
| <b>Anhysteretic Remanent Magnetization</b>      | <b>ARM</b>     | <b>Magnetization acquired by the combined effects of a large alternating field and a small DC field</b>          |
| <b>Depositional Remanent Magnetization</b>      | <b>DRM</b>     | <b>Magnetization acquired by sediments when grains settle out of water in an external field</b>                  |
| <b>Post Depositional Remanent Magnetization</b> | <b>PDRM</b>    | <b>Magnetization acquired after depositions due to mechanical effects in wet sediment</b>                        |

**Table 3.1:** Types of Remanent Magnetization and their magnetization processes.



To study Paleomagnetism, it is very important to understand and identify the materials which are responsible for acquisition of magnetic field. It is essential to know the type of magnetic minerals, their formation and behavior so as to develop a better understanding of the types of environments they may exist. Magnetic iron compounds are the most important and most common type of magnetic mineral for paleomagnetic studies. The different types of magnetic minerals, their composition and magnetic state are given in the table below.

| Mineral         | Composition                                    | Magnetic state                           | $M_s(10^3 \text{ Am}^{-1})$ | Tc (°C)      |
|-----------------|--|--|-----------------------------|--------------|
| Magnetite       | $\text{Fe}_3\text{O}_4$                        | Ferrimagnetic                            | 480                         | 580          |
| Titanomagnetite | $\text{Fe}_{2.4}\text{Ti}_{0.6}\text{O}_4$     | Ferrimagnetic                            | 125                         | 150          |
| Ulvospinel      | $\text{Fe}_2\text{TiO}_4$                      | Antiferromagnetic                        |                             | -153         |
| Hematite        | $\alpha\text{Fe}_2\text{O}_3$                  | Canted antiferromagnetic                 | $\infty 2.5$                | 675          |
| Ilmenite        | $\text{FeTiO}_3$                               | Antiferromagnetic                        |                             | -233         |
| Maghemite       | $\gamma\text{Fe}_2\text{O}_3$                  | Ferrimagnetic                            | 380                         | 590-675      |
| Pyrrhotite      | $\text{Fe}_{1-x}\text{S}$ ( $0 < x \leq 1/8$ ) | Ferrimagnetic                            | $\infty 80$                 | 320          |
| Greigite        | $\text{Fe}_3\text{S}_4$                        | Ferrimagnetic                            | 125                         | $\infty 330$ |
| Goethite        | $\alpha\text{FeOOH}$                           | Ferrimagnetic with defect ferromagnetism | $\infty 2$                  | 120          |
| Iron            | Fe   | Ferromagnetic                            | 1715                        | 765          |
| Cobalt          | Co   | Ferromagnetic                            | 1422                        | 1131         |
| Nickel          | Ni   | Ferromagnetic                            | 484                         | 358          |

**Table 3.2:** Types of magnetic minerals their composition and magnetic properties responsible for magnetization (Collinson, 1983).

### **3.2 LITERATURE SURVEY**

Several materials like journal, publication (local and regional), and books in the field of paleomagnetism and Magnetostratigraphy recorded and collected by the Paleomagnetic laboratory, Department of Geology, Mizoram University were thoroughly turned. Besides the field of study, book and journals on other related disciplines including stratigraphy, paleontology and any previous works pertaining to geology in Mizoram area were collected from Central library, Mizoram University. The internet also served as a very important source of literature through which many books and research works were accessed, downloaded and printed for discourse. Literatures collected were marked, referenced and cross checked carefully for any dissimilarity in method and principles.

### **3.3 PRELIMINARY SURVEY**

Selection of the study area was the first step for initiation of the research work which was done using toposheets and Google earth images. Champhai district was selected and in particular the areas around Champhai town as it was known to expose Barial group of rocks. Selection was done based on the availability of roads and continuous rock exposures which is necessary of magnetostratigraphic studies.

### **3.4 FIELDWORK**

Field visits were carried out on several occasions for different purpose throughout the course of study. The first field work was conducted for the selection of sections in various parts of the study area. Three ideal sections namely, Ruantlang, Zote and Ngur were selected meeting the necessary requirements for magnetostratigraphic discourse.



### **3.4.1 Preparation of litholog**

After the selection of ideal sections detailed field investigation was carried out in the fields of sedimentology, lithology, stratigraphy and structural geology so as to carefully correlate and identify the facies relationship between the three sections.

1. The location and elevation of each study area was carefully taken using GPS device.
2. The attitudes of bed were carefully taken using different measuring equipments and applications like Brunton compass, Silva compass and Field Move Clino software, which are then crosschecked for any possible errors.
3. Each individual bed within the sections was carefully measured using bamboo scale and measuring tape and the thickness was recorded.
4. The beds were carefully examined for geological structures for interpretation and correlation.
5. Lithological variations based on rock type, color, textures and weathering patterns so as to differentiate the different changes in rock facies within the area.
6. All data collected in the field were recorded in a field note along with landmarks in the form of poles, waiting shed, houses, water point etc.
7. The field data was input into computer using surfer and corel draw software (version 5.5 ) which was used to prepare a detailed litholog and description of all the sections.

### 3.4.2 Collection of samples

For paleomagnetic studies rock samples are taken in alternating order from different spots within the section. A number of specimens may be produced from a single sample taken from a specific site. Specimens are prepared in such a way that they are cut into specific dimensions for measurement of paleomagnetic measurement. A typical specimen has volume  $\sim 10 \text{ cm}^3$ .

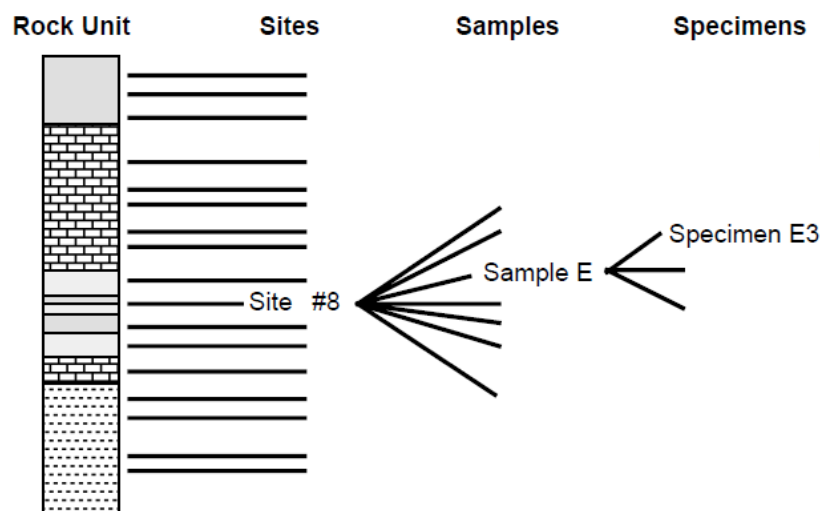


**Fig 3.3:** Generalized paleomagnetic sampling scheme. Multiple samples are collected from different sites and individually marked (Butler, 1998).

Sample cored with Portable Driller: - This is the sampling method employed for this particular research. The different steps are given below

1. Using a portable gasoline powered hand held driller with water pump; a cylinder is drilled into the outcrop to a depth not less than 6cm. While drilling, the drilling machine should be held as steady as possible so as to obtain straight samples and avoid curved samples. The cylinders should

be drilled at about 2.54cm in diameter and should not be taken out before measuring the orientation. A number of 4-6 drilling is done in a single site depending on the length of the rock sample obtained.

2. After drilling of cylinders the orientation of bedding is determined with the help of an orientation fixture so as to make tilt corrections for deformed beds. A geological compass is fixed on the Orienting Fixture in such a way that the letter S on the compass scale is oriented towards the slit for marking the drilled cylindrical specimens on the cylindrical part of the fixture.
3. The screw for controlling the dip level is loosened and the orienting fixture is inserted into the drilled cylindrical specimen. The orientation fixture is leveled in such a way that the bubble in the compass is right in the middle. After proper orientation is achieved the dip screw is tightened. Azimuth reading ( $0^{\circ}$  - $360^{\circ}$ ) and plunge/hade ( $0^{\circ}$  - $90^{\circ}$ ) measured from a scale in the fixture is taken which is recorded on a field note.
4. The orientation fixture posses a small slit parallel to the length of the cylinder. A line is drawn along the length of this slit to mark the top direction of the oriented samples. Usually a thin copper wire or pencil or water proof pen is used to prevent secondary magnetization.
5. Break the cylinder from the outcrop using the orientation fixture with caution so as to preserve the length of the sample. In case of strong samples hammers, screw drivers may be used. Remove the cylinder for marking.

6. After taking out the cylinders make sure it is dried up using a piece of cloth or paper so as to ensure that proper marking can be achieved. After excess moisture is removed, arrows (fiducial marks) are drawn on or parallel to the marking made with the copper wire and write the name and number of the specimen with pencil or marker. For example, sample taken from section RT site no.4, specimen c will be marked as RT4C.
7. Pack each specimen using paper or plastic bag and put samples from different sections in separate containers to avoid mixing up of samples.

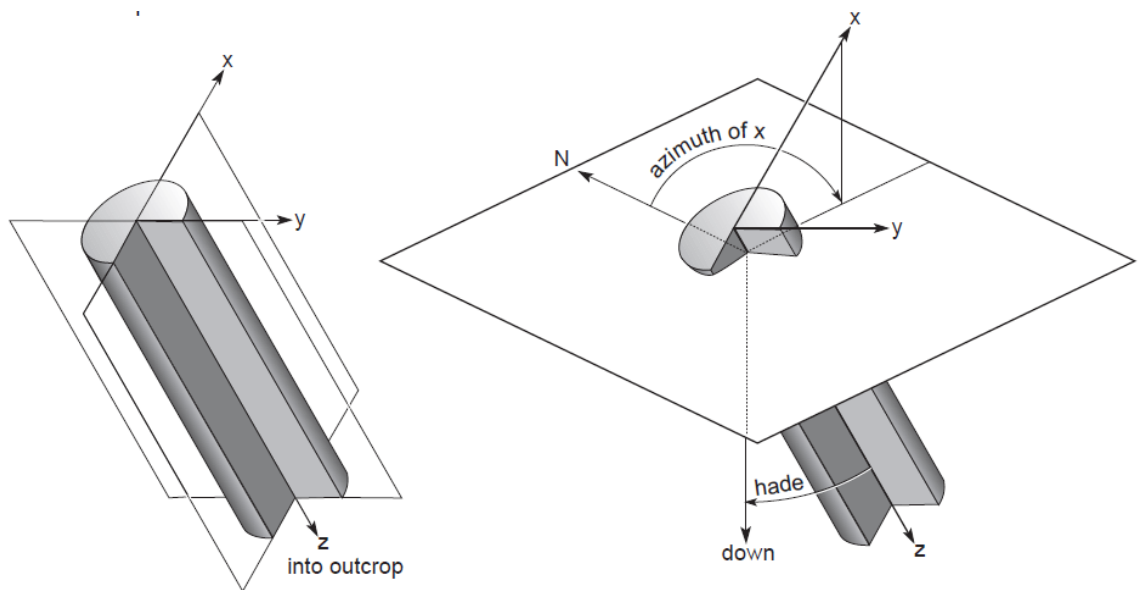


**Fig.3.4.** Orientation system for sample collected by portable core drill. Left is a schematic representation of core sample in situ. The z axis points into outcrop; the x axis is in the vertical plane; the y axis is horizontal. Diagram on the right shows orientation angles for core samples (Butler, 1998).

### **3.5 LABORATORY WORK**

Laboratory works consists of various steps including cutting the samples into desirable lengths which can fit perfectly in the equipments. This will be followed by demagnetization processes using thermal and alternating field, the step wise demagnetization will be measured and recorded into a computer attached to the spinner magnetometer. In this study laboratory induced magnetism is also involved for magnetic mineralogy studies which follow a separate approach mentioned in 4.6.

#### **3.5.1 Cutting and marking of samples**

Since the size shape and length of the samples must match the requirement of the laboratory equipments the samples are made ready for cutting in the laboratory. Cutting of samples is done with the help of a Dual-blade cutting machine with the lower portion of the blades immersed in water to ensure smooth cutting and prevent dust particles from scattering. Each cylinder is cut into 21 to 22 mm in height and fiducial marks are carefully drawn with the help of marker and pencil. The sample site and specimen numbers are also carefully marked in each specimen.

#### **3.5.2 Demagnetization**

This is one of the most crucial parts of this experiment as to find out the ChRM, which is the stable component of NRM contained within the samples. The secondary magnetic fields attained by the rocks must be removed; this may be regarded as a cleaning process. Cleaning is done with the help in two techniques namely; thermal and alternating field demagnetization. Pilot study was carried out for selected specimen from each site to have a better understanding of behavior and properties of magnetic minerals and their attained magnetism. At each step of

demagnetization the direction and intensity of magnetic field within the specimen is measured using the JR6 Dual Spinner Magnetometer (JR-6 model of Agico, Czech with a sensitivity of  $2 \times 10^{-6}$  A/m) in 4 directions.

### **3.5.2.1 Alternating field demagnetization**

Alternating field (AF) demagnetization is done using LDA-3A Alternating Field Demagnetizer of Agico, Czech, where samples are exposed under alternating field current generated magnetic field. Pilot study is carried out for 2 specimen from each site an treated at the interval of 10 mT, 20mT,30 mT, 40 mT, 50 mT, 60 mT, 70mT, and 80 mT. The remaining samples are treated at the interval of 20mt, 40mt, 60mt and 80mt. The AF demagnetization process is effective in removing secondary NRM and isolation of ChRM in rocks which comprises of ferrimagnetic minerals but may not be quite as effective for high coercivity minerals like Hematite (Butler, 1992).

### **3.5.2.2 Thermal Demagnetization**

Thermal demagnetization (TD) is done using MMTD-80 model of Magnetic Measurements, UK Thermal Demagnetizer. Two methods are followed, one called continuous thermal demagnetization involves monitoring the change in remanance of a sample as it is heated (Wilson, 1962). The other method, called progressive thermal demagnetization, consists of a number of partial demagnetization steps using successively higher temperatures which is much faster than the continuous method (Thellier, 1938). Pilot study was carried out for 1 specimen from each site at intervals of 50°C and 100°C up to 600°C (100, 200, 300, 350, 400, 450, 500, 530, 560 and 600). The remaining samples were treated at longer intervals after the behavior and

magnetic patterns of the samples was observed. Thermal demagnetization process is useful for finding out the minerals responsible attained magnetism within rocks by sudden drop of magnetization while reaching the Curie point (Butler, 1992: Mc Elhinny and Mc Faden, 2000)

### **3.6. GRAPHICAL REPRESENTATIONS AND CALCULATIONS**

With each step of demagnetization, paleomagnetic measurement was carried out using Digital spinner magnetometer (Dual Spin Spinner magnetometer (JR-6) model of Agico, Czech with a sensitivity of  $2 \times 10^{-6}$  A/m.) The direction and intensity of the samples was measured in four directions where the resultant mean direction was taken using the remasoft 3.0 software (Paleomagnetic data browser and analyzer, Agico). Data is recorded and displayed in different forms of graphical representations.

During the stepwise demagnetization the intensity and direction of field at each step changes. Stereonet is used for displaying the change in direction of NRM of the samples at each stage of demagnetization. The intensity decay curves show the change in intensity of magnetic field from the progressive demagnetization. The Zijderveld diagrams are a graphical representation of both the direction and intensity of magnetic field and are presented in the form of a Cartesian plot where vector components are projected over two orthogonal planes (Zijderveld, 1967). The NRM vector of each component during the step wise cleaning process is measured in four directions; north (N), east (E), and 2 vertical (Down, Z) components. These measurement of remnant vectors may be somewhat scattered in trajectories, as a result the Principal Component Analysis (PCA) is used in determining the direction

of best fit line among the scattered trajectories, whose precision is estimated by the Maximum Angular Deviation (MAD).

British statistician R.A Fisher, (1953) came up with a probability density function which applies to paleomagnetic directions called the Fisher distribution. Each direction is given unit weight and is represented by a point on a sphere of unit radius.

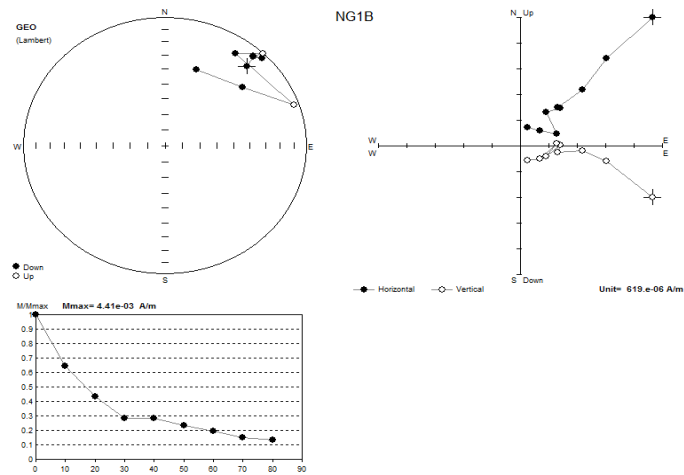


**Fig: 3.5:** Demagnetization plots shown using Stereonet, Zijdeveld diagram (Zijderveld 1967) and intensity decay curves for a specimen.

Calculation of mean is done with the help of software called CEMP PMag Tools version 3.3 developed by Mark W. Hounslow, (1997-2003). The mean is taken from the series of data collected from alternating field and thermal demagnetization. The Inclination mean ( $I_m$ ) and declination mean ( $D_m$ ) along with  $\alpha_{95}$  which is the confidence limit measured with precision for estimating the true mean direction. Tilt correction is done with using this software to ensure true bedding directions of and the above parameters will be used for the generation of the Virtual geomagnetic pole

Virtual geomagnetic pole (VGP) is any pole position that measures the



geomagnetic field from a point of observation. This is the position of the pole of a geocentric dipole that can account for the observed magnetic field direction at one location and at one point in time.

Variation in VGP in the section is expressed as VGP latitude which represents the latitude of individual VGP in the coordinates of the overall paleomagnetic pole. VGP latitude close to  $+90^{\circ}$  is considered as normal polarity, and VGP latitudes close to  $-90^{\circ}$  represents reverse polarity. The polarity representation of usually presented as black (normal) and white (reversal) bar diagrams (Opdyke and Channel, 1996).

### **3.7 GEOMAGNETIC POLARITY TIME SCALE (GPTS) AND SEDIMENT ACCUMULATION RATE (SAR)**

The Geomagnetic Polarity Time scale (GPTS) is not an important asset in the field of geochronology especially in areas devoid of age diagnostic features. Magnetic polarity stratigraphy on land and in deep sea cores provides the link between the GPTS and biozonations/bioevents and hence geologic stage boundaries (Opdyke and Channel, 1996).

With the generation of polarity zones from the VGP latitudes a series of normal and reverse polarity zones occur which may be correlated with different segment of GPTS. GPTS correlation is aided by other dating methods like radiometric and biostratigraphy (planktonic foraminifera, nanno-fossils) to ensure clinical matching. Correlations made between Magnetic polarity reversal sequences and fossil assemblages with resulting in establishment of GPTS chrons for stronger results. From the duration of events (normal and reversal) within the paleomagnetic

data, the ratio of thickness of the section and the time interval of the polarity zones may give the rate at which sediment is accumulated during the time of deposition or lava flow in case of igneous rocks. Sediment Accumulation Rate (SAR) is estimated from GPTS of Cande and Kent, (1995) records in correlation with the Magnetic Polarity Time Scale (MPTS) obtained from the study area. It was initially believed that SAR is more or less constant but there can be many changes due to tectonics within the depositional basin so cautious approach and investigation is required.

### **3.8 SAMPLING AND LABORATORY TECHNIQUES OF ROCK MAGNETISM**

Cylindrical samples were taken from various outcrops with an interval selected in accordance with the change in rock facies. The samples were reduced to a size of 21-22mm in height which is similar to the samples for magnetostratigraphy following similar procedures. The samples were dried up to remove moisture contained within the rock due to its porosity. The dried samples were then weighted in the laboratory by using an electronic balance; the weight of each sample is recorded.

Bartington MS2B magnetic susceptibility meter (sensitivity  $2 \times 10^{-6}$  SI) is used for measurement of magnetic susceptibility. The samples were measured in six orthogonal directions under low frequency field (Lf) and high frequency field (Hf) (Singer and Fine, 1989; Evans and Heller, 2001). The susceptibility of magnetic minerals is different based on the composition (e.g. ferrimagnetic, antiferromagnetic, paramagnetic, and diamagnetic), concentration and granulometry {e.g. Superparamagnetic (SP), single domain (SD), and Multidomain (MD)} of the magnetic minerals (Verosub and Robert, 1995; Han and Jiang, 1999; Oreilly, 1984).

The difference in susceptibility between the low and high frequency is called frequency dependence of susceptibility ( $\chi_{fd}$ ). Under an applied field of 0.465 kHz and 4.65 kHz susceptibility is measured under various frequencies. This helps to distinguish quantifying certain grain sizes, taking advantage of the phenomenon of magnetic viscosity (Stacey and Banerjee, 1974; Oreilly, 1984). Thus, SP particle can be estimated simply by changing the frequency of the applied field (See, Thompson and Oldfield, 1986; Dearing *et al.*, 1996; Dekkers, 1997).

$$\chi_{fd} \% = \left( \frac{\chi_{lf} - \chi_{hf}}{\chi_{lf}} \right) \times 100$$

Where,  $\chi_{lf}$  is the susceptibility at low frequency (0.465 kHz) of applied field and  $\chi_{hf}$  is the high frequency (4.65 kHz) susceptibility.

Using the alternating field demagnetizer Anhyseric Remanent Magnetization (ARM) was imparted on the sample under 80 mT and was measured using JR6 dual spinner magnetometer. Isothermal Remanent Magnetization (IRM) is carried out using ASC Scientific Impulse Magnetizer (IM-10-30) in forward and backward positions. Stepwise magnetization was carried out accordingly at 10/50/100mT intervals up to 1000 mT. Forward field was imparted in the following steps 50,100, 200, 300, 400, 500, 600, 700, 800, 900, 1000 and back field in the order -10, -20, -30, -40, -50, -100, -150, -200, -250, -300 until the sample reaches it saturation point where it can no longer acquire magnetization (Robertson and France, 1994; Kruiver *et al.*, 2001). This field limit is referred as Saturation Isothermal Remanance Magnetization (SIRM) and varies with the composition and concentration of the magnetic minerals (Dekkers, 1989).

Data generated is plotted on excel spread sheet and used for calculation of various parameters that will provide information regarding the type of magnetic minerals, their relative grain size etc. Saturation Isothermal Remanent Magnetization (SIRM) is strongly affected by grain size variations but is not affected by the diamagnetic and paramagnetic minerals, as they do not carry remanence (Lepland and Stevens, 1996). The ratio of saturation remanence to susceptibility ( $SIRM/\chi_{if}$ ) can be used as a rough estimate of magnetic grain sizes of ferrimagnetic and antiferromagnetic minerals (Sangode *et al.*, 2007) and also used as an indicator of Greigite in the samples. S-ratio provides a measure of the relative proportions of higher coercivity/hard (Haematite, Goethite) to lower coercivity and magnetically soft (Magnetite, Greigite) magnetic minerals (Thompson and Oldfield, 1986; King and Channel, 1991; Verosub and Roberts, 1995). HIRM is used to indicate the presence of magnetically hard minerals like Haematite and Goethite (Walden *et al.*, 1999). Coercivity of remanence  $B_{(0)CR}$  is a simple and straightforward parameter which used to determine magnetic mineralogy and grain size to characterize magnetic mixtures (Thompson and Oldfield, 1986).  $IRM_{soft}$  also known as low field acquisition of IRM is the parameter derived from 20 mT back field of IRM.  $\chi_{ARM}/SIRM$  ratio is used to determine the size of magnetic grains, if the ratio of high the magnetic grains will be finer and vice versa. Summary of the rock magnetic parameters and derivatives are given in the Table 3.3.

|   |   |
|---|---|
| Low and high-high susceptibility $\chi_{lf}$ and $\chi_{hf}$                                    | Proportional to the concentration of magnetic minerals  |
| Frequency dependent susceptibility $\chi_{fd}$ (%)  | ~10% or 5-10% would indicate a large fine viscous (magnetite) component of SP range.  |
| Anhysteretic remanent magnetization (ARM) $\chi_{ARM}$  | Proportional to the concentration of magnetic minerals of stable single domain size range.  |
| Isothermal remanent magnetization (IRM) and Saturation Isothermal remanent magnetization (SIRM) | Proportional to the concentration of magnetic minerals and also biased towards coarser magnetic grain size.   |
| Hard Isothermal Remanent Magnetization HIRM (SIRM-IRM300mT)                                     | Proportional to the concentration of magnetically hard minerals like Haematite and Geothite.  |
| $\chi_{ARM}/\chi_{lf}$  | Indicative of magnetic grain size of ferrimagnetic minerals.  |
| SIRM/ $\chi$  | Useful to distinguish between different types of magnetic behaviors. For example, if both $\chi$ and SIRM are low, but SIRM/ $\chi$ is relatively high, there may be a large amount of haematite. If $\chi$ is positive but there is little or no remanence, then the magnetic minerals in the sample will probably be mostly paramagnetic. |
| SIRM/ $\chi$ , ARM/ $\chi$ and ARM/SIRM   | SIRM/ $\chi$ , ARM/ $\chi$ and ARM/SIRM values denote significant SSD (magnetite) grains.   |
| ARM/SIRM  | Low ARM/SIRM values indicate a large MD (magnetite)   |
| S-ratio (IRM 300mT/SIRM)  | Relative proportions of ferrimagnetic and anti-ferromagnetic minerals (high ratio equals high proportion of magnetite)  |

**Table 3.3:** Summary of the rock magnetic parameters after Thompson and Oldfield, 1986; Maher, 1988; Oldfield, 1991.

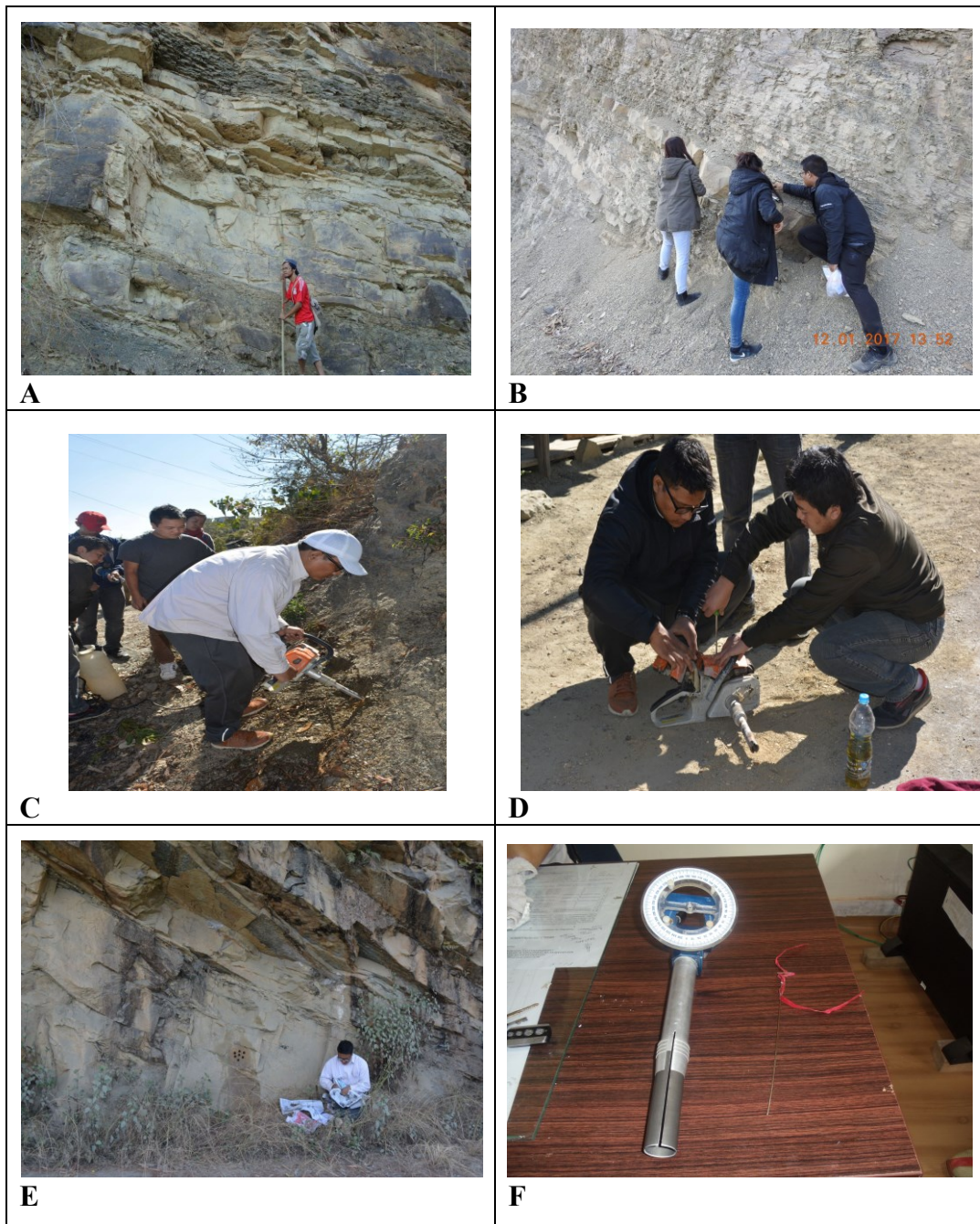


**Fig.3.6. (a)** Field photographs: A) Measuring thickness of beds using bamboo scale. B) Measuring attitude and recording sedimentary structures. C) Drilling with portable handheld driller connected with water pump. D) Refueling driller. E) Cleaning, marking and packing of samples. F) Orientation fixture.



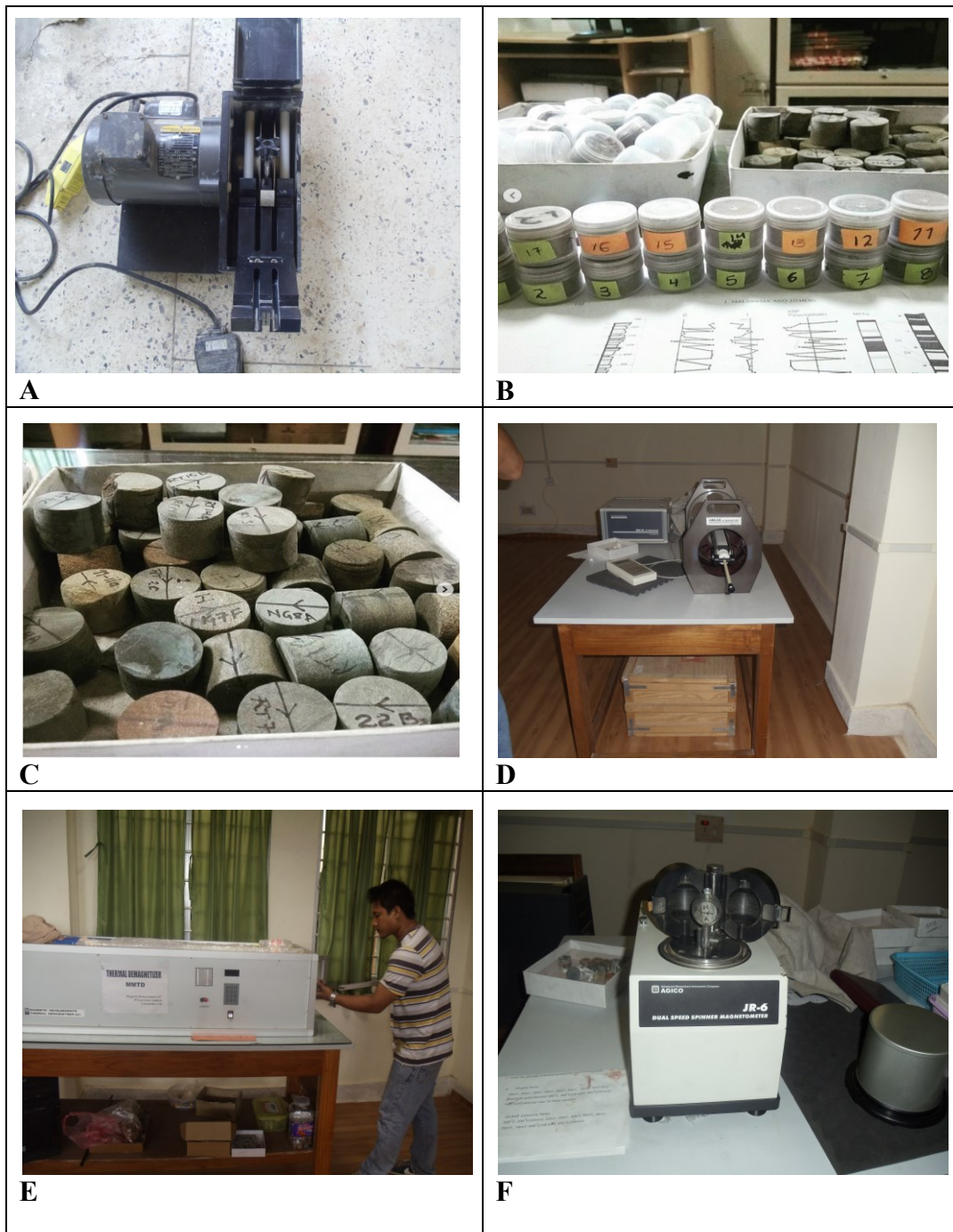


**Fig.3.6. (b)** Laboratory photographs: A) Dual-blade cutter. B) Marked samples for magnetostratigraphy and magnetic minerals study. C) Samples for demagnetization process. D) Alternating field demagnetizer (AFD). E) Thermal demagnetizer F) JR6 dual spinner magnetometer.



**Fig.3.6. (c)** Laboratory photographs: A) Bartington MS2 Magnetic susceptibility meter. B) ASC Scientific Impulse magnetizer. C) Electronic Digital balance. D) Paleomagnetic laboratory, Dept of Geology, MZU E) Panoramic view of laboratory.



## CHAPTER IV

### RESULTS

#### 4.1 MAGNETIC MINERALOGY

To develop a better understanding regarding the influence of magnetic minerals in rocks, the nature of the magnetic materials has to be worked out in terms of several parameters including mineralogy, grain size and concentration. Investigation of magnetic minerals will help to establish authentic magnetostratigraphic correlation. The sections are analyzed based on the change in lithofacies within the sections. The study area is divided into two sections for this study viz. Ruantlang section and Zote-Ngur section. Representative samples were collected from selected sites within the sections. A total of 52 samples were analyzed with 28 representative samples from Ruantlang and 24 samples from Zote-Ngur section.

##### 4.1.1 Ruantlang Section

The section is divided into 6 zones based on the behavior of magnetic parameters. Unit I shows a decreasing trend of SIRM and  $\chi_{ARM}$  which suggest decrease in the concentration of magnetic minerals and the presence of paramagnetic minerals. The S-ratio increases as a result of soft magnetic minerals like magnetite. The  $\chi_{ARM}/SIRM$  ratio increases as due to larger percentage of fine grained SD grains. Unit II show a stable linear trend and increases toward the top with corresponds with the S-ratio due to increase in the concentration of fine grained SD magnetic minerals. Unit III shows similar trends of dormancy in almost all the parameters with increase in the coercivity. This may be a result of dominant shale

beds within the zone thus depicting reducing environment. Unit IV shows varying trends of magnetic parameters. The SIRM value increases rapidly and then decreases following a linear stable pattern toward the end with an overall high  $\chi_{ARM}$  value which may reflect increase in magnetic minerals concentration of SD ferrimagnetic grains. Unit V shows a period of quiescence with linear trends. The SIRM value decreases slightly to the top which may indicate decrease in concentration and increasing coercivity shown by BoCR increasing trend. Unit VI is characterized by increasing soft magnetic minerals concentration and MD grains shown by  $\chi_{ARM}/SIRM$  ratio and decreasing ARM values.

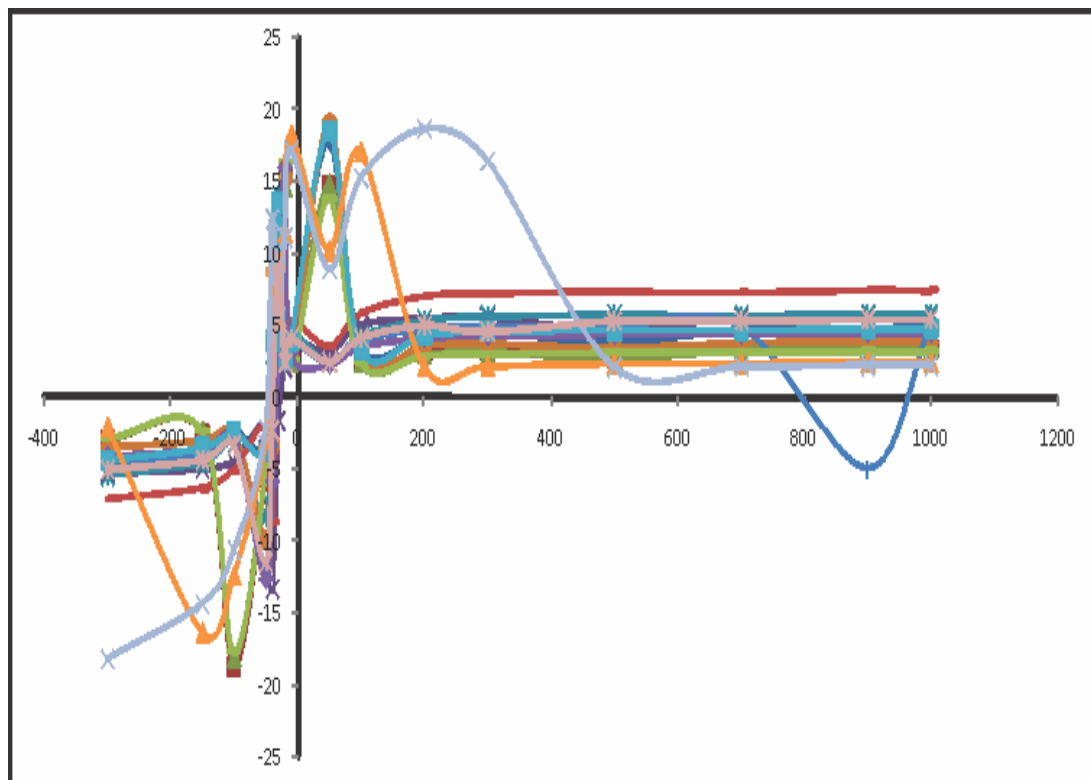


**Fig. 4.1:** The Isothermal Remanent Magnetization curves for representative samples of varied lithology within Ruantlang section.

| SAMPLE NAME | Elv (meter) | $\chi_{ARM}$ | SIRM/ $\chi_{lf}$ | $\chi_{ARM}/\chi_{lf}$ | $\chi_{ARM}/SIRM$ | Soft IRM | HIRM   |
|-------------|-------------|--------------|-------------------|------------------------|-------------------|----------|--------|
| 1A          | 633         | 1.601        | 0.510             | 3.620                  | 7.101             | 0.061    | 0.127  |
| 1B          | 626         | 3.022        | 0.471             | 6.823                  | 14.496            | 0.049    | 0.103  |
| 2A          | 582         | 3.454        | 0.266             | 7.977                  | 29.961            | -0.216   | 0.065  |
| 2B          | 575         | 2.545        | 0.344             | 6.062                  | 17.632            | -0.256   | 0.081  |
| 3A          | 567         | 2.251        | 0.334             | 4.763                  | 14.266            | -0.269   | 0.088  |
| 3B          | 540         | 5.326        | 0.582             | 23.625                 | 40.603            | -0.243   | 0.070  |
| 4A          | 405         | 0.424        | 4.488             | 9.397                  | 2.094             | 0.065    | 0.107  |
| 4B          | 400         | 8.543        | 3.513             | 128.141                | 36.479            | 0.073    | 0.123  |
| 5A          | 383         | 0.196        | 0.634             | 0.535                  | 0.843             | 0.062    | 0.122  |
| 5B          | 379         | 0.850        | 3.136             | 13.153                 | 4.195             | 0.051    | 0.107  |
| 6A          | 364         | 2.970        | 0.445             | 7.715                  | 17.338            | -0.244   | 0.091  |
| 6B          | 350         | 7.502        | 0.389             | 19.261                 | 49.472            | -0.223   | 0.083  |
| 7A          | 324         | 4.791        | 0.503             | 13.314                 | 26.493            | 0.050    | 0.096  |
| 7B          | 320         | 3.070        | 0.430             | 8.702                  | 20.237            | 0.039    | 0.081  |
| 8A          | 294         | 1.934        | 0.748             | 5.007                  | 6.697             | 0.089    | 0.151  |
| 8B          | 292         | 1.420        | 0.712             | 3.740                  | 5.249             | 0.081    | 0.142  |
| 9A          | 270         | -2.830       | 0.323             | -7.932                 | -24.574           | -0.237   | 0.064  |
| 9B          | 265         | 3.687        | 0.351             | 10.335                 | 29.483            | -0.249   | 0.069  |
| 10A         | 176         | 0.524        | 0.452             | 1.429                  | 3.162             | -0.213   | 0.090  |
| 10B         | 160         | 1.448        | 0.550             | 3.950                  | 7.179             | -0.187   | 0.109  |
| 11A         | 136         | 5.515        | 0.479             | 14.152                 | 29.533            | 0.044    | 0.100  |
| 11B         | 136         | 6.158        | 0.498             | 14.812                 | 29.745            | 0.051    | 0.113  |
| 12A         | 118         | 5.520        | 0.244             | 14.716                 | 60.426            | -0.171   | 0.053  |
| 12B         | 95          | 4.156        | 0.239             | 11.039                 | 46.134            | -0.183   | 0.051  |
| 13A         | 50          | -3.074       | 0.220             | -8.291                 | -37.631           | -0.166   | -0.258 |
| 13B         | 46          | 4.622        | 0.211             | 12.449                 | 58.926            | -0.165   | -0.247 |
| 14A         | 34          | 7.782        | 0.547             | 20.324                 | 37.154            | 0.059    | 0.113  |
| 14B         | 25          | 4.964        | 0.553             | 12.694                 | 22.967            | 0.059    | 0.116  |

**Table 4.1:** The average detrital components and various parameters calculated for Ruantlang Section: Units: BOCR = mT,  $\chi_{ARM} = 10^{-8} \text{ m}^3 \text{ kg}^{-1}$ , SIRM =  $10^{-5} \text{ Am}^3 \text{ kg}^{-1}$ , SIRM/ $\chi_{lf} = 10^3 \text{ Am}$  and Soft-IRM =  $10^{-2} \text{ A/m}^2$ .

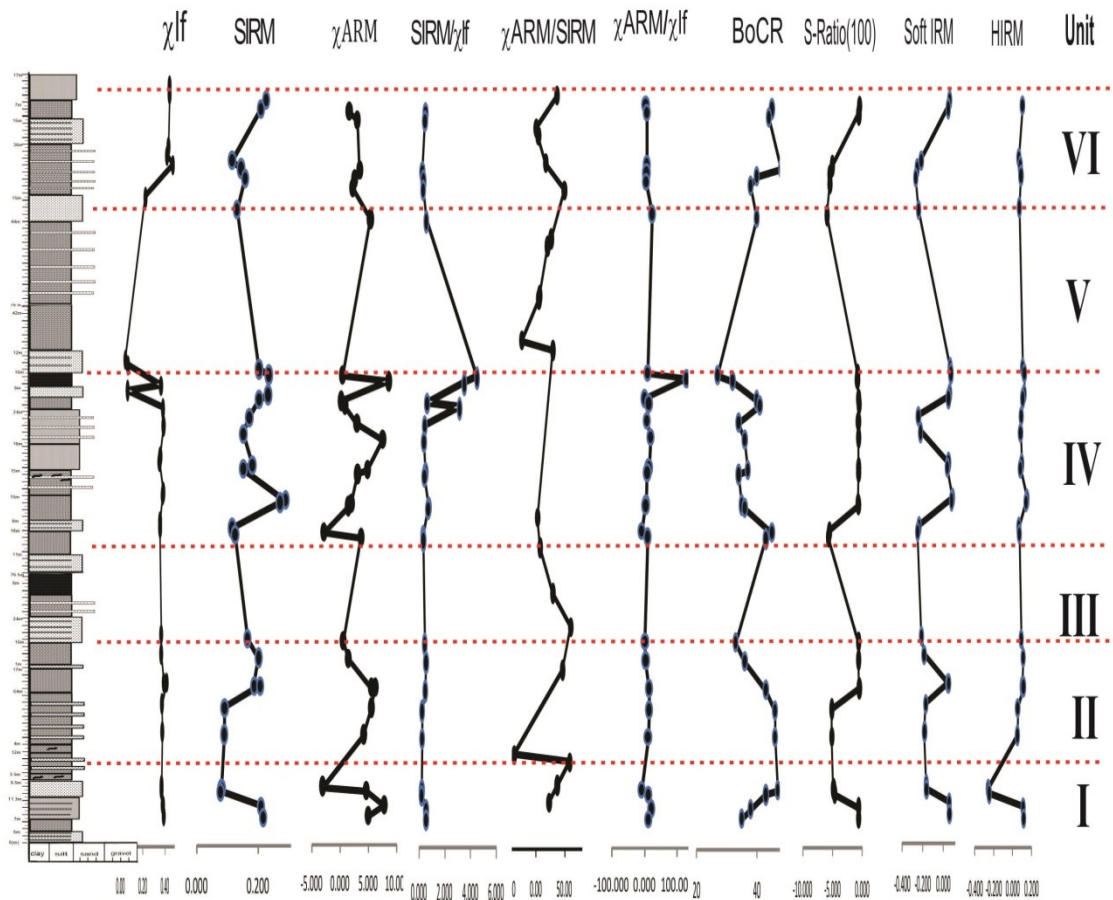


**Fig. 4.2:** Temporal distribution of the representative mineral magnetic parameters for Ruantlang section.

#### 4.1.2 Zote-Ngur Section

Zote-Ngur section represents the upper part of the study area with a noticeable change in lithology from argillaceous to sand dominated facies and is divided into VIII zones. Unit I shows a sequence of coarsening upward environment from shale, siltstone to massive brown sandstones. The  $\chi_{ARM}/SIRM$  ratio, SIRM and  $\chi_{lf}$  all show increasing trend which suggest increasing concentration of SSD-SD grains. The S-ratio decreases toward the top which may be due to increase coercivity of magnetic minerals. In Unit II the concentration of magnetic minerals decreases

slightly and then follows an increasing trend from  $\chi_{lf}$  and SIRM values. The lower part of the zone may have larger concentration of MD grains and from S-ratio and BoCR the concentration of hard magnetic minerals increases and decreases rapidly at the topmost portion of the zone. Unit III shows a linear upright S-ratio pattern which may indicate a stable environment with ferrimagnetic and anti-ferromagnetic minerals. The magnetic mineral grain size is constant throughout the zone with slight decrease in concentration from decreasing SIRM value. Unit IV is a zone which is dominated by sandstones alternating with thin shale beds. The  $\chi_{ARM}$ , SIRM and  $\chi_{lf}$  patterns and high values of  $\chi_{ARM}/SIRM$  and  $\chi_{ARM}/\chi_{lf}$  ratio all show increase in the concentration of fine grained SD ferrimagnetic minerals. Decrease in S-ratio and increase in HIRM indicates high percentage of hard magnetic minerals possibly hematite which shows a rapid decline from mid point to top. Unit V shows decrease in the concentration of magnetic minerals and increase in MD-PSD grains. The percentage of hard magnetic follows the same pattern as that of Unit IV and may depict a shallower oxidizing depositional environment. Unit VI show similar trend with the underlying Unit IV and Unit V and show fluctuating values of magnetic parameters which may indicate a periodic change in shallow depositional environment conditions. Unit VII shows moderate concentration of mixed SD-MD grains toward the upper levels by linear SIRM and  $\chi_{lf}$  patterns. At the upper level the concentration of magnetic minerals decreases rapidly with SIRM/  $\chi_{lf}$  ratio indicating the presence of MD magnetite grains. The HIRM value increases and then decrease toward the higher zone which may be a result of fluctuating depositional environment. Increase in S-ratio at the upper part of the section indicates a change in the depositional environment which increases the number of soft magnetic minerals.

Unit VIII consists of the topmost part of the section, the low values of  $\chi_{ARM}$  and  $\chi_{ARM}/\chi_{lf}$  which may be due to the increase in coarse grained MD ferrimagnetic minerals. But the concentration of magnetic minerals gradually increases toward the upper portion maintaining a stable pattern influenced by the presence of fine SD magnetite grains.

| Sr No. | Sample name | Elv. (mtr.) | XARM   | SIRM/ $\chi_{lf}$ | XARM/XLF | Xarm/SIRM | SOFT IRM | HIRM  |
|--------|-------------|-------------|--------|-------------------|----------|-----------|----------|-------|
| 1      | ZT2F1       | 26          | -0.055 | 0.303             | -0.077   | -0.255    | 0.001    | 0.007 |
| 2      | ZT3Di       | 28          | -0.036 | 0.440             | -0.039   | -0.088    | 0.004    | 0.006 |
| 3      | ZT4F        | 33          | 0.034  | 0.754             | 0.036    | 0.048     | 0.007    | 0.030 |
| 4      | ZT4.5Ei     | 42          | 0.106  | 0.873             | 0.123    | 0.141     | 0.006    | 0.237 |
| 5      | ZT5Gi       | 48          | 0.000  | 1.220             | 0.000    | 0.000     | -0.004   | 0.228 |
| 6      | ZT6Aii      | 56          | 0.047  | 0.880             | 0.067    | 0.076     | 0.000    | 0.266 |
| 7      | ZT7F        | 65          | 0.026  | 0.407             | 0.020    | 0.048     | 0.004    | 0.010 |
| 8      | ZT8i        | 70          | 0.001  | 0.573             | 0.001    | 0.002     | 0.005    | 0.007 |
| 9      | ZT9A        | 78          | 0.006  | 0.238             | 0.006    | 0.025     | 0.003    | 0.006 |
| 10     | ZT9.5Dii    | 92          | 0.001  | 0.434             | 0.001    | 0.002     | 0.003    | 0.007 |
| 11     | ZT10Aii     | 103         | 0.179  | 0.533             | 0.179    | 0.337     | 0.008    | 0.201 |
| 12     | ZT11Dii     | 113         | -0.055 | 1.186             | -0.086   | -0.073    | 0.005    | 0.008 |
| 13     | ZT13Cii     | 135         | -0.044 | 0.612             | -0.053   | -0.087    | -0.003   | 0.198 |
| 14     | ZT13.5Aii   | 150         | 0.069  | 0.535             | 0.099    | 0.184     | 0.004    | 0.142 |
| 15     | ZT14Aii     | 158         | 0.055  | 1.085             | 0.103    | 0.095     | 0.010    | 0.226 |
| 16     | ZT15G       | 170         | 0.033  | 1.913             | 0.070    | 0.037     | 0.008    | 0.081 |
| 17     | ZN1Fi       | 182         | 0.032  | 0.691             | 0.032    | 0.046     | 0.011    | 0.269 |
| 18     | ZN2Fii      | 198         | 0.004  | 0.509             | 0.003    | 0.006     | 0.005    | 0.301 |
| 19     | ZN3Gi       | 207         | 0.096  | 0.286             | 0.114    | 0.399     | 0.000    | 0.021 |
| 20     | ZN4Di       | 211         | 0.045  | 0.266             | 0.029    | 0.109     | 0.006    | 0.160 |
| 21     | ZN5Cii      | 217         | 0.004  | 0.504             | 0.004    | 0.007     | 0.000    | 0.041 |
| 22     | ZN6Fi       | 222         | -0.146 | 0.754             | -0.222   | -0.294    | 0.008    | 0.140 |
| 23     | ZN8Bi       | 233         | 0.026  | 1.198             | 0.047    | 0.039     | 0.011    | 0.259 |
| 24     | ZN9D        | 240         | 0.006  | 1.057             | 0.011    | 0.010     | -0.004   | 0.252 |

**Table 4.2:** The average detrital components and various parameters calculated for Zote-Ngur section. Units: BOCR = mT,  $\chi_{ARM} = 10^{-8} \text{m}^3 \text{kg}^{-1}$ ,  $\text{SIRM} = 10^{-5} \text{Am}^3 \text{kg}^{-1}$ ,  $\text{SIRM}/\chi_{lf} = 10^3 \text{Am}$  and Soft-IRM =  $10^{-2} \text{A/m}^2$ .

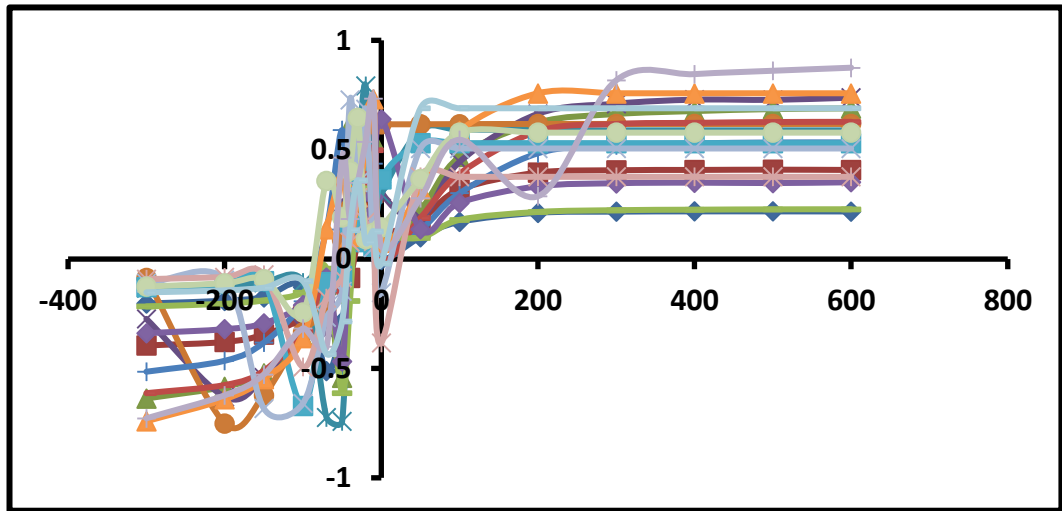


**Fig. 4.3:** The Isothermal Remanent Magnetization curves for representative samples of varied lithology within Zote-Ngur section.

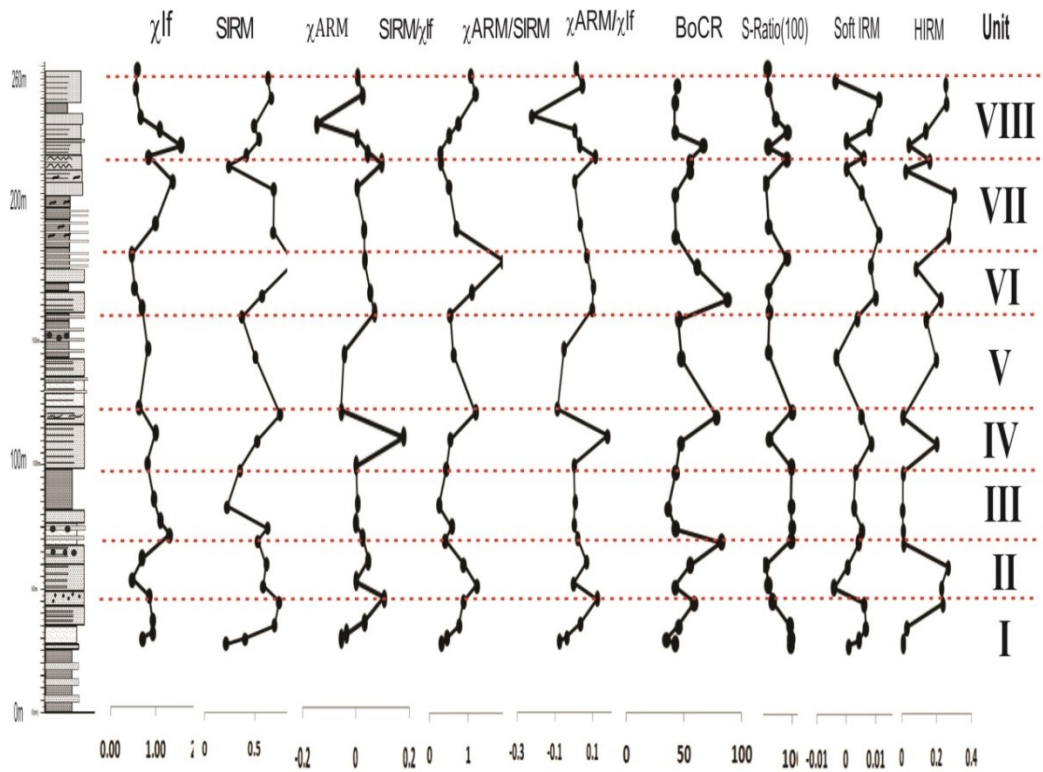


**Fig. 4.4:** Temporal distribution of the representative mineral magnetic parameters for Zote-Ngur section.

## **4.2 MAGNETOSTRATIGRAPHIC RESULTS**

Magnetostratigraphic discourse in all three sections Ruantlang, Zote and Ngur was completed, with the details mentioned in the lithostratigraphy and methodology section. Pilot study was carried out on selected specimen from each site for alternating field and thermal demagnetization. The remaining samples were treated at higher intervals based on the magnetic mineralogy analysis and correlation with pilot studies.

### **4.2.1 Ruantlang Section (RT)**

Ruantlang section exposes a 514.3m thick succession of rocks representing the lower part of the Barail exposures in this area. 31 distinct units were recorded in the section where a total of 108 specimen collected from 18 sites was demagnetized under alternating field and thermal demagnetization. Demagnetization of representative samples from Ruantlang Section is given below.

#### **4.2.1.1 Thermal Demagnetization**

**RT1C:** Demagnetization of RT1C shows a steep decrease in intensity till 300°C and then a steady drop from 350°C to 450°C which is selected as the ChRM for this particular specimen. There is a slight increase in intensity at 550°C and 650°C which indicates secondary components.

**RT2D:** There is a sharp decrease in intensity at 200°C followed by a linear decline from 400 to 530°C which is taken as the ChRM for this sample due to the presence of a stable component. The vector direction shows an increase in intensity at 530°C and drops at 600°C which may be due to unstable secondary fields.



**RT3C:** From 100°C to 350°C the sample shows a gentle decay and then a slight change in direction and intensity till 450°C at which all the secondary component have been removed. The sample then shows a stable component vector between 450°C and 500°C which is taken as the ChRM for this sample.

**RT4D:** This sample shows an intensity decay curve which is almost similar to the previous sample. There is a steady decline in intensity till 450°C which represents a stable component ChRM.

**RT5H:** The intensity decay curve shows the presence of 2 stable components which show a stable decay path from 100°C to 350°C and 400°C to 530°C. The latter component is taken as ChRM due to directions depicted in the Zijderveld diagrams.

**RT6F, 6A:** The samples show linear decay pattern throughout each step of demagnetization till 530°C which may indicate a unicomponent system. After 530°C the patterns show an increase in susceptibility and intensity which may be post induced magnetism after treatment.

**RT7C:** From the intensity decay curves and Zijderveld diagrams the sample shows unicomponent behaviour. The intensity decreases at a very gradual and stable way and no scattering in direction is observed. The ChRM is taken between 450°C and 500°C.

**RT8E:** Two components are witnessed in this graph, one between 100°C and 350°C and the other at 400°C to 500°C. The intensity decay rate is higher in the former compared to the latter with a slight change in resultant vector. ChRM direction is obtained between 400°C and 450°C.

**RT9D, 9B:** The intensity decay curve shows removal of a weak secondary field at 100 followed by a rapid drop at 300°C where 80% of the intensity is lost. After 300°C it shows the presence of a stable component with steady decrease between 300°C and 450°C along which the ChRM direction for the sample is taken.

**RT10C, 10A:** The samples show a linear decay path from 100°C to 300°C that indicate the removal of a strong secondary component. The ChRM direction is taken between 450°C and 500°C based on the decay curve and Zijdeveld diagrams. However, after 550°C the samples show scattering and anomalies in terms of susceptibility and intensity.

**RT11A, 11B:** Intensity decay curves show the removal of two secondary components. The second secondary component shows a very gradual decay path from 350°C to 400°C and is considered a weaker field compared with the former. The ChRM direction is taken between 450°C to 500°C with zero angular deviation. The intensity increases exponentially after 560°C showing false directions which may be caused by due to magnetism acquired in the laboratory during measurement.

**RT12B:** ChRM direction for this sample is taken between 350°C and 400°C where the maximum angular deviation (MAD) is 0. A strong secondary component is encountered between 100°C and 300°C where more than 50% of the intensity has decayed. At 500°C there is a sharp drop in intensity and the overall intensity drops by 90%.

**RT13C, 13A:** The sample shows a more or less linear decay till 500°C which may be attributed to the presence of a unicomponent system. This linear decay path indicates

primary ChRM directions from 400°C to 500°C. Spurious vector direction with increase in intensity is observed after 530°C.

**RT14E:** The decay pattern is very similar to the previous sample maintaining a linear decay path till 500°C thus suggesting a unicomponent system. The intensity goes on decreasing till 560°C where almost all the field has decayed.

**RT15D:** Quite a strong and stable component is observed between 100°C and 300°C showing linear decay path. The main component is witnessed between 350°C and 500°C represented by a strong and stable linear decay direction without scattering. After this the intensity increases showing false directions which may be a result of secondary fields during measurement.

**RT16A, 16B:** The samples show 2 components of secondary magnetization of differing intensities. The first component which show a linear decay path between 100°C and 300°C is quite strong compared with the one removed between 350°C and 400°C. ChRM direction is taken between 530°C and 560°C where a linear decay path and stable direction is observed.

**RT17C:** From 100°C and 300°C the sample show a very rapid loss in intensity where more than 80% is decayed, indication a strong and stable secondary component. The stable ChRM component is witnessed from 450°C to 500°C showing linear decay path.

**RT18C:** Linear decay path from 100°C to 400°C indicates a very strong and stable secondary component comprising of about 60% of total intensity. The main ChRM component displays a linear and rapid decay series between 500°C to 560°C.

#### **4.2.1.2 Alternating Field Demagnetization**

**RT1B, 1D, 1G:** From the intensity decay curve there is a rapid decay between 10mT and 20 mT showing the removal of a strong but unstable secondary magnetization. There is a slight increase in intensity at 30mT followed by a gradual decrease till 60mT which indicates a stable field component taken as the ChRM direction for this sample.

**RT2C:** At 10 mT there is a rapid drop which consumes about 70% of the intensity followed by a linear decay path from 20mT to 30 mT. The intensity again increases from 40mT to 50mT. A linear decay path is observed between 60mT and 70 mT indicating the ChRM direction. After 70 mT there is a sharp increase in intensity and scattering directions.

**RT3C, 3E, 3F:** The samples show similar decay paths and directions following a rapid and linear path from 10mT to 30mT. A very gradual decrease is observed between 40mT and 60mT indicating a stable ChRM component at this interval. False directions are observed after this point with increase in intensity.

**RT4A, 4B, 4C:** All the representative samples show the same pattern where there is a sharp and decay at 10mT followed a very gradual decay path till 80mT. This would indicate a unicomponent system with a more or less constant direction falling under the same quadrant.

**RT5, RT6, and RT7:** These three representative samples from adjacent site show similar decay pattern and directions. There is a constant decay path from 10mT to 60mT which as the path for ChRM for respective samples. This is followed by a

gentle decay path from 70mT to 80mT where more than 90% of the magnetization has been removed.

**RT8B:** Almost 80% of the intensity is lost at 40mT following a gradual decay path from 10mT indicating the removal of a strong secondary component. There is a slight increase followed by a rather stable path from 50mT to 60 mT thus signifying ChRM in this region.

RT9A: The intensity rapidly decreases at 10mT where more than 50% decay has occurred. This is followed by a gradual and linear decay path till 40mT indicating a strong secondary component. The decay path from 50mT to 80mT indicates a stable component and ChRM is taken at 60mT showing 104/60.6/0 PCA directions.

**RT10B, 10D:** Representative samples from this site shows a rapid decay rate from 10 to 30mT where more than 80% of the intensity has been removed. This would indicate a strong secondary component. There is a linear increase in intensity with a gradual drop at 70mT. This region signifies the presence of a stable component hence taken as the ChRM direction for the samples.

**RT11C:** Sharp decrease in intensity at 10mT followed by a linear decrease till 50mT indicates a strong but instable component followed by removal of a stable component in this area. The PCA direction is 105/57.9/0.

**RT12A:** PCA direction for this sample is 60.4/54.5/0 taken from 40mT to 60mT which shows a decay characteristic and directions of a stable component.

**RT13B:** The sample shows a decay path quite similar to that of RT12A. There is a rapid drop in intensity at 10mT followed by a linear decrease till 40Mt indicating the

removal of a secondary component. The ChRM direction for this samples falls between 50mT and 60mT with 152.2/16/0 as the PCA direction.

**RT14A:** From 10mT to 40mT there is a rapid linear decline in intensity where 90% decay is observed. There is a slight increase at 50mT followed by a linear decay path till 70mT which is taken as the ChRM direction showing PCA direction 195.6/60.9/0.

**RT15B:** The sample shows the characteristic of a unicomponent system with a sickle shape decay pattern. There is a rapid loss of intensity at 10mT followed by a curved and gradual decrease till 40mT. A linear pattern is observed from 40mT to 60mT and the intensity rapidly increases at 70 mT. The PCA direction is 275/-331/0 and the ChRM direction falls between 50mT to 60mT.

**RT16C:** Similar decay path is observed as with the previous sample but a weaker increase in intensity at 70mT. ChRM component is taken from 40mT to 60mT with 29.8/-9.7/0 PCA direction.

**RT17B:** Intensity drops by 40% at 10 mT with a linear decay path till 40mT indicating the removal of a stable component. PCA direction for this sample is 92.9/27.8/0 taken from 50mT to 60mT where a stable decay component has been observed.

**RT18A:** The sample shows a gradual decay path from 10mT to 30mT losing more than 70% of the total field intensity. A stable direction in the zijderveld diagram and decay pattern indicates the ChRM for this sample at 40-60mT. The PCA direction for this sample is 65.6/-24.1/0.

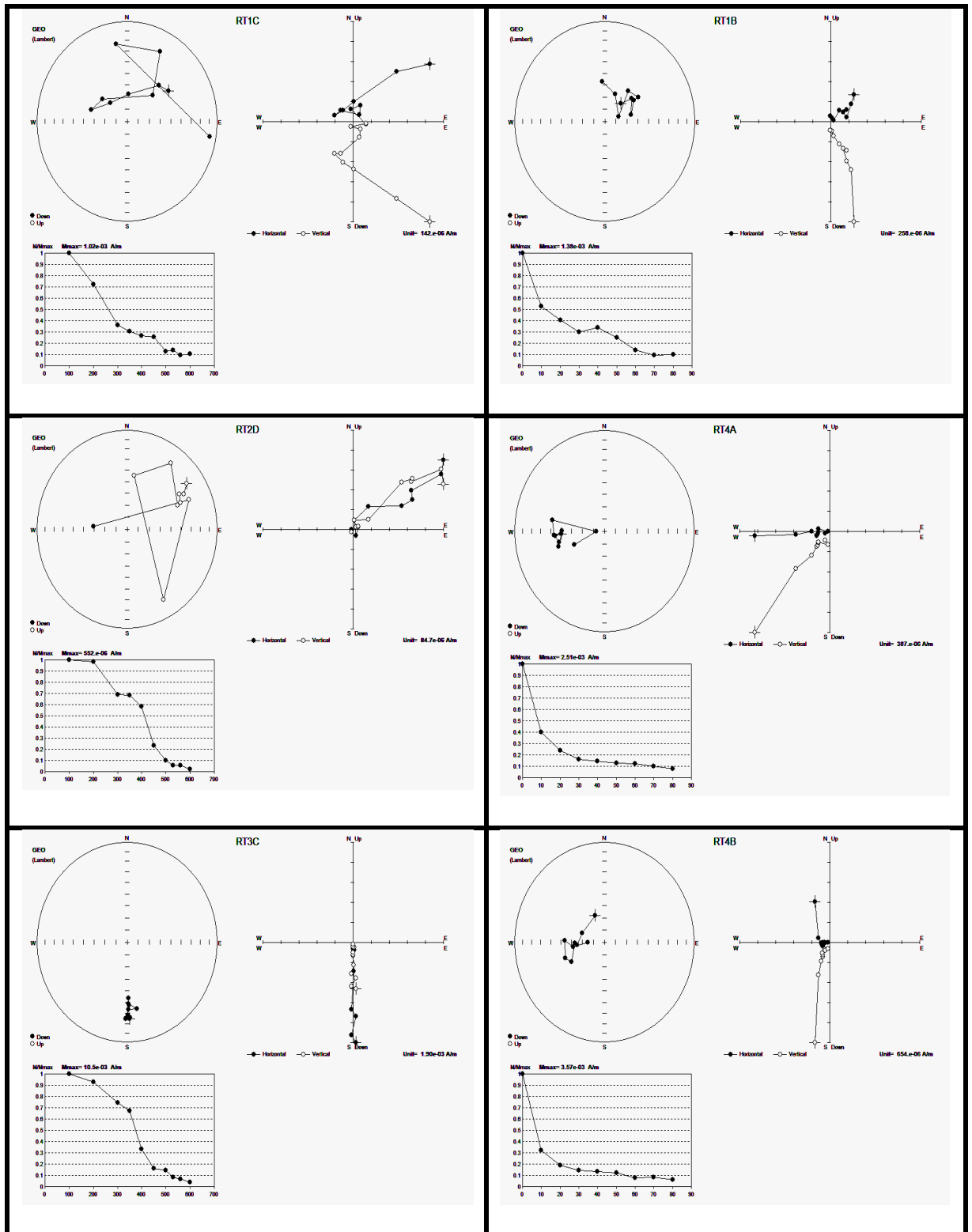


**Fig. 4.5 (A):** Demagnetization plots [Stereonet, Zijderveld diagram (Zijderveld 1967) and intensity decay curve] for representative samples from Ruantlang Section.

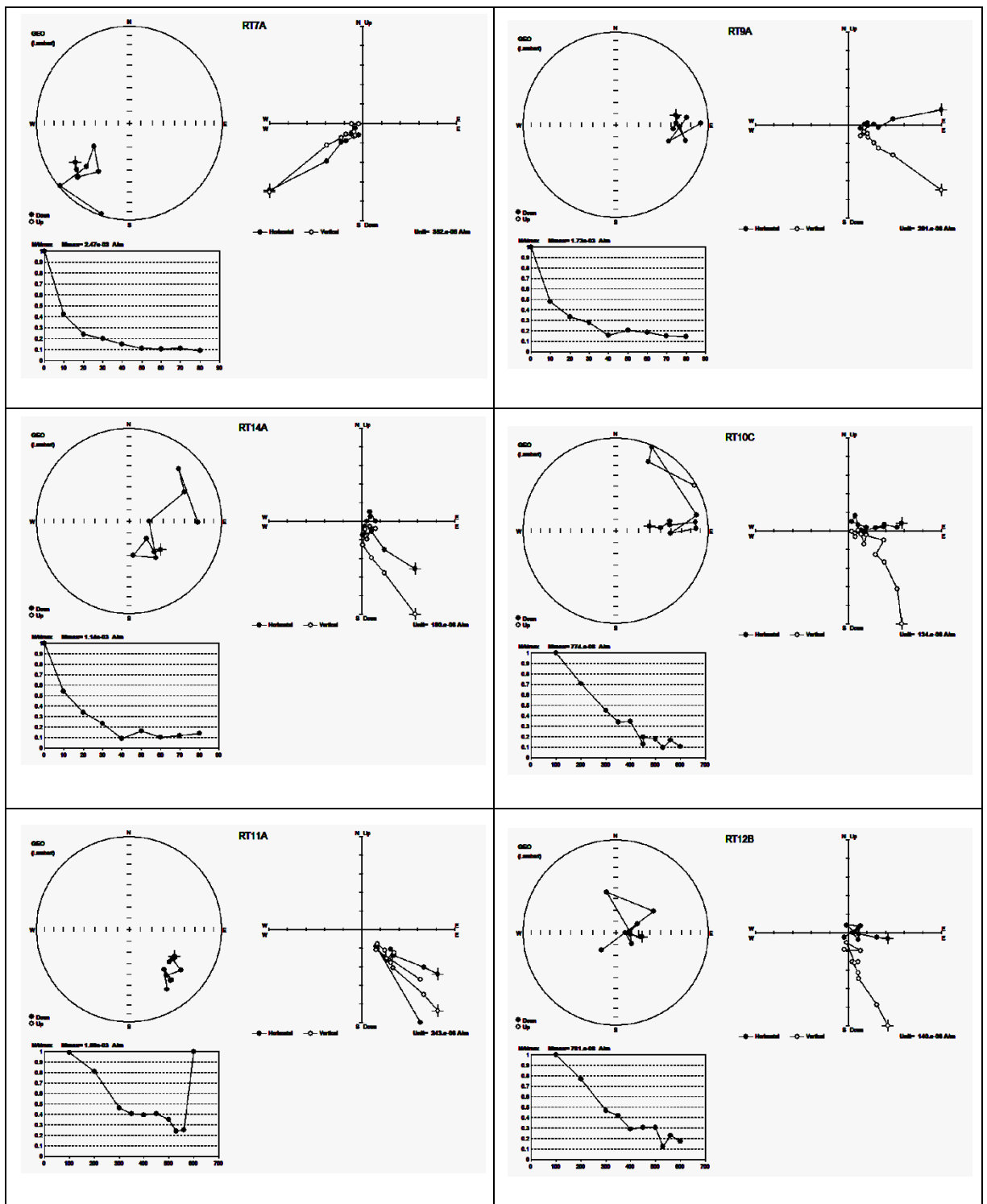


**Fig. 4.5 (B):** Demagnetization plots [Stereonet, Zijderveld diagram (Zijderveld 1967) and intensity decay curve] for representative samples from Ruantlang Section.



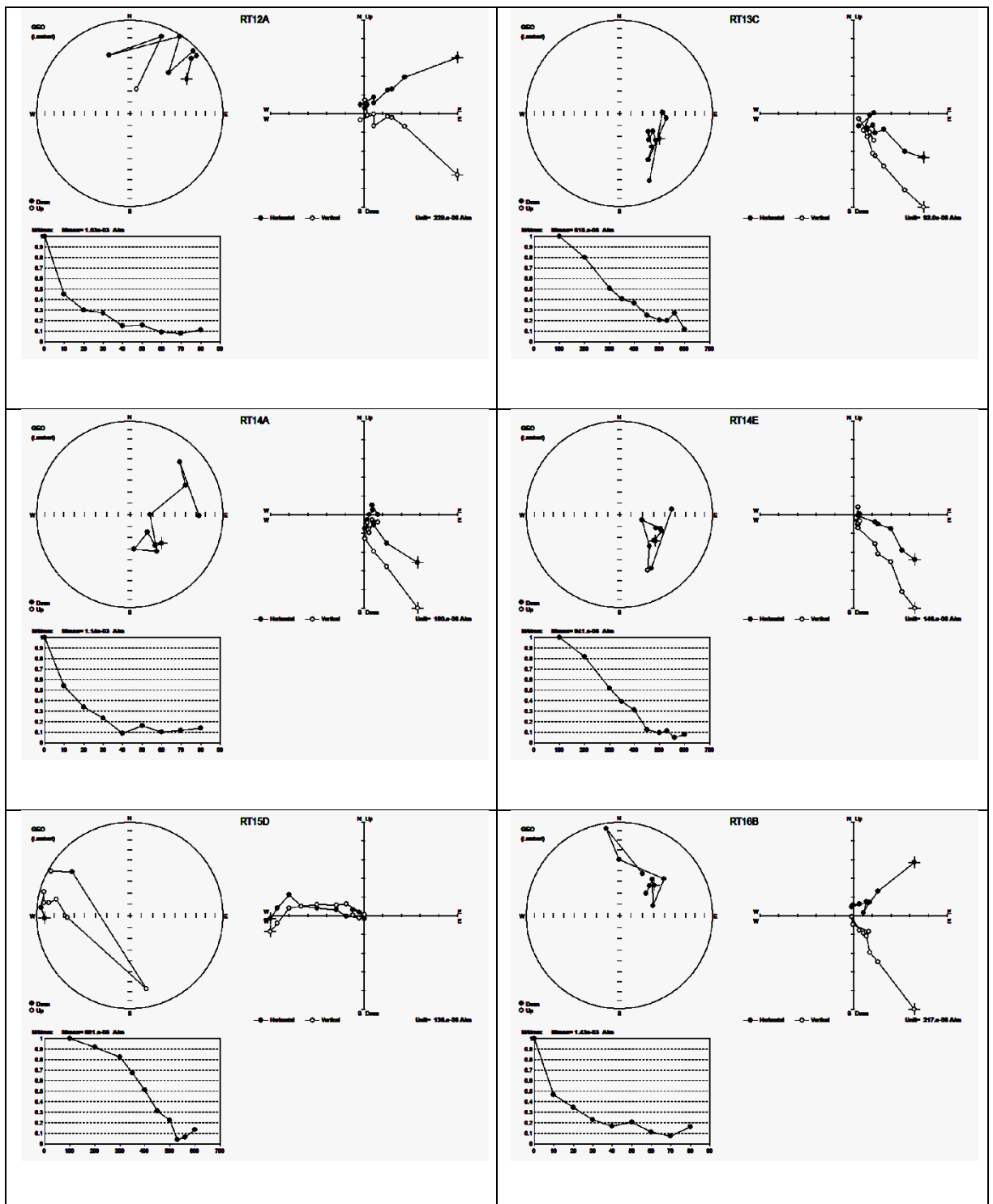


**Fig. 4.5 (C):** Demagnetization plots [Stereonet, Zijderveld diagram (Zijderveld 1967) and intensity decay curve] for representative samples from Ruantlang Section.

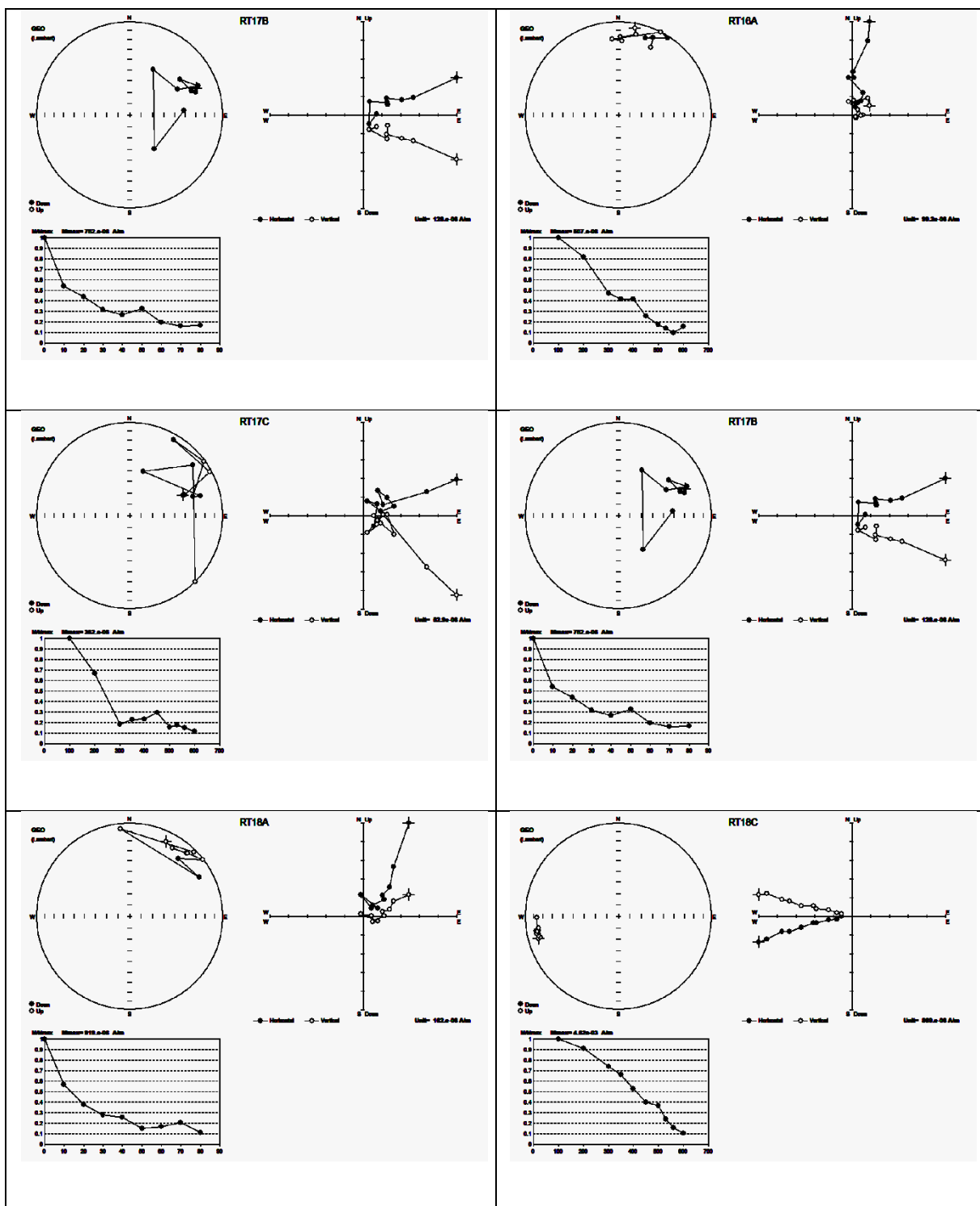


Fig. 4.5 (D): Demagnetization plots [Stereonet, Zijderveld diagram (Zijderveld 1967) and intensity decay curve] for representative samples from Ruantlang Section.

**Table: 4.3:** Number of samples and name, declination and inclination mean, sample height,  $k\alpha_{95}$  (Fisher statistical parameters; concentration parameter and 95% cone of confidence, VAP latitude (normal and reversal))

| Site | Height (m) | n | Dm    | Im   | alpha 95 | k    | V.lat | dp    | dm    | P. Lat |
|------|------------|---|-------|------|----------|------|-------|-------|-------|--------|
| RT1  | 31         | 6 | 38.2  | 48.3 | 44.2     | 3.25 | 43.1  | 47.1  | 64.5  | 37.9   |
| RT2  | 56         | 6 | 50.1  | 28.7 | 35.2     | 4.58 | 36.6  | 23.7  | 40.8  | 19.9   |
| RT3  | 74         | 6 | 58.1  | 16.1 | 78.4     | 1.69 | 29.6  | 43.8  | 82.8  | 11.4   |
| RT4  | 202        | 5 | 259.2 | 42   | 37       | 5.1  | -10.5 | 26.3  | 44.1  | 22.09  |
| RT5  | 206        | 6 | 356.8 | 63.1 | 59.7     | 2.21 | 47.9  | 103.8 | 111.3 | 65.3   |
| RT6  | 224        | 5 | 162.6 | 36.5 | 31.6     | 6.81 | -51.6 | 1.2   | 7.3   | 11.8   |
| RT7  | 257        | 6 | 216.6 | -9.2 | 75.1     | 2    | 50.5  | 40.9  | 78.4  | -10    |
| RT8  | 268        | 5 | 53.2  | 18.2 | 45.6     | 3.77 | 34.3  | 43.4  | 80.7  | 13.18  |
| RT9  | 281        | 6 | 88.3  | 30   | 43.7     | 3.3  | 0.5   | 26.2  | 47.9  | 15     |
| RT10 | 307        | 6 | 73.3  | 49.3 | 27       | 7.13 | 16.6  | 24.1  | 36.1  | 30.9   |
| RT11 | 332        | 6 | 150.1 | 38.4 | 52.5     | 2.5  | -44.8 | 30.4  | 56.5  | 30.4   |
| RT12 | 349        | 6 | 87.4  | 38.9 | 4.46     | 6    | 0.9   | 3.06  | 5.22  | 20.6   |
| RT13 | 364        | 5 | 170.2 | 3.43 | 48.9     | 3.4  | 69.8  | 25    | 49.5  | -5.3   |
| RT14 | 408        | 6 | 153   | 49.8 | 87.8     | 1.7  | -41.2 | 59.8  | 102   | 44.8   |
| RT15 | 429        | 5 | 226.3 | 11.7 | 100      | 1.5  | 41.2  | 49.4  | 94.3  | -10.4  |
| RT16 | 450        | 5 | 25.8  | 24.1 | 61.5     | 2.5  | 58.9  | 44.1  | 73.7  | 22.4   |
| RT17 | 468        | 5 | 62.5  | 26.5 | 40.8     | 4.4  | 21.4  | 25.3  | 45.5  | 16.5   |
| RT18 | 484        | 6 | 64.1  | 47.6 | 116.1    | 1.3  | -21.2 | 66.6  | 109.5 | -23.6  |

#### **4.2.1.3 Magnetic Polarity reconstruction of Ruantlang section**

Ruantlang section, as stated in the lithography section consists of rock facies which is dominated by shales. Since drilling and obtaining samples from such type of rock units is not possible and with the scarcity of competent sandstone beds, the spacing between sample sites are quite far off in some parts. The alternating field and thermal demagnetization data presented is analysed and the mean direction is taken from a collection of 5-7 specimen from each site. This is used to determine the VGP latitude and MPTS as described in section 4.6 of methodology chapter.

The normal and reversal determined in the VGP latitude of each samples taken from different horizons is then arranged coinciding with the sample positions in the litho-column created using corel draw software. Since there is no datum plane for matching the local polarity reversal pattern with Geomagnetic Polarity Time scale (GPTS) due to absence of geologic age markers, matching is done using careful examination of reversal pattern and periodicities within the Magnetic Polarity Time Scale (MPTS).

Ruantlang Section (RT) displays 5 normal and 4 reversal magneto-zones showing differing normal periodicities and quite similar interval among the reversal stage. The GPTS correlated ages of Ruantlang section falls between ~29.662 Ma at the base to 27.087 Ma at the top as shown in Table. 4.4.

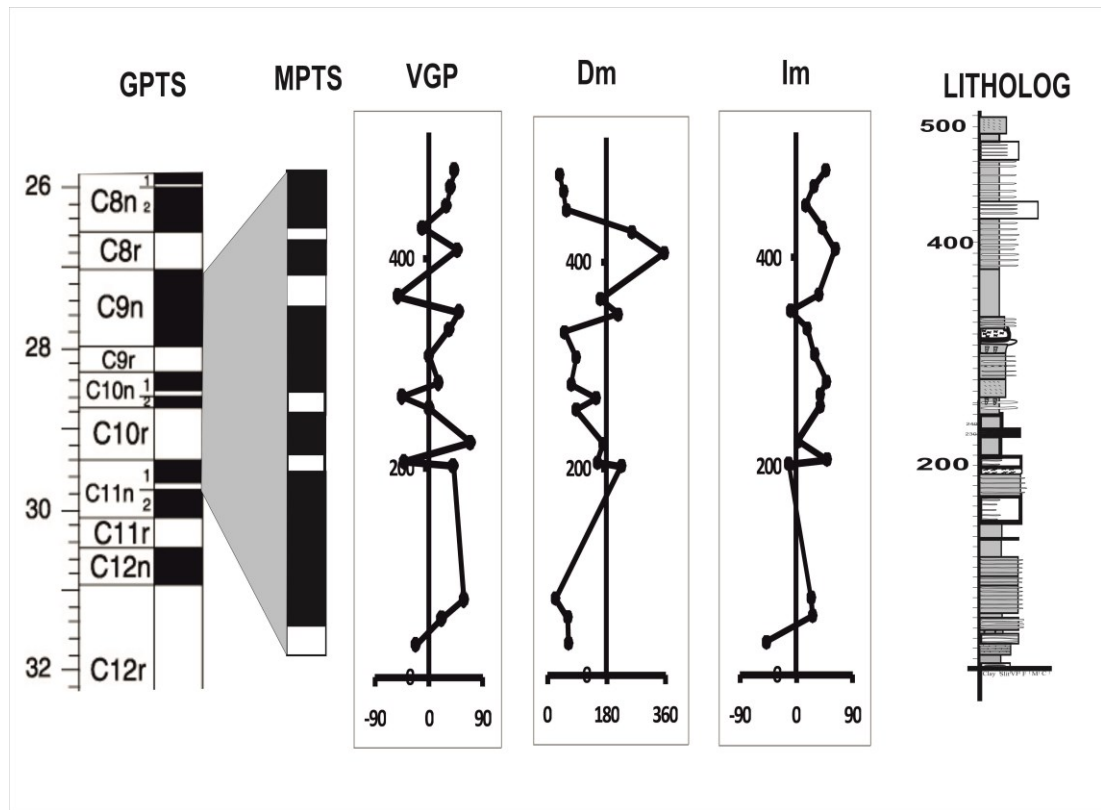


**Fig 4.6:** Magnetic polarity reconstruction of Ruantlang Section

| S.N | GPTS EVENTS | Duration      | Stratigraphic level (m) |
|-----|-------------|---------------|-------------------------|
| 1   | C11n.1n     | 29.401-29.662 | 56-202                  |
| 2   | C10n.2n     | 28.578-28.745 | 224-257                 |
| 3   | C10n.1n     | 28.283-28.512 | 281-349                 |
| 4   | C9n         | 27.027-27.972 | 408-484                 |

**Table 4.4:** Normal polarity events of Ruantlang Section

### **4.3.2 ZOTE SECTION (ZT)**

Zote Section lies in the middle part of the study area and exposes a 177.5m thick succession of sandstone and shale alternation with coarsening upward type of environment. 102 samples were demagnetized under alternating field and thermal methods. 20 distinct rock units have been recorded in this section where samples were taken from 17 sites.

#### **4.3.2.1 Thermal Demagnetization**

**ZT1A1, 1C:** The samples show a sharp linear decay pattern from 200°C to 400°C and a gentler and stable direction between 450°C to 500°C with the components completely removed at 600°C. The spherical plot shows that the components are clustered in a single quadrant and zijderveld plots showing a stable directional pattern. From the graphical representation of data the sample are unicomponent systems with PCA directions 48.6/40.4/0.

**ZT2C:** There is a steady linear decay pattern from 100°C to 400°C indicating the removal of one component. ChRM direction is taken from 400°C to 500°C after a sharp rise from removing the previous component. 44.1/10.5/3 is the PCA direction for this representative sample.

**ZT3A:** The samples show a more or less linear decline in intensity throughout the various demagnetization steps. Stereographic plots, zijderveld diagrams and intensity decay curves all indicate a unicomponent system. The PCA is 33.0/-8.6/0 with ChRM direction taken from 450°C and 500°C.

**ZT4BII:** The decay pattern is similar to that of the previous sample with the stereographic plots concentrated in the East quadrant and consistent directions in the zijderveld diagrams. The PCA is 20.2/37.4/0.

**ZT5CI:** The specimen show a sharp inclined step like decay path till 300oC indicating a secondary component. The ChRM direction is taken from 350°C to 450°C with PCA direction 66.3/20.4/0. The remaining steps follow a gradual stepwise decrease in intensity throughout the remaining plots.

**ZT6DI:** A sharp drop in intensity is observed from 100°C to 300°C followed by a gentler pattern from 350°C to 400°C. There is an increase at 450°C dropping sharply to 450°C and then a pyramid pattern from 450oC to 600°C. The PCA for this sample is 72.5/-27.5/0 taken between 300°C and 400°C.

**ZT7EII:** A linear decay pattern in shown in the intensity decay curve with persistent direction in zijderveld plots. This signifies a unicomponent system with ChRM direction taken between 500°C and 550°C. After this the intensity increases sharply at 600°C which may be due to induced magnetism in laboratory.

**ZT8AI:** Consistent linear decay pattern and direction is displayed in all graphical plots due to the presence of a unicomponent system. The ChRM lies between 500°C and 550°C.

**ZT9E, ZT9.5CII:** Fairly stable direction and pattern is observed within the samples. The intensity decay curves show a gentle decay path till 500°C and ChRM is taken in this area. The PCA direction for this sample is 79.5/-35.7/0 for ZT9.5CII and 80/-6.1/0 for ZT9E

**ZT10CI:** The PCA direction for this sample is 258.6/11.4/0 with the ChRM direction between 450°C and 500°C. A very gentle decay path is observed between 100°C and 500°C which is a signature of unicomponent system. The intensity rapidly rises at 600°C which may be attributed to magnetism induced after demagnetization.

**ZT11AI:** 100°C to 300°C show a rapid linear decrease in intensity where more than 60% of the field is removed. At 350°C a stable component is observed from graphical plot which is taken as the ChRM direction for the sample.

**ZT12C:** The specimen shows a rather stable decay pattern and direction from 100°C to 450°C which is the ChRM signifying a unicomponent system. PCA direction for the sample is 155.9/71.9/0. There is a small rise in intensity which gradually drops till 600°C where almost all components have been removed.

**ZT13DII, ZT13.5B:** The representative samples show similar patterns in terms of decay and directions. A linear decay path is observed from 100°C to 300°C with a slight change in direction and intensity decay rate from 350°C to 400°C. The pattern continues till 550°C then rises rapidly at 600°C. The ChRM direction is taken from 350°C to 400°C.

**ZT14E:** There is a rapid decay pattern from 100°C to 300°C followed by a stable path along 350°C which is taken as the ChRM direction for this sample and PCA is 69.4/27.7/1.0.

**ZT15A:** The intensity decay curve shows a linear decay path from start to end which may indicate a stable unicomponent system. ChRM is taken between 450°C and 500°C having PCA direction of 79.5/-35.7/0.



#### **4.3.2.2 Alternating Field Demagnetization**

**ZT1B, ZT1D, ZT2A, ZT2EI:** The samples show a sharp drop in intensity at 10mT which is followed by a steady decay path till 40mT where nearly all the magnetization has been removed. The ChRM is taken between 30mT to 40mT where a stable component is observed. There is a gradual rise at 50mT which may be referred to laboratory induced magnetization.

**ZT3BI, ZT4CI, ZT5GII, ZT6BI:** These three adjacent representative samples show similar patterns of demagnetization. The intensity decay curve show a linear decay path from 10mT to 25mT where about 90% of the field have been removed. This is followed by a slight rise in intensity at 30mT. The ChRM direction lies between 25mT and 30mT for each sample. Higher demagnetization notes indicate spurious directions.

**ZT7AI, 7BII:** More than 70% of the field is removed at 20mT which indicates the removal of a strong secondary field. The decay curve follows a linear pattern till 40mT showing characteristic of a stable component where the ChRM direction is taken. PCA direction for this sample is 73.6/38.3/0.

**ZT8EII:** PCA direction for this sample is 154/-26.6/0 with ChRM taken between 30mT and 35mT. The sample show a sharp drop in intensity at 20mT followed by a stable component with linear path of very low change in intensity.

**ZT9DI:** The intensity falls at a rapid rate at 20mT and about 80% of total intensity is decayed. The stable component is found between 25mT and 35mT where ChRM direction is taken. PCA for the specimen is 116.7/-42.7/1.

**ZT9.5EII:** 90% of the total intensity decayed at 20mT followed by a stable component till 30mT after which the intensity increases exponentially. The ChRM direction is selected between 20mT and 25mT. This specimen show two component removed during demagnetization.

**ZT10AI:** The specimen shows two components based on the graphical representations. The first component which is regarded as the secondary component shows a steady linear decline in intensity from 10mT to 25mT. The second component shows a linear, rather straight decay path which is considered the ChRM direction. The PCA value is 238.4/-0.9/0.

**ZT11EII:** The intensity decay curve shows two components system removed at 30mT. The first component show a steady linear decline in intensity at 20mT where more than 70% of the field has been removed. The stable ChRM component from 25mT to 30mT shows a steady decline in intensity followed by a rapid rise at 35mT.

**ZT12D:** The ChRM for this specimen lies between 20 and 30mT and PCA direction of 26/-78.9/0. The intensity decay curves show two components removed during demagnetization.

**ZT13DI:** 90% of total intensity is removed at 20mT which indicates a strong but unstable component followed but a partial rise at 25mT and fall at 30mT again followed by a rise which may be considered induced magnetism in laboratory settings. The ChRM is taken between 25mT and 30mT.

**ZT13.5EI:** The decay path follows a steady linear pattern up to 30mT which indicates a unicomponent system. ChRM lies between 20mT and 30mT.

**ZT14BI:** At 20mT the intensity decay curve shows a decrease of more than 90% followed by scattered directions and increase in intensity. The specimen is a unicomponent system with PCA direction 145.1/9.6/2.0.

**ZT15B:** 20mT shows about decay percentage of about 90 of total intensity that indicates the presence of a strong but unstable component. This is follow by a linear decay path with slight increase in intensity till 35 mT, indicative of a stable ChRM component. The PCA direction for the specimen is 61.7/10.5/1.0.

### **4.3.3 ZOTE-NGUR SECTION (ZN)**

Zote-Ngur (ZN) Section is a small section between Zote and Ngur Sections. It exposes a 76.5m thick succession of 13 distinct lithological units. The lithological description is included in the first part of Ngur section as it is considered a continuation of the lower part of Ngur section from structural and lithological correlation. The demagnetization part is included in Zote section as it was initially a part of the section and is more convenient for calculations. 41 specimens from 9 sites are analyzed for demagnetization process.

#### **4.3.3.1 Thermal Demagnetization**

**ZN1C:** From the intensity decay curve the samples show a linear decay of more than 80% of total field from 100°C to 400°C. The intensity rises by a small amount at 450°C followed by a steady decrease till 550°C thus indicating the ChRM component. The PCA direction is 67/25.9/0 for ZN1C. Two main components are observed the sample.

**ZN2C:** About 90% of the total intensity is decayed following a steady decline from 100°C to 400°C which is quite similar to the previous sample. The decay pattern then

gently drops from 450°C to 700°C which is indicative of the stable ChRM component.

**ZN3E:** From 100°C to 300°C the intensity drop at a sharp rate signifying the removal of a strong component consisting of 80% of the total intensity. A stable component pattern is witness at 350°C to 450°C indicating a second component. The intensity again rises by a small amount which may be due to small induced field during treatment process after which the sample is completely demagnetized.

**ZN4F:** The decay pattern and directions from graphical plots show a unicomponent system which gently declines with each demagnetization step. The ChRM is selected from 350°C to 450°C having a PCA value of 34.9/-21.9/0.

**ZN5C:** More than 70% of total intensity is decayed between 100°C and 300°C which is followed by a uniform linear path till 400°C taken as the ChRM direction. The intensity then drops gently at 500°C followed by a slight increase at 550°C after which the specimen has completely demagnetized at 700°C.

**ZN6A:** The intensity rapidly decays from 100°C to 400°C with a loss of 90% of the total intensity. This is followed by rather stable component from 400°C to 500°C from which ChRM component is taken having PCA value 101.5/8.5/0.

**ZN7D:** The intensity decay curve and zijderveld plots show a stable and consistent pattern and direction which indicates a unicomponent system. The ChRM is between 450°C and 500°C with PCA direction 47.3/16.5/0.

**ZN8A:** The specimen show similar decay path and direction as the previous specimen. It is a unicomponent system ChRM direction between 450°C and 500°C with PCA values 298.6/-40.9/0.

**ZN9A:** The sample shows a rapid decrease in intensity from 100oC to 300oC where 70% of the field is removed. There is a slight rise in intensity at 350°C followed by a gradual decay path till 500°C which is considered the stable component with PCA values 52.7/44.2/0. The intensity then slightly rises then fall with scattering directions after which the sample is completely demagnetized.

#### **4.3.3.2 Alternating Field Demagnetization**

**ZN1DII:** The specimen shows a sharp decay path where 80% of the intensity is decayed at 20mT which represents a strong but unstable secondary component. From 25mT to 35mT there is a stable component decay pattern which is taken as the ChRM for this sample. At 40mT there is a slight drop and then increases at 45mT with scattered directions showing acquisition of induced laboratory field.

**ZN2EI:** The intensity decay curve indicate a bicomponent system as the pattern follows a linear decay path till 25mT then slightly increasing intensity curve like pattern ending at 30mT which is taken as the main component vector. The PCA direction is 17.2/18.3/2.

**ZN3B:** The first component is removed at 20mT showing a linear decay path which is deviated in a gentler pattern till 35mT. The second component is taken as the ChRM direction for this specimen. The intensity then rises rapidly at 40mT after removal of the NRM components.

**ZN4C:** Rapid decay pattern is shown at 20mT removing 80% of total intensity. The decay path then gradually decline till 30mT indicating the stable component vector. The intensity then decreases at a linear path till the sample is completely demagnetized.

**ZN5D:** Three components are seen in this specimen, the first one shows a rapid decay path at 20mT followed by a stable vector component till 30mT. The third component shows an increase in intensity which is characteristic of spurious secondary magnetization. The PCA direction for this specimen is 10.8/-25.6/0.

**ZN6B1:** 90% of the field is removed at 20mT which is considered the secondary component. The decay path then follows a linear pattern till 35mT which is the direction for stable ChRM component.

**ZN7C:** The intensity decay curve shows two components in this specimen. The secondary component is removed at 20mT which shows a huge decrease in intensity. The ChRM direction is from 25mT and 30mT following a linear path till 40mT.

**ZN8EII:** 80% of the field is removed at 20mT in a linear fashion from origin. The decay path then display about 25% increase at 35mT then rapidly fall at 40mT. The stable components is taken from 25mT to 30mT with PCA values 337.1/-10.7/0.

**ZN9BI:** The representative specimen shows two components based on interpretation from the intensity decay paths and plots shown in zijderveld diagrams. The ChRM for this sample lies at 25mT after which a gradual increase in intensity is observed with scattered directions.

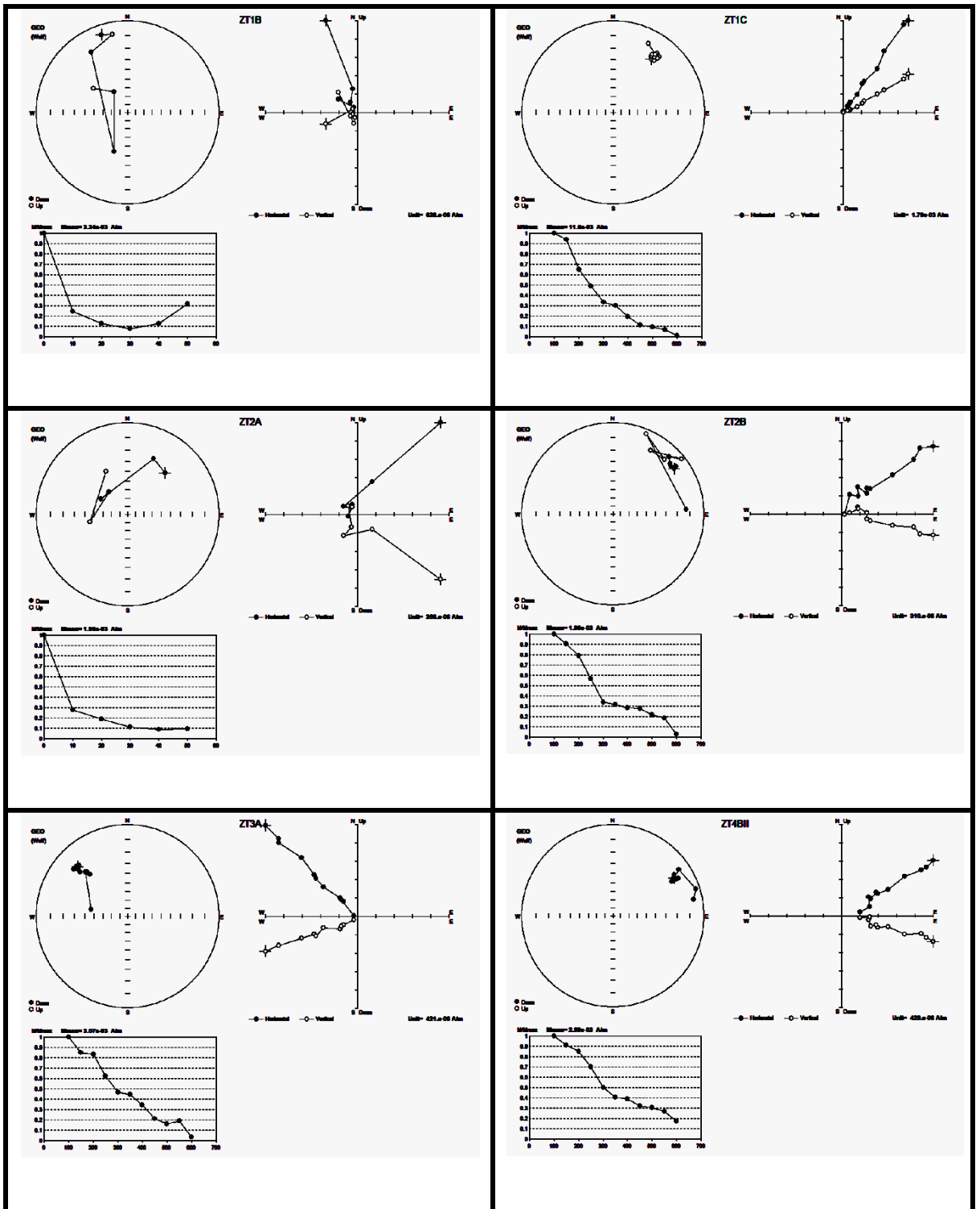


**Fig. 4.7 (A):** Demagnetization plots [Stereonet, Zijderveld diagram (Zijderveld 1967) and intensity decay curve] for representative samples from Zote Section.

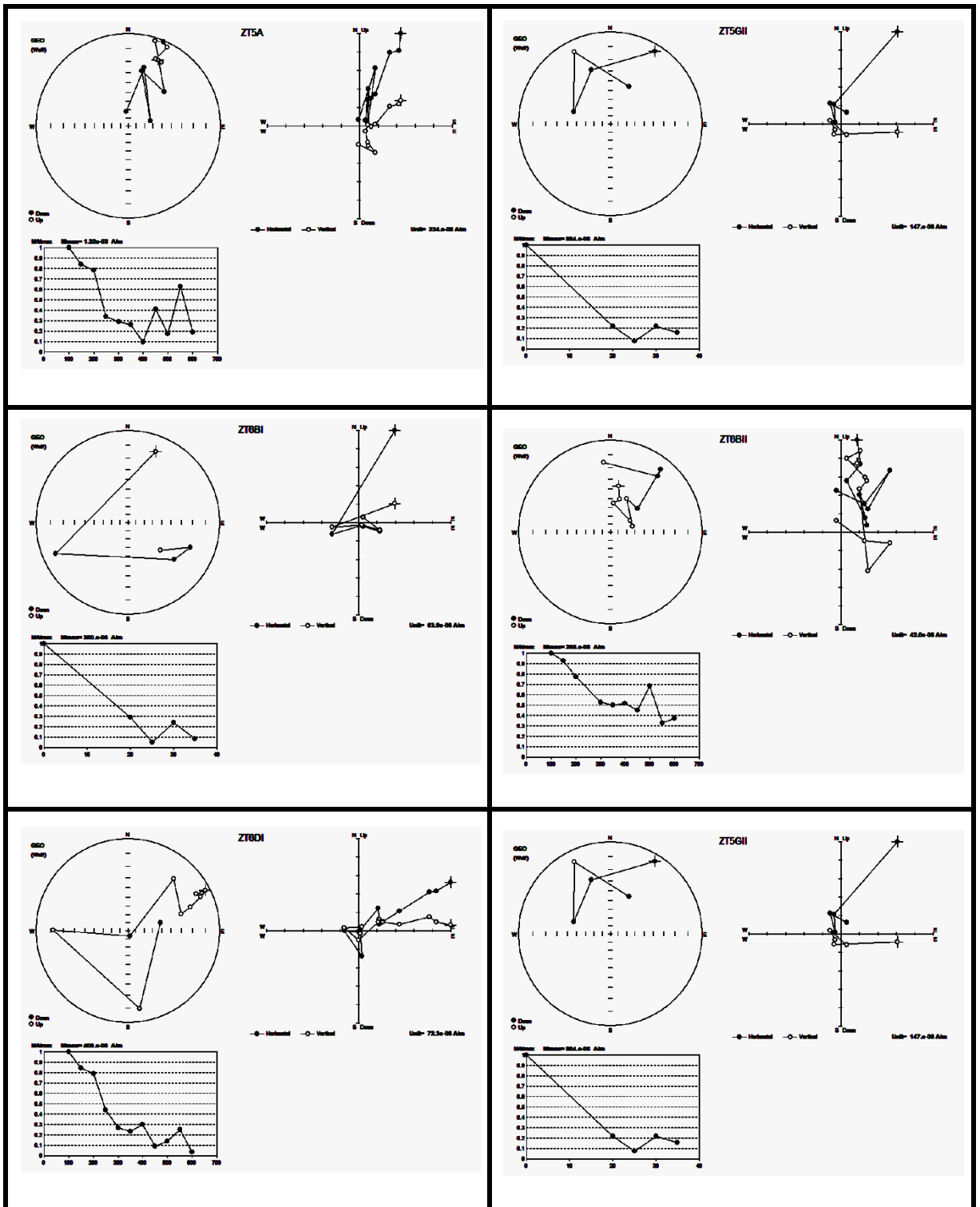


**Fig. 4.7 (B):** Demagnetization plots [Stereonet, Zijderveld diagram (Zijderveld 1967) and intensity decay curve] for representative samples from Zote Section.



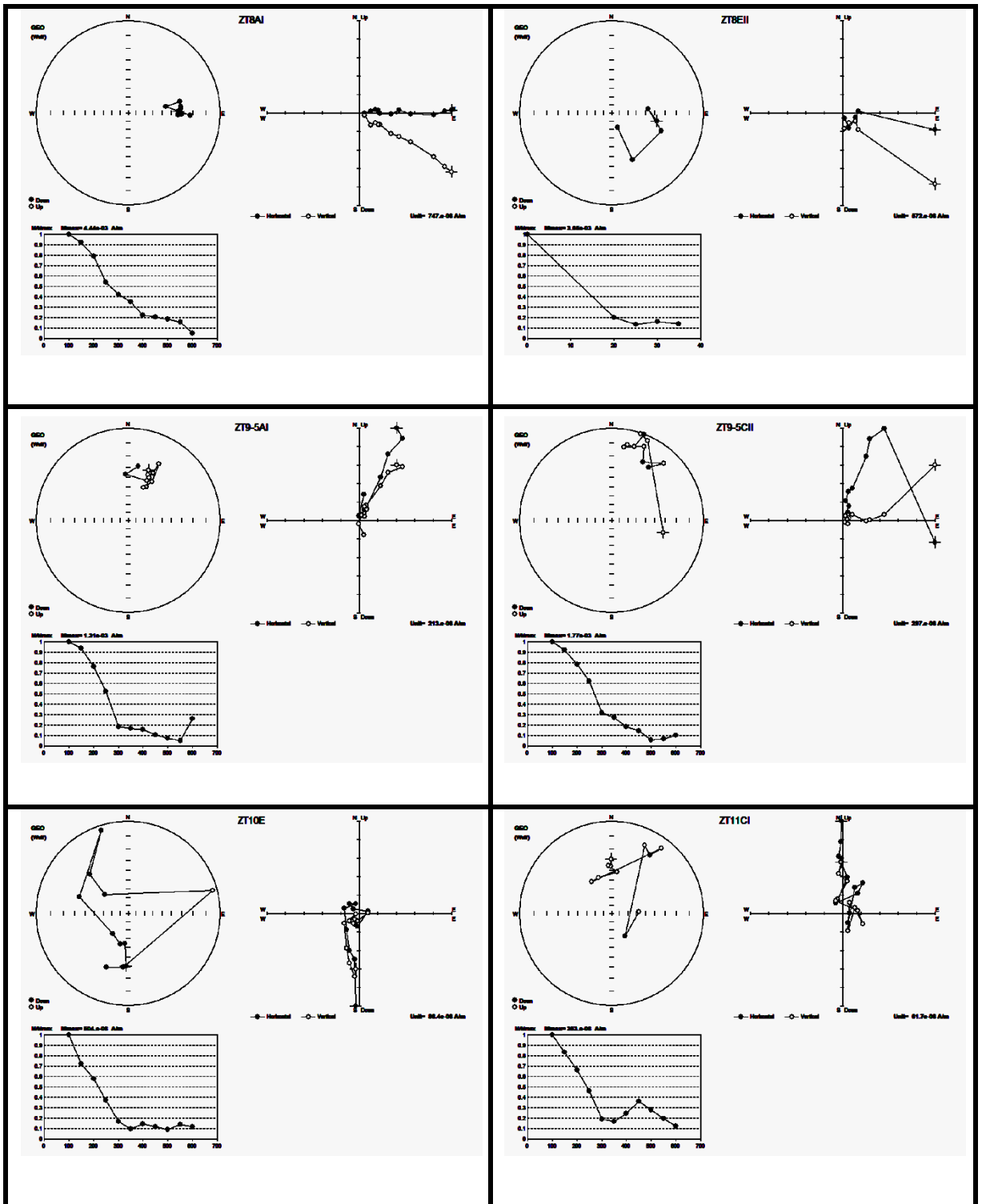


**Fig. 4.7 (C):** Demagnetization plots [Stereonet, Zijderveld diagram (Zijderveld 1967) and intensity decay curve] for representative samples from Zote Section.

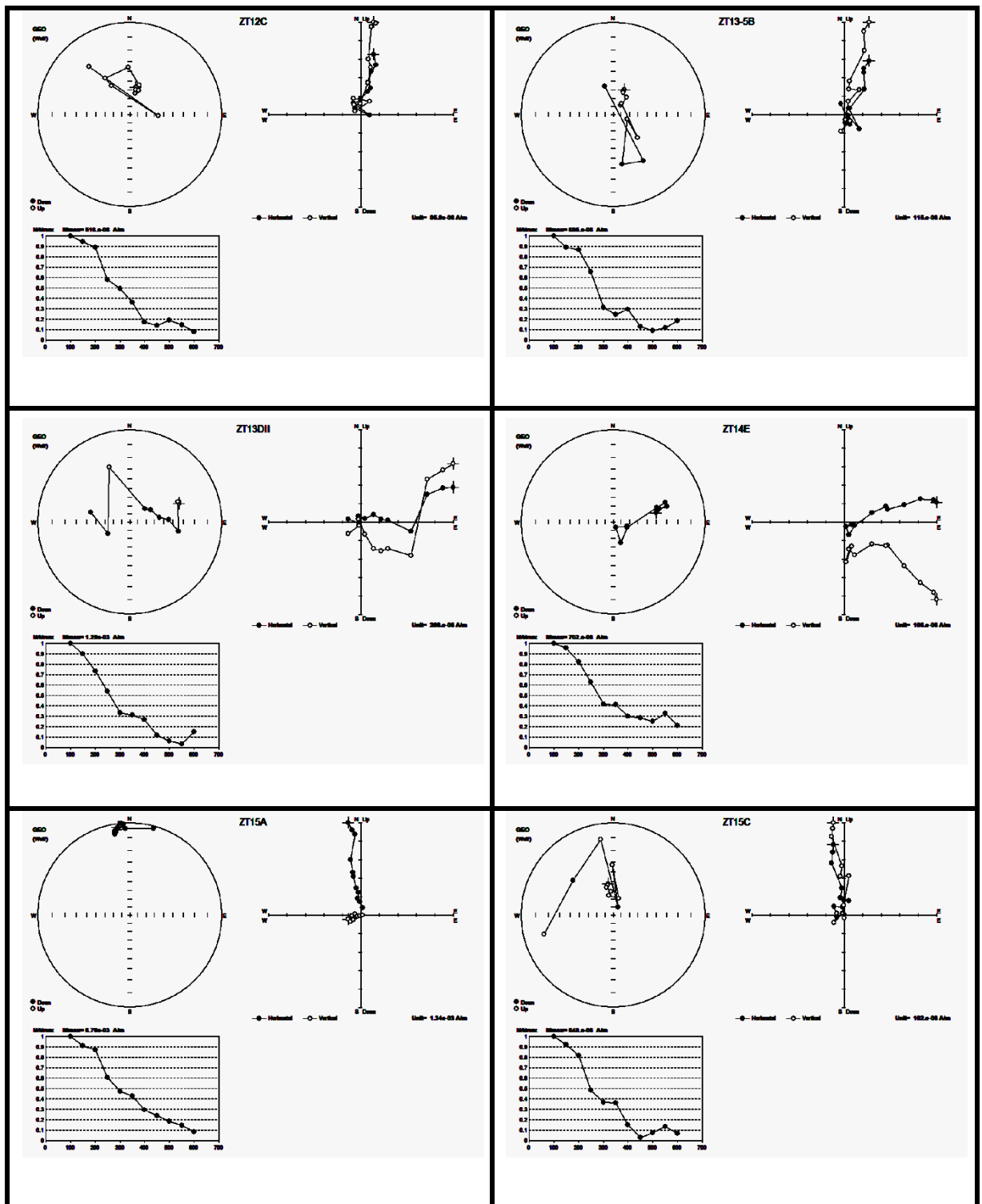


**Fig. 4.7 (D):** Demagnetization plots [Stereonet, Zijderveld diagram (Zijderveld 1967) and intensity decay curve] for representative samples from Zote Section.

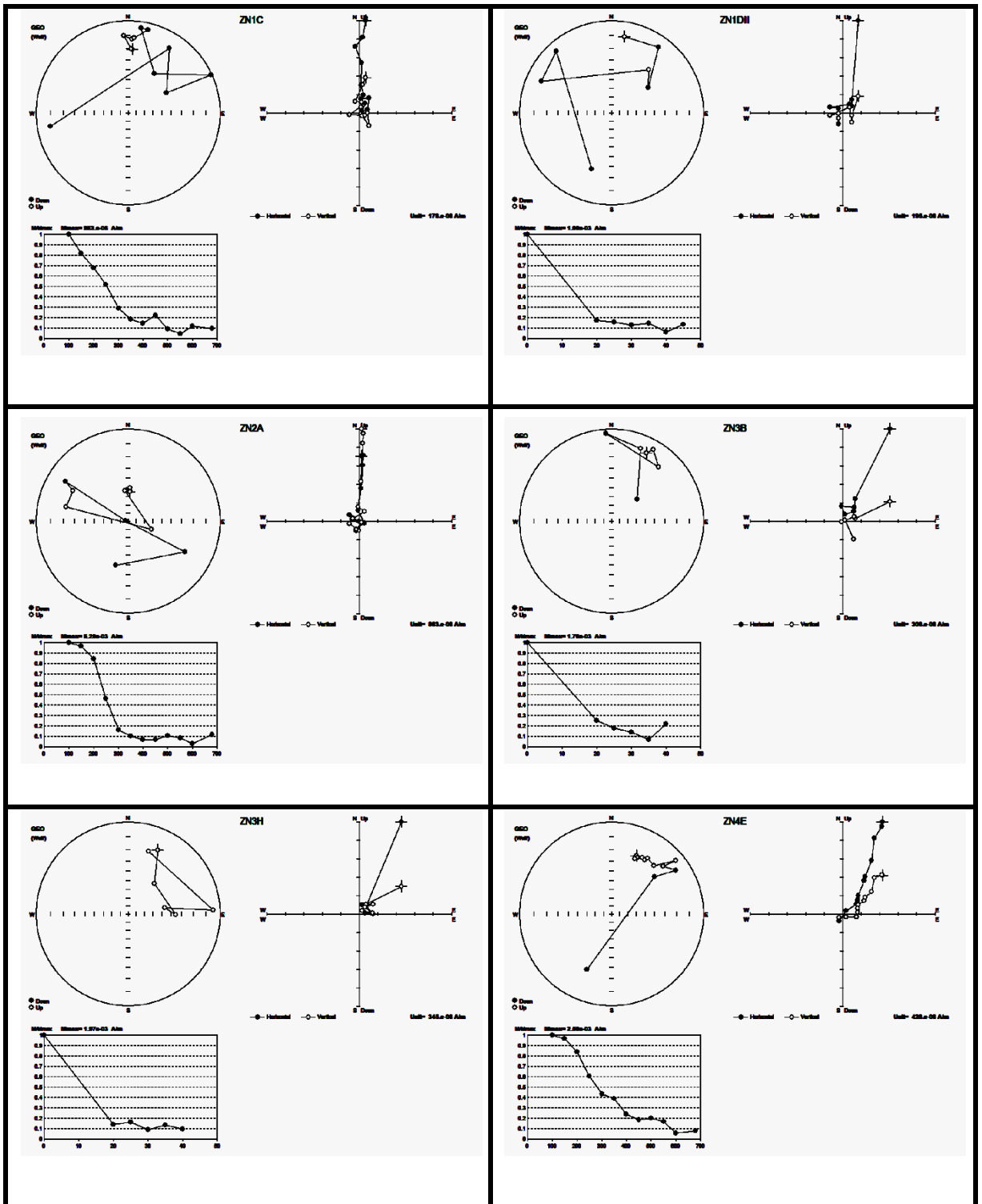


**Fig. 4.7 (E):** Demagnetization plots [Stereonet, Zijderveld diagram (Zijderveld 1967) and intensity decay curve] for representative samples from Zote-Ngur Section.

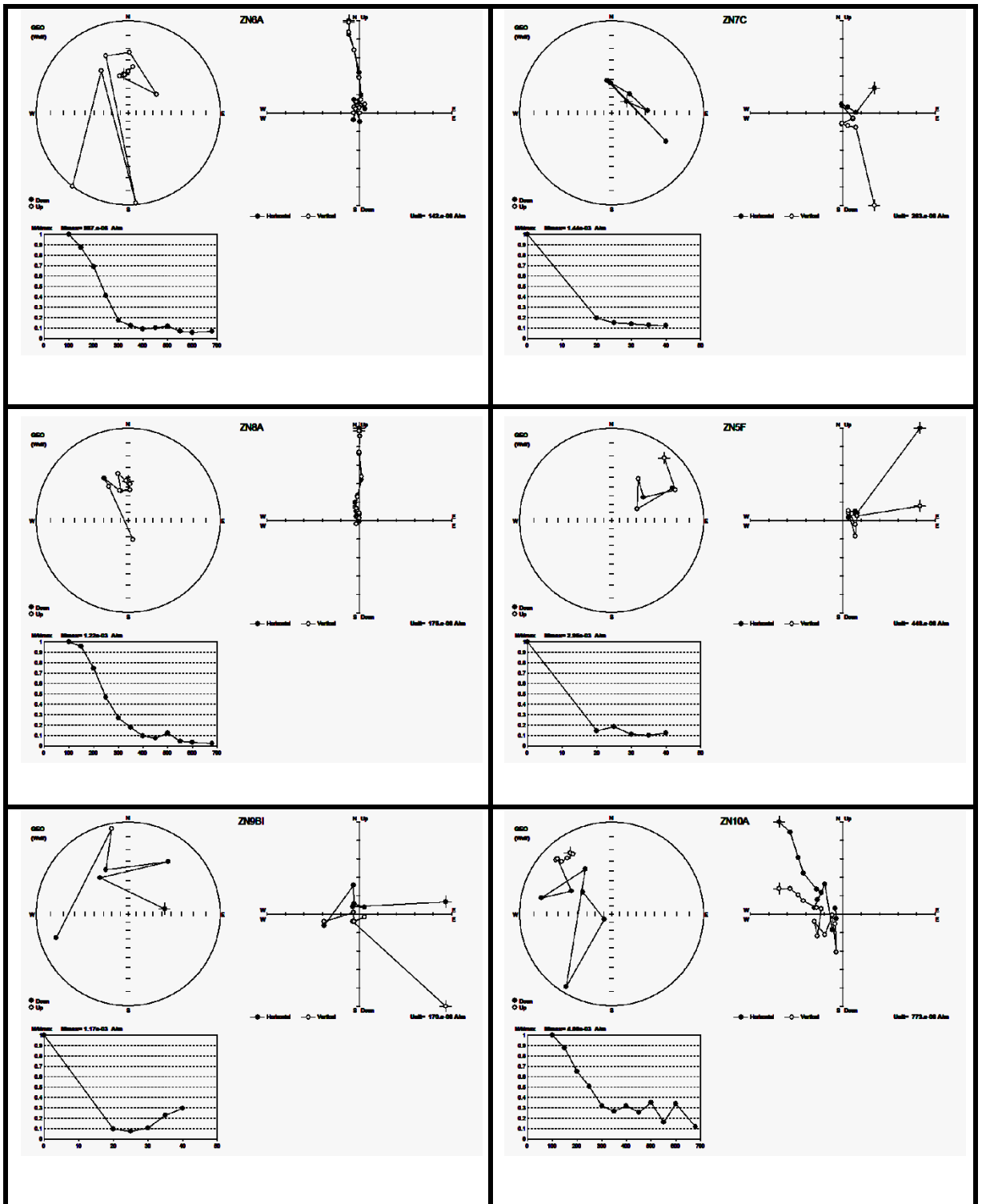


**Fig. 4.7 (F):** Demagnetization plots [Stereonet, Zijderveld diagram (Zijderveld 1967) and intensity decay curve] for representative samples from Zote-Ngur Section.

**Table: 4.5:** Number of samples and name, declination and inclination mean, sample height,  $k\alpha_{95}$  (Fisher statistical parameters; concentration parameter and 95% cone of confidence, VGP latitude (normal and reversal)

| Site   | Height (m) | n | Dm    | Im    | Alpha 95 | k    | V.Lat | dp    | dm    | P.Lat |
|--------|------------|---|-------|-------|----------|------|-------|-------|-------|-------|
| ZT1    | 6          | 4 | 8.1   | 15.5  | 63.3     | 3.09 | 75.4  | 36.45 | 67.93 | 12.99 |
| ZT2    | 27         | 5 | 64.1  | 22.7  | 94.6     | 1.6  | 23.6  | 49.9  | 94.8  | 11.04 |
| ZT3    | 31         | 5 | 8.7   | -4.1  | 57.8     | 2.71 | 67.7  | 29    | 57.9  | 2.6   |
| ZT4    | 43         | 5 | 53.7  | 7.2   | 29.3     | 7.77 | 33.4  | 14.8  | 29.5  | 4.19  |
| ZT5    | 54         | 5 | 1.3   | 49.5  | 92.2     | 1.66 | 70.7  | 0.8   | 134   | 40    |
| ZT6    | 58         | 5 | 74.5  | -20.1 | 102      | 1.54 | -13.2 | 6316  | 4656  | -11.7 |
| ZT7    | 65         | 5 | 45.3  | 5.3   | 66.9     | 2.86 | 41.1  | 33.9  | 67.4  | 4.12  |
| ZT8    | 78         | 5 | 99.3  | 26.2  | 47.2     | 3.59 | -8    | 25.48 | 49    | 9.3   |
| ZT9    | 80         | 6 | 126.3 | -3.4  | 73.2     | 1.8  | 34.9  | 38.3  | 74.9  | -7.29 |
| ZT9.5  | 90         | 5 | 106   | 6     | 59.5     | 2.6  | 15.2  | 79.8  | 54.8  | -1.33 |
| ZT10   | 100        | 5 | 248.5 | 24.4  | 29.2     | 7.8  | -18.3 | 16.9  | 31.4  | 13.5  |
| ZT11   | 115        | 5 | 9.4   | -4.9  | 50.2     | 3.28 | 67.1  | 25.2  | 50.3  | 2.19  |
| ZT12   | 124        | 4 | 142.5 | 16.6  | 123.2    | 1.58 | -45.3 | 45.2  | 90    | 2.35  |
| ZT13   | 130        | 5 | 10.6  | -12   | 77.6     | 1.94 | -63.6 | 38.8  | 77.6  | -1.4  |
| ZT13.5 | 155        | 5 | 311.8 | -31.3 | 37.7     | 5.07 | -33   | 20.58 | 39.3  | -10   |
| ZT14   | 166        | 5 | 86.2  | 24.7  | 45.9     | 3.73 | 3.4   | 9298  | 47.8  | 9.76  |
| ZT15   | 178        | 5 | 14.1  | -10.6 | 68.2     | 2.22 | -62.6 | 34.1  | 68.2  | -0.95 |
| ZN1    | 185        | 5 | 0.4   | -7.7  | 110.6    | 1.46 | 68    | 45    | 90    | 1.3   |
| ZN2    | 203        | 5 | 92.2  | -45.2 | 106.9    | 1.49 | 4.1   | 81.4  | 121   | -31   |
| ZN3    | 213        | 5 | 126   | -12.1 | 49       | 3.39 | 36.1  | 27.6  | 52    | -11.9 |
| ZN4    | 217        | 5 | 47.1  | -0.6  | 44.2     | 3.96 | 39.1  | 22.1  | 44.2  | 1.03  |
| ZN5    | 226        | 5 | 39.5  | 33.9  | 41.3     | 4.39 | 45.8  | 28.4  | 48.5  | 20.8  |
| ZN6    | 232        | 5 | 149.5 | 1.3   | 46.9     | 3.62 | 55.2  | 24    | 47.5  | -5.39 |
| ZN7    | 240        | 3 | 84.8  | 32.9  | 68.2     | 4.35 | 4.8   | 40.4  | 74.2  | 14.4  |
| ZN8    | 247        | 5 | 317.1 | -17.8 | 53.7     | 2.99 | -41.1 | 27    | 53.9  | -3.05 |
| ZN9    | 258        | 4 | 358.4 | 52.5  | 50.8     | 4.2  | 68.1  | 62    | 79.3  | 43.9  |

#### 4.3.3.3 Magnetic Polarity reconstruction of Zote section

Calculation for the magnetic polarity of Zote section includes Zote-Ngur (ZN) section as mentioned in 4.3.3. ZN section lies between Zote and Ngur section connecting the two sections. Since the lithological facies exposed within the section is more similar and with Zote section, and the attitude of rock layers more closely resembled they are grouped to represent a continuous section. By combining the two sections, a total of 143 samples collected from 26 distinct horizons were analysed. Several samples, especially from the topmost part of the section were discarded due to their fragile nature as they break during spinning procedures.

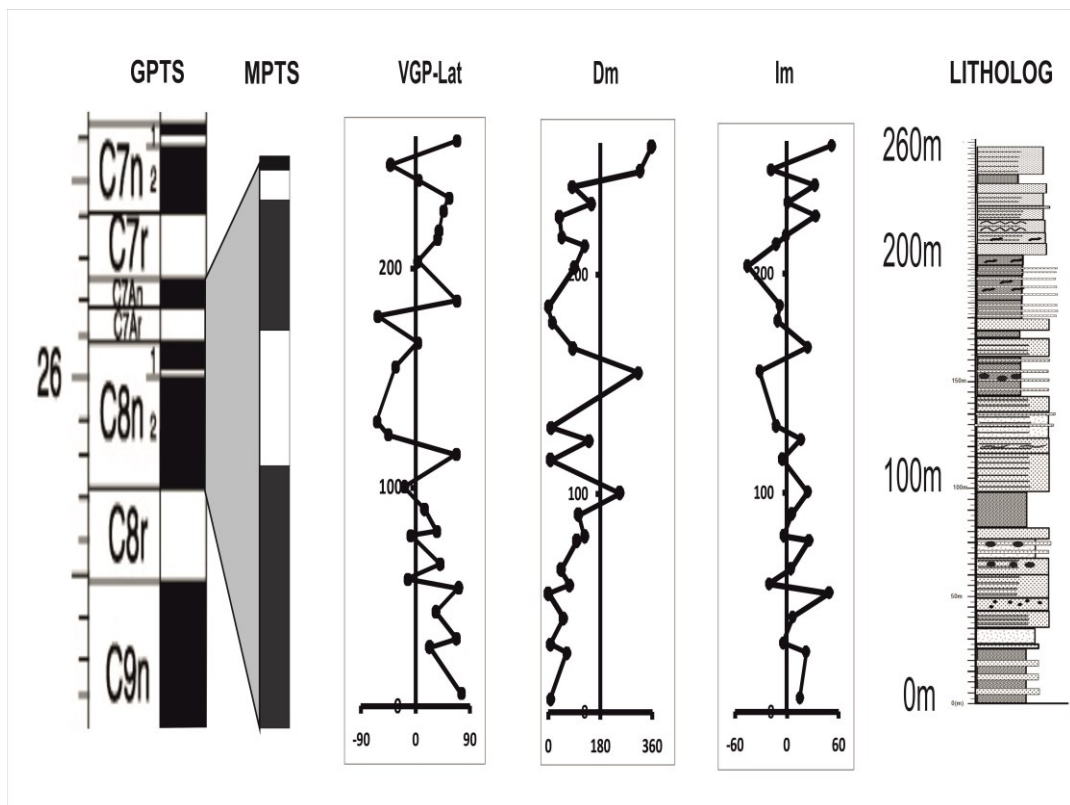


**Fig 4.8:** Magnetic polarity reconstruction of Zote (ZT) and Zote-Ngur (ZN) Section

Due to the absence of any age diagnostic features and previous work done in the Barail of Mizoram, matching the MPTS with GPTS of Cande and Kent (1995) was based on careful examination of the time interval between normal and reversal recorded in the rocks. Since this is the first discourse in determining the Chronostratigraphy of the area the MPTS and GPTS correlation can be questionable or not exactly precise.

From the VGP latitudes produced for the section, 3 normal and 2 reversal magneto-zones are obtained. The ages fall between ~26.554 Ma at the base to ~25.600 Ma at the top by matching with the GPTS magneto zones as shown in Table. 4.6. Total duration for the accumulation of 254m thick succession is estimated as ~0.954 Ma.

| S.N | GPTS EVENTS | Duration      | Stratigraphic level (m) |
|-----|-------------|---------------|-------------------------|
| 1   | C8n.2n      | 25.992-26.554 | 0-115                   |
| 2   | C8n.1n      | 25.823-25.951 | 185-240                 |
| 3   | C7An        | 25.600-25.648 | 258                     |

**Table 4.6:** Normal polarity events of Zote (ZT) and Zote-Ngur (ZN) Section

#### **4.3.4 Ngur Section (NG)**

This is the topmost part of the study area with an elevation of more than 1600m from mean sea level. The section exposes a 387m (excluding the 76.5m thick ZN section) thick succession of sandstone and shale where sandstone dominates the upper part of the section. 21 distinct units are recorded and 54 samples undergo demagnetization process taken from 9 sites.

##### **4.3.4.1 Thermal Demagnetization**

**NG1F:** From 100°C to 600°C the intensity decay curve shows a linear decrease in intensity with consistent direction all clustered in east quadrant of the spherical plot. This indicates a stable unicomponent system with the ChRM directions taken 500°C and 550°C having PCA value of 37.0/46.3/0.

**NG2C:** This specimen show similar pattern with the previous one with ChRM directions taken between 500°C and 550°C having PCA values 33.5/-25.2/0. The intensity decay, zijderveld and stereographic plots are also quite similar.

**NG3C:** From 100°C to 500°C the decay path follows a relatively linear path which indicates the presence of a strong and stable component. After this the intensity increases sharply followed by a rapid decline which may be a result of secondary magnetization during treatment process. ChRM direction is taken from 350°C and 400°C having PCA values 74.2/57.6/0.

**NG4F:** 80% of the intensity is removed at 100°C followed by a very gradual decay path till 400°C indicating the presence of two components. The intensity then rises by small amount at 450°C which is relatively stable till 500°C where it rises sharply till 600°C. The rapid increase may be due to acquisition of induced magnetism in



laboratory. 300°C-350°C is the point for stable ChRM component with PCA direction 48.8/10.3/0.

**NG5B:** Two components are identified in this specimen based on the decay curve and vector plots. The first component is completely removed at 400°C with a linear decay path from 100°C. The intensity then falls rapidly at 450°C followed by a steady decline till 550°C. The second component is identified as the stable ChRM component.

**NG6D:** The stereographic plot shows that the direction is clustered in the NNE quadrant with consistent pattern in the zijderveld diagram. The intensity decay curve shows a linear decay path from 100°C to 500°C along which the ChRM is taken. The specimen is a unicomponent system with PCA values 29.3/-47.7/0.

**NG7F:** From 100°C to 450°C the intensity decay curve shows a linear decay path followed by a slight increase with spurious directions. From the data presented the specimen is concluded as a unicomponent system having PCA of 51.4/-18.5/0.

**NG8B:** The intensity drops by 40% at 100°C which signifies the removal of a secondary component. From 300°C to 500°C the decay path maintains a gradual decline removing about 90% of total intensity. This is taken as the main component vector direction.

**NG9D:** The specimen shows a unidirectional signature with a linear decay pattern from 100°C to 450°C removing 90% of total intensity. The PCA direction is 90.4/-18.1/0 after which scattering in direction is observed.

#### 4.3.4.2 Alternating Field Demagnetization

**NG1A:** The specimen show similar pattern which is characteristic of 2 components. There is a steep decay path from 10mT to 30mT followed by a stable direction and decay path till 60mT. The stable component is selected between 30mT to 50mT with PCA value 53.3/30/0.

**NG2A:** There is sharp drop in intensity at 10mT where 80% of the intensity has been removed. After this the decay path follows a plateau like pattern till 80mT. The ChRM direction is taken from 30mT to 40mT.

**NG3C:** The intensity decreases by about 40% at 20mT, which signifies the removal of a secondary component having PCA values 56.5/6.7/5.0. The intensity then follows a linear decay path till 40mT which is where the stable vector component is taken with PCA direction of 27.8/5.2/0. The intensity then increases at 50mT due to secondary field attained during laboratory treatment.

**NG4B:** The ChRM direction is taken between 30mT and 50mT giving a PCA value of 74.6/-17/0 which shows a linear decline pattern. The first component follows a decrease pattern from 10mT which is completely removed at 20mT showing a PCA direction of 220/43.6/0.2.

**NG5D:** There are 3 components witnessed within this specimen all showing varying vector properties. The first component is removed at 10mT where more than 70% of the intensity is reduced showing a PCA value 338.7/0.3/5.0. The second component which is considered the stable ChRM direction is taken at 20mT with PCA value 18.4/44/0. The intensity then rises at 30mT descending to 40mT followed by a slight

increase at 50mT and falling to more than 80% of total intensity at 60mT after which it rises till 80mT.

**NG6D:** The sample shows a unicomponent system which shows a linear decay pattern from 10mT to 60mT removing 90% of total intensity. ChRM direction is taken from 20mT and 30mT showing PCA values 38.6/-2.2/0.

**NG7E:** There is a rapid and linear decay path observed between 10mT and 20mT with PCA direction 33.3/-0.6/0 which is considered the secondary component. The intensity then follows a constant path from 30mT to 40mT with a slight increase at 60mT. 30mT is taken as the point for ChRM direction having PCA values of 98.5/13.6/0.

**NG8D:** 10mT to 20mT there is a 70% removal of intensity with PCA value 30.8/-7.7/0 which is considered the first component. The second component shows a gradual rise in intensity till 40mT. This is followed by a stable component till 50mT which is taken as the region for ChRM direction giving PCA directions 7.5/26.7/0.

**NG9B:** Two components are removed from this specimen at 40mT and 70mT. The first component, which is considered the stable ChRM component, follows a gradual decay curve and consistent direction in zijderveld diagrams from 20mT to 40mT with PCA values 41.9/74.2/0. The path then experience a slight increase at 50mT which then gradually decline to 70mT with a PCA value of 29.2/33.5/22.5. The MAD is too high due to spurious directions due to attained laboratory induced field.

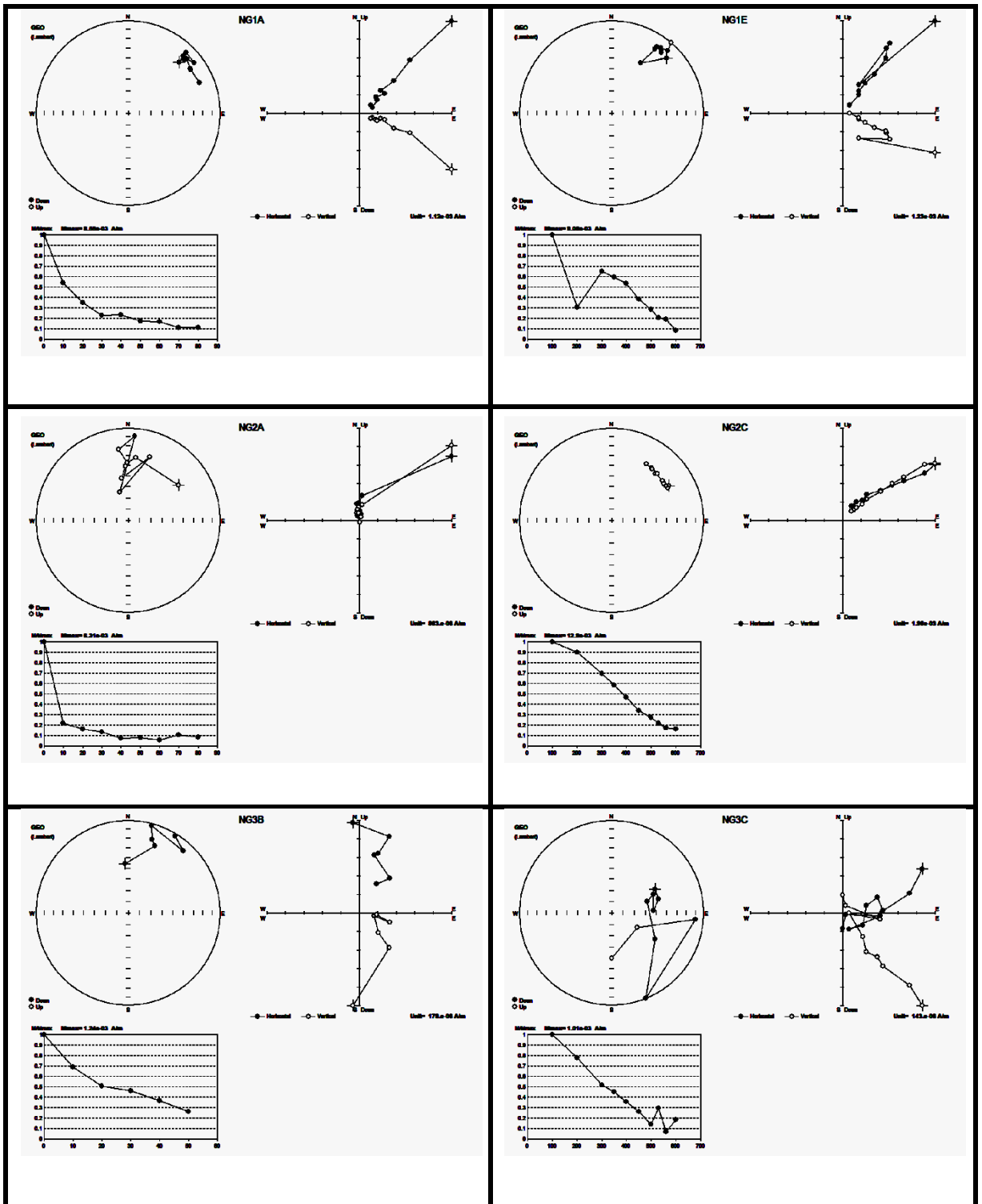


**Fig. 4.9(A):** Demagnetization plots [Stereonet, Zijderveld diagram (Zijderveld 1967) and intensity decay curve] for representative samples from Ngur Section.

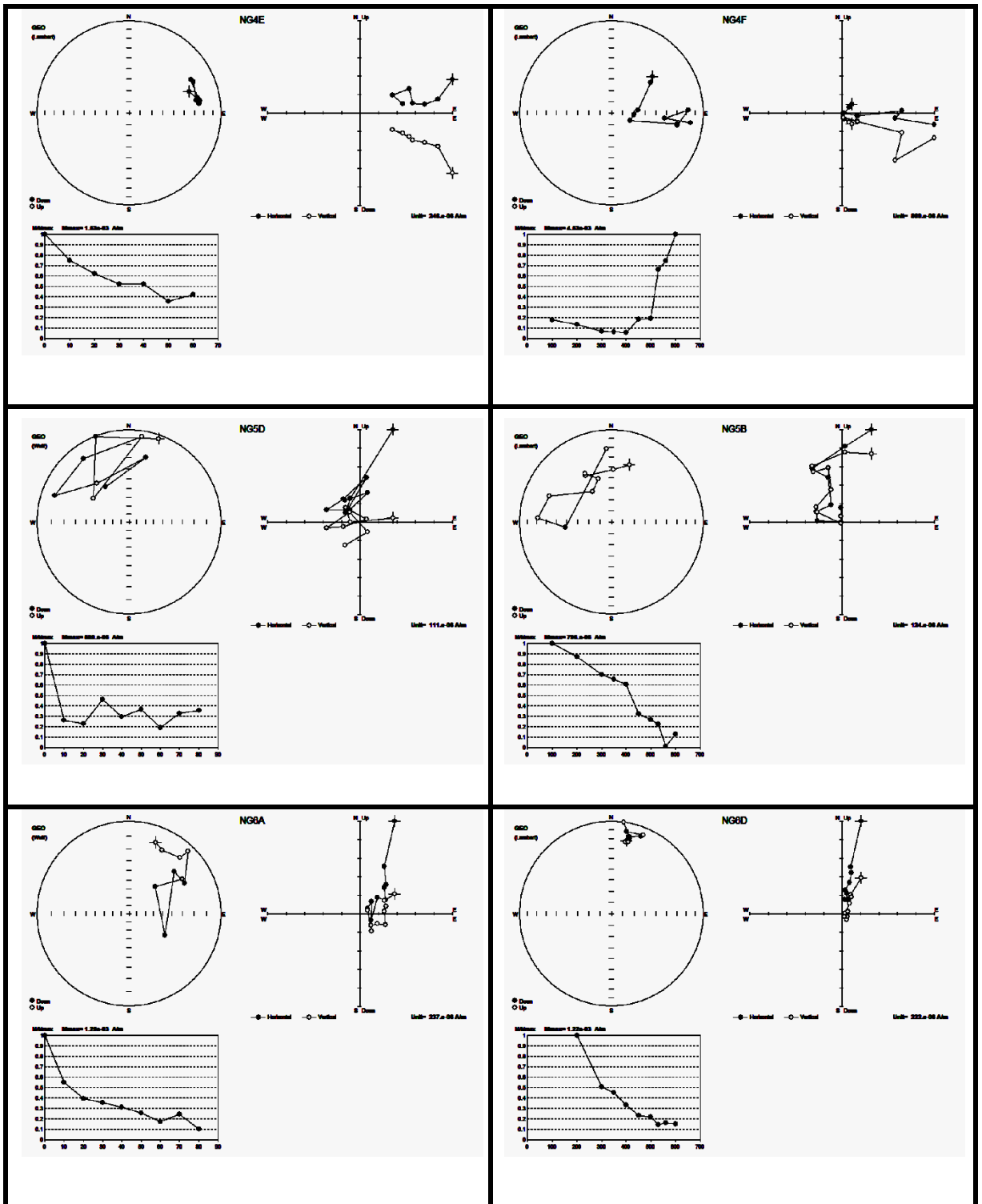


**Fig. 4.9(B):** Demagnetization plots [Stereonet, Zijderveld diagram (Zijderveld 1967) and intensity decay curve] for representative samples from Ngur Section.

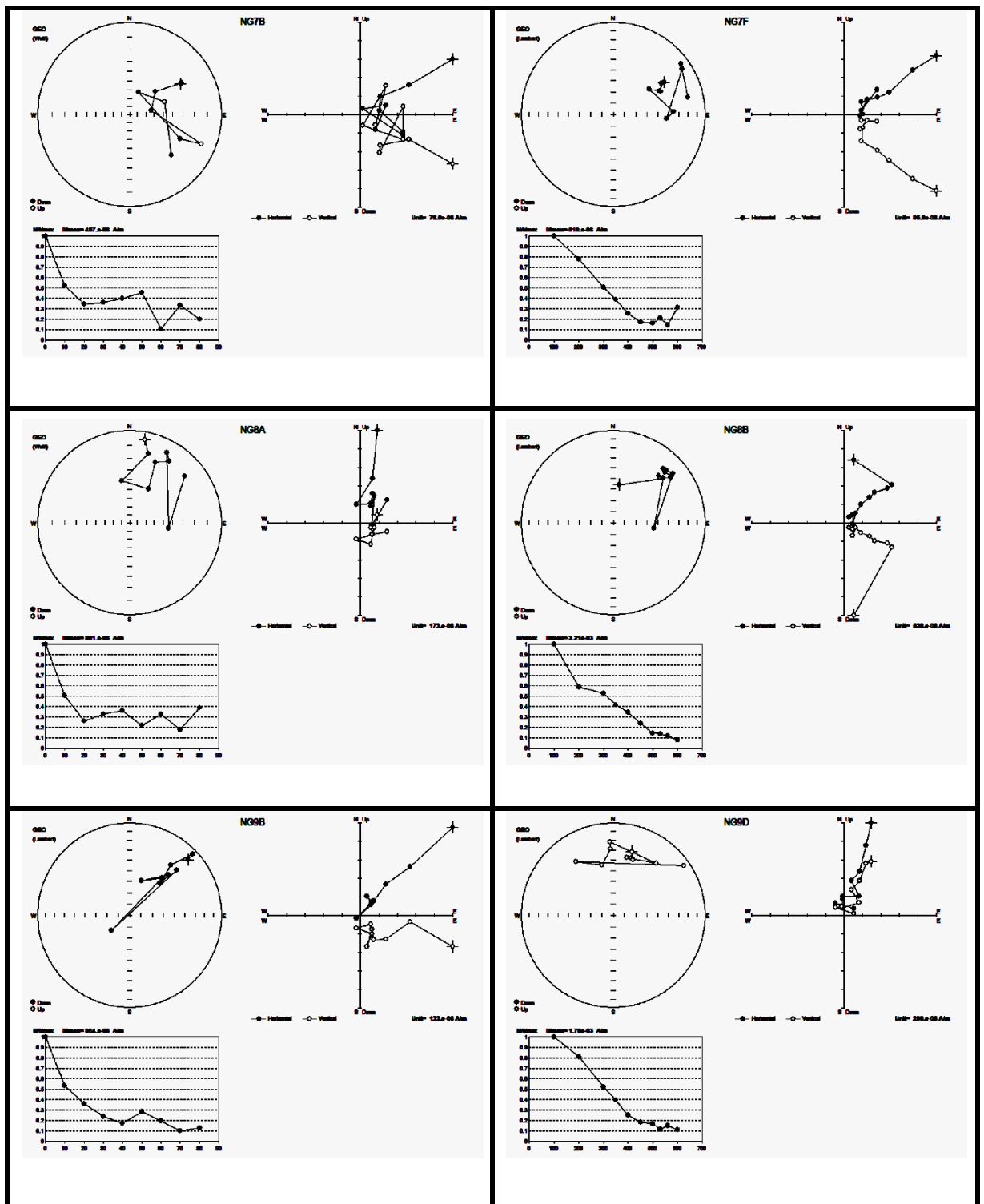


**Fig. 4.9(C):** Demagnetization plots [Stereonet, Zijderveld diagram (Zijderveld 1967) and intensity decay curve] for representative samples from Ngur Section.

#### 4.3.4.3 Magnetic Polarity reconstruction of Ngur section

The samples show overall good results in term of alternating field and thermal demagnetizations. Majority of the samples are of unicomponent system with gradual decay paths and consistent directions. Some of the samples which have a secondary component are of high intensity but relatively unstable. The ChRM direction generally falls at 20mT to 40mT for alternating field and 250°C to 500°C for thermal demagnetization. The total number of sites and samples collected from the end section is restricted due to damaged drill bit and problems with the drilling machine. 3-5 specimens for each site undergo demagnetization as a result of breakage of some specimen during cutting and spinning process.

| Site | n | Height (m) | Dm    | Im    | alpha 95 | k     | V.lat | dp   | dm   | P.lat |
|------|---|------------|-------|-------|----------|-------|-------|------|------|-------|
| NG1  | 6 | 25         | 40.6  | 22.5  | 17.4     | 15.72 | 44.9  | 10.2 | 18.8 | 13.9  |
| NG2  | 6 | 50         | 22.8  | -38.6 | 26.4     | 7.39  | -60.2 | 13.5 | 26.7 | -5.19 |
| NG3  | 6 | 87         | 58    | 47.2  | 38.1     | 4.04  | 25    | 31   | 48.6 | 27.2  |
| NG4  | 6 | 120        | 66.2  | 16    | 18.7     | 13.75 | 21.2  | 9.7  | 19.1 | 7.1   |
| NG5  | 4 | 165        | 343.5 | -21.6 | 88.3     | 2.07  | -57.9 | 44.7 | 88.9 | -3.99 |
| NG6  | 6 | 220        | 41.3  | -32.4 | 47       | 2.99  | -39.9 | 27.8 | 51.1 | -14.3 |
| NG7  | 6 | 270        | 44.6  | -0.2  | 40.01    | 3.7   | 41.4  | 20   | 40   | 1.7   |
| NG8  | 6 | 340        | 45.3  | -1.1  | 33.4     | 4.9   | 40.7  | 16.7 | 33.4 | 1.2   |
| NG9  | 6 | 385        | 81.1  | 37.9  | 59.4     | 2.23  | 6.8   | 37.5 | 66.7 | 17.2  |

**Table: 4.7.** Number of samples and name, declination and inclination mean, sample height,  $k$  &  $\alpha_{95}$  (Fisher statistical parameters; concentration parameter and 95% cone of confidence, VGP latitude (normal and reversal)

Calculation is done following the steps and techniques mentioned in the methodology chapter. All the demagnetized specimens from each site and the mean direction are calculated using fisher statistics (Fisher, 1953). The Virtual Geomagnetic Pole (VGP) is then given after calculation of mean inclination and declination directions, correction of bedding directions.

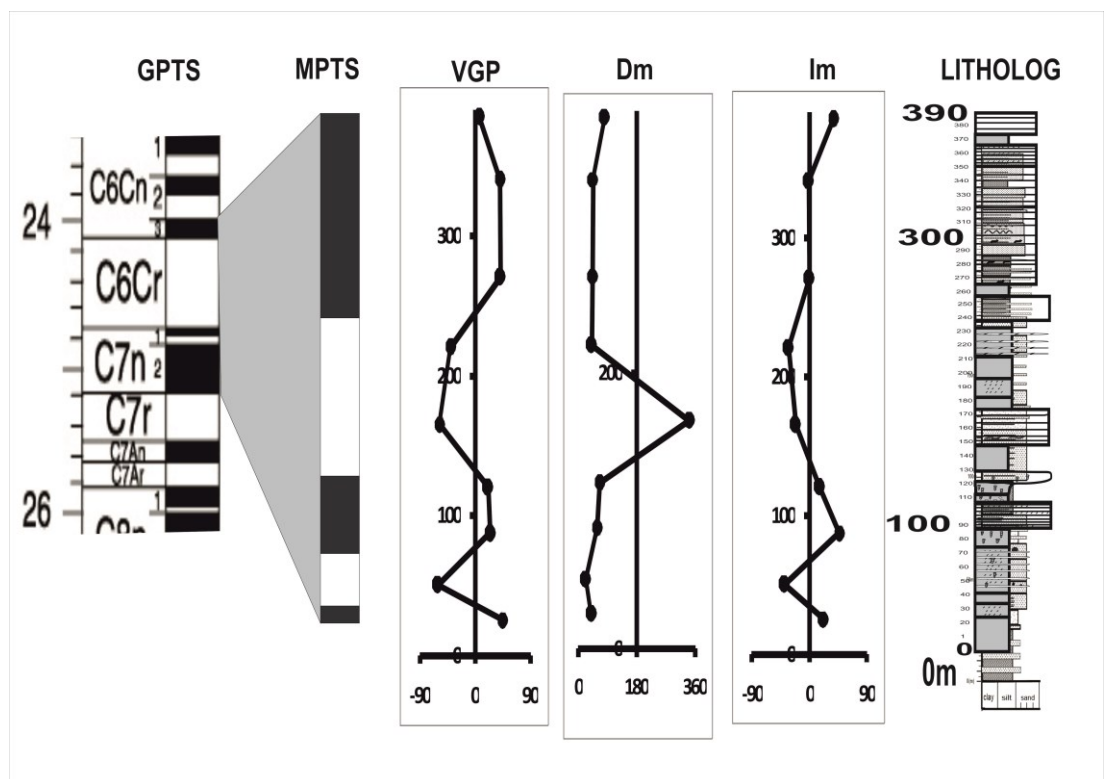


**Fig 4.10:** Magnetic polarity reconstruction of Ngur (NG) Section

Since there is no datum line for any of the Barial rocks exposed in Mizoram, and in particular the study area, correlation of MPTS with the GPTS of Cande and Kent, (1995) was challenging. The correlation is made based on experienced opinions and careful calculation of interval and pattern of magneto-zones combined field experience in stratigraphic and sedimentology.



3 normal and 2 reversal magneto-zones are generated from the VGP latitudes. The age of the oldest part (base) of the section is ~25 Ma with the youngest (top) at ~23.999 Ma after correlation with GPTS magneto zones as shown in Table. 4.8. Total duration for the accumulation of 387m thick succession is estimated as ~1Ma.

| <b>S.N</b> | <b>GPTS EVENTS</b> | <b>Duration</b> | <b>Stratigraphic level (m)</b> |
|------------|--------------------|-----------------|--------------------------------|
| 1          | C7n.2n             | 24.835-25.000   | 0-25                           |
| 2          | C7n.1n             | 24.730-24.781   | 87-120                         |
| 3          | C6Cn.3n            | 23.999-24.118   | 270-385                        |

**Table 4.8:** Normal polarity events of Ngur Section

## **CHAPTER V**

### **RATE OF SEDIMENTATION AND STRATIGRAPHIC CORRELATION OF MIZORAM**

#### **5.1 INTRODUCTION**

The rate at which sediments may accumulate within a depositional basin may be controlled by various factors like tectonic evolution, paleoenvironment and depositional environment etc. The normal and reversal pattern generated from the VGP is plotted against the measured litholog for the generation of Magnetic Polarity Time Scale (MPTS) for the area. The MPTS is then correlated with the Global Polarity Time Scale (Cande and Kent, 1995). The time interval and duration of events taken from the GPTS is compared with the thickness of the sections where MPTS is obtained, giving the pace at which the thickening of sediments takes place and the variations in the speed of deposition. Sediment Accumulation Rate (SAR) is measured in terms cm/ka.

#### **5.2 SEDIMENT ACCUMULATION RATE OF RUANGLANG SECTION (RT)**

Ruantlang section constitutes of the lowest part of the study area for the present research which comprises of a 514.3 m thick succession of sedimentary units dominated by shales. Sediment Accumulation Rate (SAR) was calculated for the section which shows 5 normal and 4 reversals falling between ~29.662 Ma at the base to 27.087 Ma at the top with a total duration of ~2.635 Ma. The SAR at the bottom part of the section (33.5 cm/ka) is much higher compared to the younger beds dropping to 28.93 cm/ka in the middle section to 11.05 cm/ka at the top as shown in

figure 6.1. The difference in the rate of sedimentation for the given section is reflected by the change in facies within the section as the lower part shows more abundance of sandstone formations compared to the upper parts which is dominantly composed of argillaceous materials. The average sedimentation rate for the section is 19.5 cm/ka.

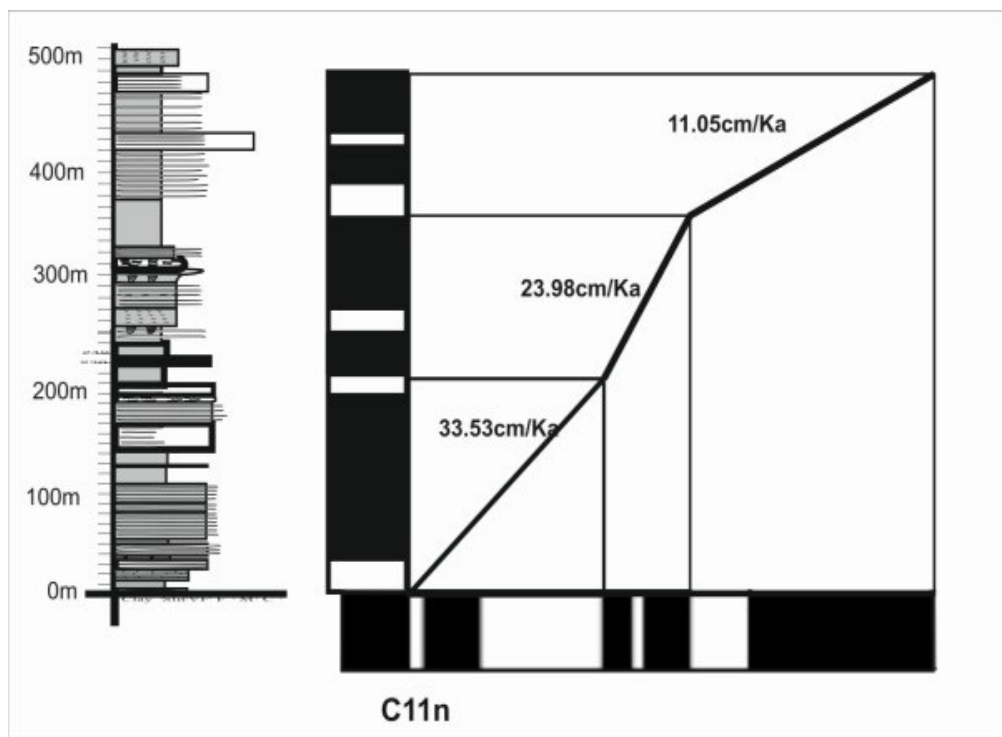


**Fig. 5.1:** Sediment Accumulation Rate (SAR) of Ruantlang Section.

| S.N | GPTS EVENTS      | Duration             | Thickness (m) | Rate (Cm/ka) |
|-----|------------------|----------------------|---------------|--------------|
| 1   | C11n.1n-C10r     | 29.662-28.744(0.918) | 206           | 33.53cm      |
| 2   | C10n.2n- C10n.1n | 28.745-28.283(0.462) | 206-349       | 23.98        |
| 3   | C9r- C9n         | 28.282-27.027(1.255) | 349-484       | 11.05        |

**Table 5.1:** Estimation of SAR using magnetostratigraphic ages from Ruantlang section.

### 5.3 SEDIMENT ACCUMULATION RATE OF ZOTE SECTION (ZT)

The sediment accumulation rate for Zote section was calculated by correlating the 3 normal and 2 reversal magneto zones with the corresponding GPTS polarity events. The total duration for accumulation of 254m thick succession was estimated as ~0.954 Ma with an average sedimentation rate of 27.5 cm/ka. SAR calculated for the lower part of the section is 48.32 cm/ka which was quite high compared to the upper section with a SAR of 21.87 cm/ka. The lower part of the section is composed of massive brown sandstones with mud clast and ball and pillow structure which indicate a high velocity depositional environment.

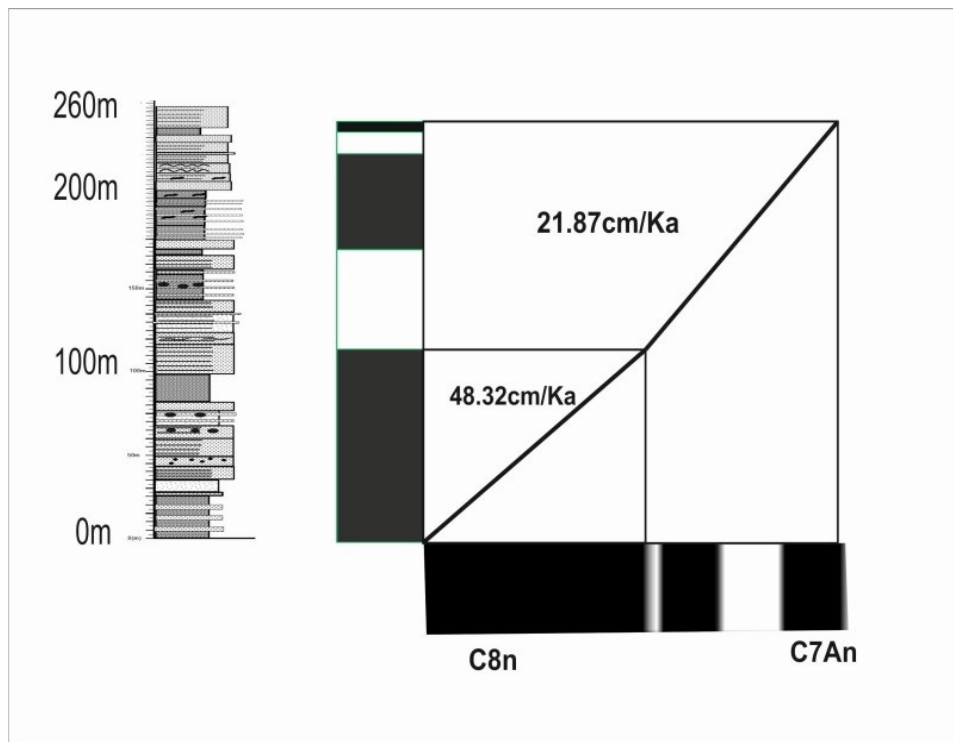


**Fig. 5.2:** Sediment Accumulation Rate (SAR) of Zote (ZT) Section

| S.N | GPTS EVENTS | Duration               | Thickness (m) | Rate (cm/ka) |
|-----|-------------|------------------------|---------------|--------------|
| 1   | C8n.2n      | 26.554- 25.992 (0.562) | 115           | 48.32        |
| 2   | C8n.1r-C7An | 25.991-25.648 (0.343)  | 115-258       | 21.87        |

**Table 5.2:** Estimation of SAR using magnetostratigraphic ages from Zote section.

#### 5.4 SEDIMENT ACCUMULATION RATE OF NGUR SECTION (NG)

3 normal and 2 reversal magneto-zones are generated from Ngur section. Total duration for the accumulation of 254m thick succession is estimated as ~1Ma with an average rate of 38.9 cm/ka, which is the highest in the study area. The lower portion which is dominated shales show a low SAR of 8.92 cm/ka while the Upper part which is composed of sandstones have a moderate SAR value of 41.03cm/ka.

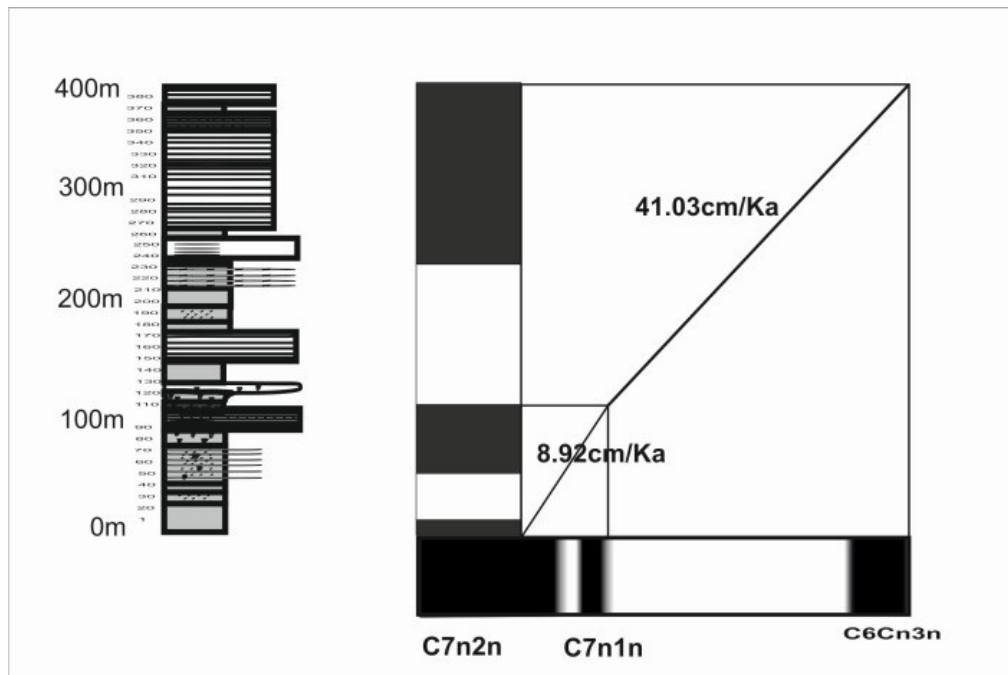


**Fig. 5.3:** Sediment Accumulation Rate (SAR) of Ngur (NG) Section

| <b>S.N</b> | <b>GPTS EVENTS</b>    | <b>Duration (Ma)</b>       | <b>Thickness (m)</b> | <b>Rate (cm/ka)</b> |
|------------|-----------------------|----------------------------|----------------------|---------------------|
| <b>1</b>   | <b>C7n.2n- C7n.1n</b> | <b>25.000-24.730(0.27)</b> | <b>120</b>           | <b>8.92</b>         |
| <b>2</b>   | <b>C6Cr- C6Cn.3n</b>  | <b>24.729-23.999(0.73)</b> | <b>120-385</b>       | <b>41.03</b>        |

**Table 5.3:** Estimation of SAR using magnetostratigraphic ages from Ngur section.

## **5.5 SEDIMENT ACCUMULATION RATE (SAR) SUMMARY FOR ALL SECTIONS**

Generation of Sediment Accumulation Rate (SAR) is one of the primary objectives of the present study as it helps to better understand the dynamics of the depositional history of the area. The SAR calculated for the study area is quite low compared to the overlying Surma and Tipam group of rocks as mentioned in the review of literature chapter. Since tectonic evolution, paleo-environment, location etc. can play a crucial role in the rate at which sediment accumulate within a depositional environment, careful examination and correlation is required.

The overall lithostratigraphy and geology of the sections in the study area depicts a coarsening upward environment comprising of sediment from deeper, low energy environments to a much shallower high velocity environment. Shales and siltstones dominates the lower parts with a gradual increase in grain size from very fine to fine and fine to medium sandstones in the upper part of the study area. Hence the average rate of sedimentation for each section increases from bottom to top from low rate of sedimentation to moderate to moderate high SAR. Comparison of SAR for the different sections is given in the table below.

|                               | <b>Ruantlang Section</b> | <b>Zote Section</b> | <b>Ngur Section</b> |
|-------------------------------|--------------------------|---------------------|---------------------|
| Average rate of sedimentation | 19.5 cm/ka               | 27.5 cm/ka          | 38.9 cm/ka          |
| Peak of sedimentation         | 33.53 cm/ka              | 48.32 cm/ka         | 41.03 cm/ka         |
| Lowest rate of sedimentation  | 11.05 cm/ka              | 21.87 cm/ka         | 8.92 cm/ka          |
| Thickness of sedimentation    | 514.3m                   | 254m                | 387m                |
| Duration of sedimentation     | ~2.635 Ma                | ~0.954 Ma           | ~1 Ma               |
| Magnitude of sedimentation    | Low                      | Moderate            | Moderate            |

**Table 5.4:** Comparison and summary of SAR for Ruantlang, Zote and Ngur sections.

## **5.5 STRATIGRAPHIC CORRELATION FOR MIZORAM**

The stratigraphic succession of Mizoram was constructed by various workers following the stratigraphic framework of Surma basin established of Evans, (1932,1964); Sengupta, (1966); Raju, (1968); Alam (1989; 1991; 1995; and 1997) and many more. Following the works of previous researchers Karunakaran, (1974); Ganju (1975); Tiwari and Kachhara, (2003), Mandaokar, (2000) and Tiwari *et al*, (2011; 2012) constructed the stratigraphic succession of Mizoram dividing it into three distinct units. The lowest part of the succession is the +3000m thick Barail

group of rocks of upper Paleogene period. The barail rocks are overlain by a Surma group of rocks consisting of the Bhuban and Bokabil formation with about 6000m in thickness ranging from early to middle Miocene. Rocks of upper Bhuban and middle Bhuban the most common type of formation exposed throughout the state of Mizoram. The youngest and uppermost unit is the +900m thick Tipam group of rocks which overlies the Surma group and ranges from late Miocene to early Pliocene. Tipam sandstones are considered to be fluvial deposits based on their grain size and friable nature.

The pioneer work for magnetostratigraphy in Northeast India was carried out by Worm *et al.*, (1998). Magnetostratigraphy was done in the Hari river section in Meghalaya. In Mizoram, magnetostratigraphy was done for the first time by Tiwari *et al.*, (2007) where he studied the magnetic polarity recorded in the rocks exposed along Bawngkawn and Durtlang which is located to the North- northeast of Aizawl city. The Bawngkawn-Durtlang (BD) section delineated by Tiwari marks the oldest part of the Bhuban formation which falls under middle Bhuban at ~21.7 Ma falling at the top of C6A. An magnetozone. 7 normal and 7 reverse magneto zones were recorded from the section with a total duration of 6.6 Ma. The SAR for the 560m thick succession was quite low at an average of 8.48 cm/ka. Paul *et al.*, (2014) delineated 3 normal and 4 reversals at Kolasib-Rengtekawn(KR) section ranging between ~17.2Ma to ~14.9Ma and is considered a continuation of the BD section where the uppermost part of the section is dated as ~16.014 Ma. The 445m thick successions also have a low sedimentation rate of ~21.52 cm/ka with a total duration of ~2.3 Ma. A stratigraphic level of 220m in this section was taken as datum line as it records fossils dating back to Burdigalian (Mazumder, 2004).



Malsawma *et al.*, (2010) and Malsawma, (2011) carried out magnetostratigraphic study in Tuirial and Sairang section which was considered as the Upper Bhuban formation from sedimentology and lithological analysis. The two sections were correlated falling into the same age range between ~12.5 to ~8Ma and ~9.8 to ~8.3 Ma respectively. The average SAR for the sections was also quite high (33.6 cm/ka and 30.17 cm/ka) compared to BD and KR sections of middle Bhuban formation. Magnetostratigraphy was done for two sections in Kolasib district by Paul in 2013, where he analyzed the Tipam group of rocks. Zero point –Saihapui and Thuchhuahen sections expose Tipam sandstones and Tipam-Dupitila transition. 3 normal and 3 reversals in Zero point-Saihapu section and 1 normal and 1 reversal in Tuichhuahen section were recorded. SAR of the two sections was ~82.49 cm/ka and ~74.12 cm/ka. C2An.3n, C3n.1n, C3n.2n magnetozone were delineated for the two sections with a total time period of ~1.5 Ma. The magnetozone recorded from this section is delineated with the Hari river section obtained by Worm et al., in 1998. The correlated sections fall in the late Miocene to early Pliocene epoch both characterized by Tipam and Bokabil group of rocks and representing the youngest rocks recorded within Mizoram.

The present area of study exposes Barail group of rocks which is considered to be of Oligocene age. Ruantlang section comprises of a 514.3m thick succession where the SAR for selected intervals is 33.5cm/ka, 28.93cm/ka and 11.05cm/ka with an average rate of 19.5 cm/ka. 5 normal and 4 reversals were recorded falling between ~29.662 Ma to ~27.087 Ma with a total duration of ~2.635 Ma. Ruantlang constitutes the lowest part of the study area and the corresponding magnetozone C11n.1n (29.662) is now the oldest recorded stratigraphic layer in Mizoram. The

average SAR for Zote section (27.5 cm/ka) is calculated over a time period of ~0.954 Ma. Zote section overlies Ruantlang section by a 254m thick succession of sandstone, siltstone and shale sequence falling between ~26.554 Ma to ~25.600 Ma. The uppermost section Ngur is considered to be the youngest of the Barail rocks recorded within the study area. The upper part at 23.990 Ma almost transitioned from late Oligocene to early Miocene epoch with magnetozone C6Cn.3n. The oldest rock recorded in the BD and KR sections of the middle Bhuban formations was ~21.7 Ma falling at the top of C6A.An. The overall time duration for the recorded sections in Champhai area is ~5.663 Ma with corresponding magnetozones C6Cn.3n-23.999 and C11n.1n-29.662.

Almost all the stratigraphic horizons of Mizoram has been studied using Magnetostratigraphy ranging from Oligocene (29.662) to early Pliocene (3.330) having a total duration of ~26.332 Ma.

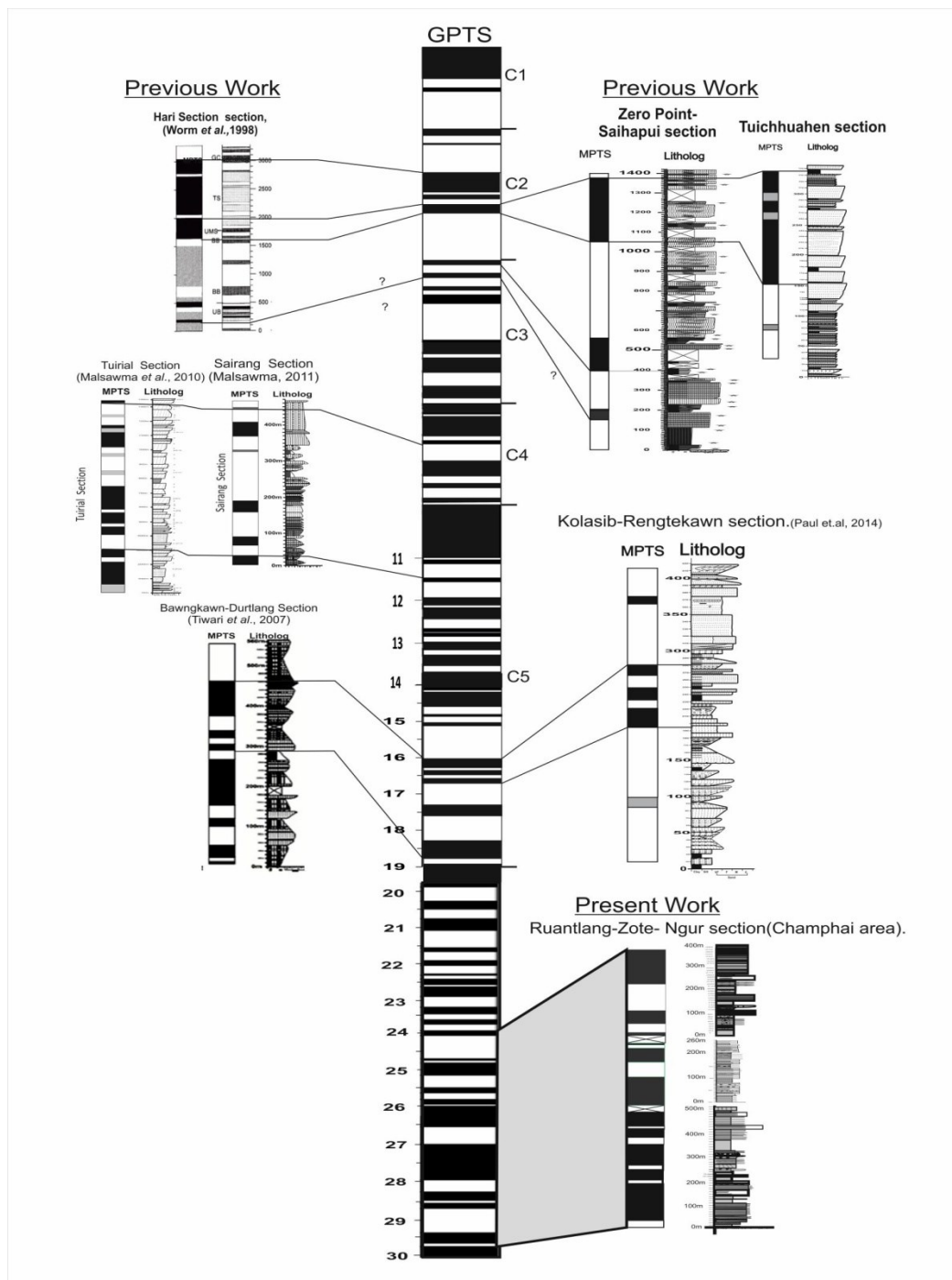


**Fig 5.4:** Correlation of established Magnetic Polarity Scales from various sections within Mizoram and Hari river section (Worm *et al.*,1998, Tiwari *et al.*, 2007; Malsawma *et al.*, 2010, Malsawma, 2011; Paul, 2013; Paul *et al.*, 2014.

## CHAPTER VI

### SUMMARY AND CONCLUSIONS

Tectonic evolution of the Bengal basin started with the collision of Indian plate with Eurasia during early Paleogene period resulting in the initiation of Himalayan orogeny. The Himalayan ranges are the most majestic inland mountain range which forms the main geological framework of the area and stretches over a length of 2500km trending east-west with a width of about 300kms in north-south direction. The hilly terrain of Mizoram is entrenched in the Surma Basin which makes part of the Greater Bengal and is one the thickest sedimentary basins in the world with ongoing sedimentation till date. Karunakaran, (1974) and Ganju, (1975) grouped the sedimentary sequence of Mizoram into 3 distinct groups which are Barail, Surma and Tipam. Over the years with more geological information as a result of advancement in science and technologies revisions have been made by Tiwari and Kachhara, (2003), Mandaokar, (2000) and Tiwari *et al.*, (2011, 2012). Establishment of a well deciphered stratigraphic framework is necessary since the area is well known for its hydrocarbon deposits and susceptibility to natural disasters especially earthquakes and landslides.

The study area is around Champhai town which is one of the district capitals of Mizoram situated to the Eastern part of the state and about 190 km from Aizawl city, the capital of Mizoram state. Three sections were selected for this study from roadside exposures running along the south to northeast and north-northeast direction from Champhai town. The proposed area of study belongs to Barail succession which

is the only Paleogene rocks reported in Mizoram till date. The existence of Barial group in Mizoram was debatable as some of the earlier geological and stratigraphic work does not acknowledge its presence. Stratigraphic correlation of parts of Mizoram have been carried out over the years using Magnetostratigraphy covering the Northern (Kolasib District) and Central (Aizawl District) part of Mizoram where Tipam and Surma group of the Mio-Pliocene periods were analyzed leading to a well established stratigraphic framework (Tiwari *et al.*, 2007; Malsawma *et al.*, 2010; Malsawma, 2011; Paul *et al.*, 2013; Paul, 2014). Since no detailed magnetostratigraphic or paleomagnetic work is available for the Barail succession of Mizoram, Magnetostratigraphy will serve as a robust tool in establishing the chronostratigraphic framework and correlation with already establish Surma sequences in various parts of Mizoram.

## **LITHOSTRATIGRAPHY**

Three sections were selected for this study from roadside exposures running along the south to northeast and north-northeast direction from Champhai town. The first section is located to the South of Champhai town and is named Ruantlang section (RT). The second section Zote (ZT) lies to the east of Champhai with plain area lying in between the first two sections. The Ngur section (NG) is the third section and runs along the roadside exposures in the north-northeast direction from Zote.

Ruantlang section (RT) exposes a 514.3m thick succession of rocks representing the lower part of the Barail exposures in this area. The rocks exposed in Ruantlang

section are dominantly argillaceous with occasional sandstone beds. The thickness of sandstone beds vary from a few centimeters to more than a meter and are mostly very fine to fine grained. Shales are dominant throughout the area showing colors ranging from light to dark grey and little pale olive green coloration. The shales are mostly clayey to silty shales and shows different form of weathering patterns like fissility, spheroidal and splintary.

Zote section exposes a 117.5m thick sedimentary succession which is mainly composed of intermixing and alternation of sandstone and shale. The section can be interpreted as a coarsening upward type of environment since shale is more common in the lower parts with an increasing grain size sequence leading to a more sandy top section. Mud clast, ball and pillow structure are occasionally found within the sandstone beds. Shale makes up a huge portion of the section and are mostly found alternating with sandstone bed and intermixing with sand, forming silty-sandstone formation in some parts of the exposure.

Ngur section exposes a 387m thick sedimentary succession which is mainly composed of sandstones, shales and sandstone shale alternations. In terms of depositional environment, the section is believed to represent the shallowest part of the study area. The sandstones show varying colors with brown sandstones with different sedimentary structures like heterolithic bedding, cross lamination and mud-clast which may be interpreted as a shallow marine environment of deposition. The shales are splintary and show spheroidal weathering structures with different shades grey color and are bioturbated.

## MAGNETIC MINERALOGY

To develop a better understanding regarding the influence of magnetic minerals in rocks, the nature of the magnetic materials has to be worked out in terms of several parameters including mineralogy, grain size and concentration. Investigation of magnetic minerals will help to establish authentic magnetostratigraphic correlation. The sections are analyzed based on the change in lithofacies within the sections. The study area is divided into two sections for this study viz. Ruantlang section and Zote-Ngur section.

Ruantlang section shows an overall dominance of ferrimagnetic fine grained SD grains. The main carrier mineral is magnetite with of varying grain size and magnetic domain. There is also increase in the concentration of high coercive minerals possibly haematite in some zones. Unit V shows a period of quiescence with linear trends. The SIRM value decreases slightly to the top which may indicate decrease in concentration and increasing coercivity shown by BoCR increasing trend. The uppermost unit is characterized by concentration and MD grains shown by  $\chi_{ARM}/SIRM$  ratio and decreasing ARM values.

Zote-Ngur section represents the upper part of the study area with a noticeable change in lithology from argillaceous to sand dominated facies and is divided into VIII zones. The general increase in the abundance of hard magnetic minerals like goethite and haematite as shown by the S-ratio and BoCR patterns may signify shallower oxidizing environments. The zones dominated by sandstones show high values of  $\chi_{ARM}/SIRM$  ratio, SIRM and  $\chi_{lf}$  all show increasing trend which suggest increasing concentration of SSD-SD grains.

## **MAGNETOSTRATIGRAPHY**

Magnetostratigraphic discourse in all three sections Ruantlang, Zote and Ngur was completed by alternating field and thermal demagnetization processes. The correlation of MPTS with the GPTS was done by iterative matching with careful consideration of the duration of magnetozones and magnetic mineralogy due to absence of datum line for precise matching.

### **RUANTALNG SECTION (RT)**

Ruantlang section exposes a 514.3m thick succession of rocks representing the lower part of the Barail exposures in this area. 31 distinct units were recorded in the section where a total of 108 specimen collected from 18 sites was demagnetized under alternating field and thermal demagnetization. Ruantlang Section (RT) displays 5 normal and 4 reversal magneto-zones showing differing normal periodicities and quite similar interval among the reversal stage. The GPTS correlated ages of Ruantlang section falls between ~29.662 Ma at the base to 27.087 Ma at the top with a total duration of ~2.635 Ma.

### **ZOTE SECTION (ZT)**

A total of 143 samples collected from 26 distinct horizons were analyzed. Due to the absence of any age diagnostic features and previous work done in the Barail of Mizoram, matching the MPTS with GPTS of Cande and Kent, (1995) was based on careful examination of the time interval between normal and reversal recorded in the rocks. Since this is the first discourse in determining the



Chronostratigraphy of the area the MTPS and GPTS correlation can be questionable or not exactly precise. From the VGP latitudes produced for the section, 3 normal and 2 reversal magneto-zones are obtained. The ages fall between ~26.554 Ma at the base to ~25.600 Ma at the top by matching with the GPTS magneto zones. Total duration for the accumulation of 254m thick succession is estimated as ~0.954 Ma.

### **NGUR SECTION (NG)**

The samples show overall good results in term of alternating field and thermal demagnetizations.. The ChRM direction generally falls at 20mT to 40mT for alternating field and 250°C to 500°C for thermal demagnetization. Since there is no datum line for any of the Barial rocks exposed in Mizoram, and in particular the study area, correlation of MPTS with the GPTS of Cande and Kent, (1995) was challenging. The correlation is made based on experienced opinions and careful calculation of interval and pattern of magneto-zones combined field experience in stratigraphic and sedimentology. 3 normal and 2 reversal magneto-zones are generated from the VGP latitudes. The age of the oldest part (base) of the section is ~25 Ma with the youngest (top) at ~23.999 Ma after correlation with GPTS magneto zones. Total duration for the accumulation of 387m thick succession is estimated as ~1Ma.

### **SEDIMENT ACCUMULATION RATE (SAR)**

The time interval and duration of events taken from the GPTS is compared with the thickness of the sections where MPTS is obtained, giving the pace at which

the thickening of sediments takes place and the variations in the speed of deposition. Sediment Accumulation Rate (SAR) is measured in terms cm/ka.

### **RUANTALNG SECTION (RT)**

The average sedimentation rate for ka for Ruantlang section is 19.5 cm/ ka. The SAR at the bottom part of the section (33.5.cm/ka) is much higher compared to the younger beds dropping to 28.93cm/ka in the middle section to 11.05cm/ka at the top. The difference in the rate of sedimentation for the given section is reflected by the change in facies within the section as the lower part shows more abundance of sandstone formations compared to the upper parts which is dominantly composed of argillaceous materials.

### **ZOTE SECTION (ZT)**

The sediment accumulation rate for Zote section was calculated by correlating the 3 normal and 2 reversal magneto zones with the corresponding GPTS polarity events. The total duration for accumulation of 254m thick succession was estimated as ~0.954 Ma with an average sedimentation rate of 27.5 cm/ka. SAR calculated for the lower part of the section is 48.32 cm/ka which was quite high compared to the upper section with a SAR of 21.87 cm/ka. The lower part of the section is composed of massive brown sandstones with mud clast and ball and pillow structure which indicate a high velocity depositional environment.

## **NGUR SECTION (NG)**

3 normal and 2 reversal magneto-zones are generated from Ngur section. Total duration for the accumulation of 254m thick succession is estimated as ~1Ma with an average rate of 38.9 cm/ka, which is the highest in the study area. The lower portion which is dominated shales show a low SAR of 8.92 cm/ka while the Upper part which is composed of sandstones have a moderate SAR value of 41.03cm/ka.

## **MAGNETOSTRATIGRAPHIC CORRELATION**

The pioneer work for magnetostratigraphy in Northeast India was carried out by Worm *et al.*, (1998) in the Hari river section in Meghalaya. In Mizoram, Tiwari *et al.*, (2007) studied the magnetic polarity recorded in the rocks exposed along Bawngkawn and Durtlang which is located to the North- northeast of Aizawl city. The Bawngkawn-Durtlang (BD) section delineated by Tiwari marks the oldest part of the Bhuban formation which falls under middle Bhuban at ~21.7 Ma falling at the top of C6A. An magnetozone. Paul *et al.*, (2014) delineated 3 normal and 4 reversals at Kolasib-Rengtekawn(KR) section ranging between ~17.2Ma to ~14.9Ma and is considered a continuation of the BD section where the uppermost part of the section is dated as ~16.014 Ma. Malsawma *et al.*, (2010) and Malsawma, (2011) delineated section two sections in Tuirial and Sairang falling into the same age range between ~12.5 to ~8Ma and ~9.8 to ~8.3 Ma respectively. The average SAR for the sections was also quite high (33.6 cm/ka and 30.17 cm/ka) compared to BD and KR sections of middle Bhuban formation. Paul, 2013, analyzed the Tipam group of rocks from Zero point –Saihapui and Thuchhuahen. 3 normal and 3 reversals in Zero point-

Saihapu section and 1 normal and 1 reversal in Tuichhuahen section were recorded. SAR of the two sections was  $\sim 82.49$  cm/ka and  $\sim 74.12$  cm/ka. C2An.3n, C3n.1n, C3n.2n magnetozones were delineated for the two sections with a total time period of  $\sim 1.5$  Ma. The magnetozones recorded from this section is delineated with the Hari river section obtained by Worm *et al.*, in 1998. The correlated sections fall in the late Miocene to early Pliocene epoch both characterized by Tipam and Bokabil rocks and representing the youngest rocks recorded in Mizoram.

Ruantlang section comprises of a 514.3m thick succession where the SAR for selected intervals is 33.5.cm/ka, 28.93cm/ka and 11.05cm/ka with an average rate of 19.5 cm/ka. 5 normal and 4 reversals were recorded falling between  $\sim 29.662$  Ma to  $\sim 27.087$  Ma with a total duration of  $\sim 2.635$  Ma. Ruantlang constitutes the lowest part of the study area and the corresponding magnetozones C11n.1n (29.662) is now the oldest recorded stratigraphic horizon in Mizoram. The average SAR for Zote section (27.5 cm/ka) is calculated over a time period of  $\sim 0.954$  Ma. Zote section falls between  $\sim 26.554$  Ma to  $\sim 25.600$  Ma. The uppermost section Ngur is considered to be the youngest of the Barail rocks recorded within the study area. The upper part at 23.990 Ma almost transitioned from late Oligocene to early Miocene epoch with magnetozones C6Cn.3n. The oldest rock recorded in the BD and KR sections of the middle Bhuban formations was  $\sim 21.7$  Ma falling at the top of C6A.An. Almost all the stratigraphic horizons of Mizoram has been studied using Magnetostratigraphy ranging from Oligocene (29.662) to early Pliocene (3.330) having a total duration of  $\sim 26.332$  Ma.

## Reference

---

- Acharyya, S.K., 1986, Tectono-stratigraphic history of Naga Hills ophiolite in geology of Nagaland Ophiolite: *Geological Survey of India, Memoir*, v. 119, p. 94-103.
- Ahmed, S. T., 1968. Cenozoic Fauna of the Cox's Bazar Coastal Cliff. *Unpubl. MSc Thesis, Univ. of Dhaka, Dhaka*, 68 pp.
- Alam, M., 1997. Bangladesh. In: Moores, E.M., Fairbridge, R.W. (Eds.), *Encyclopedia of European and Asian Regional Geology. Chapman & Hall, London*, 64-72.
- Alam, M., 1989. Geology and depositional history of Cenozoic sediments of the Bengal Basin of Bangladesh. *Palaeogeogr., Palaeoclimetol., Palaeoecol.*, **69** : 125-139.
- Alam, M., 1972. Tectonic classification of the Bengal Basin. *Geol. Soc. Am. Bull.*, **83** : 519-522.
- Alam, M., Alam, M. M., Curray, J. R., Chowdhury, M. L. R. and Gani, M. R., 2003. An overview of the sedimentary geology of the Bengal Basin in relation to the regional tectonic framework and basin-fill history. *Sedimentary Geology*, **155** : 179-208.
- Alam, M. M., 1995a. Tide-dominated sedimentation in the upper tertiary succession of the sitapahar anticline, Bangladesh. In: Flemming, B.W., Bortholma, A. (Eds.), *Tidal Signatures in Modern and Ancient Sediments. Int. Assoc. Sedimentol., Spec. Publ.*, **24** : 329-341.
- Alam, M. M., 1995b. Sedimentology and depositional environments of the Bengal Basin subsurface Neogene succession based on detailed facies and electrofacies analysis: A case study of the Kailashtila, Rashidpur and Bakhrabad structures in northeastern Bangladesh. *NORAD Project BGD-023, Bangladesh Petroleum Institute, Dhaka*, 74 pp.

- Alam, M. M. 1991. Palaeoenvironmental study of the Barail sediments exposed in the northeastern Bangladesh. *Bangladesh J. Sci. Res.*, **9(1)** : 25-33.
- Alam, M. M. and Ferdous, M. H. S., 1995. Lithofacies analysis and depositional environments of the Lichubagan Sandstone Formation in the Sitapahar anticline, southeastern Folded Belt of Bangladesh. *J. Indian Assoc. Sediment.*, **14** : 9-18.
- Badekar, A. G., Sangode, S. J., Gosh, S.K., Tiwari, R. P., Meshram, D.C., Malsawma, J. and Lalnuntluanga, P. 2013. Petromineralogic and Rock magnetic aspects of Clastic Sedimentation in the Surma Basin, Mizoram. *Journal. Geol. Soc.of India.*, **82** : 23-37.
- Bakhtine, M. I., 1966. Major tectonic features of Pakistan: Part II. The Eastern Province. *Sci. Ind.*, **4** : 89-100.
- Betka, P., Seeber, L., Thomson, S.N., Steckler, M.S., Syncavage, R. and Zoramthara, C. 2018. Slip-partitioning above a shallow, weak decollement beneath the Indo-Burman accretionary prism. *Jour. Earth and Planetary Science letters.*, **503** : 17-28.
- Butler, R. F., 1998. Paleomagnetism: Magnetic Domains to Geologic Terranes, *Blackwell Science Inc.*
- Butler, R. F., 1992. Palaeomagnetism, *Blackwell Scientific Publishers*, 237p.
- Cande, S. C and Kent, D. V., 1995. Revised calibration of the geomagnetic polarity time scale for the late Cretaceous and Cenozoic. *Jour. Geophys. Res.*, **100 (B4)** : 6093-6095.
- Chatterjee , B. P., 1972. *In:* Nandy, D.R. and Mukerjee, R.N., Geological mapping in parts of Aizawl district, Mizoram. *Geol. Surv. India. Progress Report (Unpublished)*.
- Chowdhury, S. Q., 1982. Palynostratigraphy of the Neogene sediments of the Sitapahar anticline (western flank), Chittagong Hill Tracts, Bangladesh. *Bangladesh J. Geol.*, **1** : 35-49.

- Collison, D. W., 1983. Methods in Rock Magnetism and Palaeomagnetism: Techniques and Instrumentation. *Chapman and Hall*, London.
- Curry, J. R. and Moore, D. G., 1974. Sedimentary and tectonic processes in Bengal deep-sea fan and geosyncline. In: Burk, C.A., Drake, C.L. (Eds.), *The Geology of Continental Margins. Springer-Verlag, New York*, 617-628.
- Curry, J. R., Emmel, F. J., Moore, D. G. and Raitt, R. W., 1982. Structure, tectonics and geological history of the northeastern Indian Ocean. In: Nairn, A.E.M., Stehli, F.G. (Eds.), *The Ocean Basins and Margins. The Indian Ocean, Plenum, New York*, 6 : 399– 450.
- Dasgupta. S., 1982. Synthesis and review on faunal records from the surma basin. *Rec. Geo. Sur. of India*, **112 (5)** : 31-38.
- Dasgupta, S., Nandy, D. R., 1995. Geological frame work of the Indo-Burmese convergent margin with special reference to ophiolitic emplacement. *Indian J. Geol.* 67(2),110–125.
- Dearing, J. A., Dann, R. J. L., Hay, K., Lees, J. A., Loveland, P. J., Maher, B. A. and O’Grady, K., 1996. Frequency dependent susceptibility measurements of environmental materials. *Geophysical Journal International*, **124** : 228-240.
- Dekkers, M.J., 1989. Magnetic properties of natural goethite—I. Grain-size dependence of some low- and high- field related rock magnetic parameters measured at room temperature, *Geophys. J.* 97 (1989) 323–340.
- Dekkers, M. J., 1997. Environmental magnetism: An introduction. *Geologie en Mijnbouw*, **76** :163-182.
- Evans, P., 1964. Tectonic framework of Assam. *J. Geophys. Soc. India*, **5** : 80–96.
- Evans, P., 1932. Tertiary succession in Assam. *Trans. Min. Geol. Inst. India*, **27** : 155– 260.

- Evans, M. E. and Heller, F., 2001. Magnetism of loess/paleosol sequences: recent developments. *Earth Science reviews*, **54** : 129-144.
- Ferdous, H. S., Renaut, R. W., 1996. Preservation of primary porosity in the Neogene clastic reservoirs of the Surma Basin, Bangladesh. *AAPG Bulletin* 5, p 44c
- Fisher, R. A., 1953. Dispersion on a sphere. *Proc. R. Soc. London*, **A217** : 295-305.
- Ganguly, S., 1975. Tectonic evolution of the Mizo Hills. *Geol, Min. & Met. Soc. India*, **48** : 28-40.
- Gani, M. R. and Alam M. M., 1999. Trench-slope controlled deep-sea clastics in the exposed lower Surma Group in the southeastern fold belt of the Bengal Basin, Bangladesh. *Sed. Geol.*, **127** : 221-236.
- Ganju, J. L., 1975. Geology of Mizoram. *Bull. Geol. Min. Met. Soc. India*, **48** : 17-26.
- Geological Survey of India., 2011. Geology and mineral resources resources of Manipur, Mizoram, Nagaland and Tripura. *Miscellaneous publication*, No. 30, Part IV (Vol-1) Part 2: 30-31.
- Graham, S. A., Dickinson, W. R. and Ingersoll, R. V., 1975. Himalayan–Bengal model for flysch dispersal in the Appalachian – Ouachita system. *Geol. Soc. Am. Bull.*, **94** : 273–286.
- Han, J. and Jiang, W., 1999. Particle size contributions to bulk magnetic susceptibility in Chinese loess and paleosol. *Quaternary International*, **62** : 103-110.
- Hauhnar, M., Lalnunmawia, J. and Vanthangliana, V. 2018. Petrography of Barail sandstone of Champhai Mualkawi section in Champhai District, Mizoram: Implications on Provenance and Tectonic setting. *Advancement in Engineering research*, vol., 178: 66-73.



- Hess, H.H., 1962 History of ocean basins. In *Petrologic Studies: A Volume to Honor A.F. Buddington* (A.E.J. Engel, H. James and B.F. Leonard, Eds.), pp.599-620. Geological Society of America, Boulder, CO. [149,183]
- Hiller, K. and Elahi, M., 1988. Structural growth and hydrocarbon entrapment in the Surma basin, Bangladesh. In: *H. C. Wagner*.
- Hiller, K., Elahi, M., 1984. Structural development and hydrocarbon entrapment in the Surma Basin, Bangladesh (northwest Indo-Burman fold belt): *Singapore Fifth Offshore Southwest Conference*. p 656–663.
- Holtrop, J. F. and Keizer, J., 1970. Some aspects of the stratigraphy and correlation of the Surma basin wells, East Pakistan. *ESCAPE Miner. Resour. Dev. Ser.* **36** :143–154.
- Hussain, M.F., and Bharali, B. 2019. Whole-rock geochemistry of Tertiary sediments of Mizoram Foreland Basin, NE India, implication for source composition, tectonic setting and sedimentary process. *Acta Geochim*, *14<sup>th</sup> Jan.2019.*, <https://doi.org/10.1007/s11631-019-00315-3>
- Hutchison, C. S., 1989. Geological evolution of South-East Asia. *Clarendon Press*, London, 368 pp.
- Jacob, J. A., 1994. Reversals of the Earth's Magnetic Field. *Cambridge University Press*, Cambridge.
- Jauhri, A. K., Tiwari, R. P. and Lyngdoh, B. C., 2004. Early Miocene larger foraminifera (Operculina) from the Baghmara Formation (Garo Group), Garo Hills, Meghalaya, India, *Revue de Paleobiologie, Geneve*, **23 (1)**: 227-237.
- Johnson, G. D., Opdyke, N. D., Tandon, S. K. and Nanda, A. C., 1983. The magnetic polarity stratigraphy of the Siwalik Group at Haritalyangar (India) and a new last appearance datum for Ramapithecus and Sivapithecus in Asia. *Paleogeogra., Palaeoclimatol., Palaeoecol.*, **44** : 223-249.

- Johnson, N. M., Stix, J., Tauxe, L., Cervený, P. F. and Tahirkheli, R. A. K., 1985. Palaeomagnetic Chronology, fluvial processes and tectonic implications of the Siwalik deposits near Chinji Village, Pakistan. *J. Geol.*, **93**: 27-40.
- Johnson, N. M., Opdyke, N. D., Johnson, G. D., Lindsay, E. H. and Tahirkheli, R. A. K., 1982. Magnetic polarity stratigraphy and ages of Siwalik Group rocks of the Potwar Plateau, Pakistan. *Paleogeogra., Palaeoclimatol., Palaeoecol.*, **37**: 17-42.
- Johnson, S. Y. and Alam, A. M. N., 1991. Sedimentation and tectonics of the Sylhet Trough, Bangladesh. *Geol. Soc. Am. Bull.* **103** : 1513–1527.
- Jokhanram and Venkataraman, B. 1984. Tectonic Framework and Hydrocarbon Prospects of Mizoram. *Petroleum Asia Journal.*, 2:60-65.
- Karunakaran, 1974. Geology and Mineral resources of the States of India, *Misc. Publ. Geol. Surv. India*, **30(IV)** : 93-101.
- Keller, M. H., Tahirkheli, R. A. K., Mirza, M. A., Johnson, G. D., Johnson, N. M. and Opdyke, N. D., 1977. Magnetic polarity stratigraphy of the upper Siwalik deposits, Pabbi Hills, Pakistan. *Earth Planet Sci. Lett.*, **36**: 187-201.
- Kent, R.W., Pringle, M.S., Muller, R.D., Saunders, A.D., and Ghose, N.C., 2002, Ar/Ar geochemistry of the Rajmahal Basalts, India, and their relationship to the Kerguelen Plateau, *Journal of Petrology*, v. 43, no. 7, p. 1141-1153.
- Khan, A. A., 1991. Tectonics of the Bengal Basin. *J. Himalayan Geol.*, **2(1)** : 91– 101.
- Khan, M. A. M., 1978. Geology of the Eastern and the Northeastern part of Sadar Subdivision, Sylhet District, Bangladesh, *Records of the Geol Surv Bangladesh*, p 20.

- Khandoker, R. A., 1989. Development of major tectonic elements of the Bengal Basin: a plate tectonic appraisal. *Bangladesh Journal of Scientific Research* 7, 221–232.
- King, J.W., Channell, J.E.T., 1991. Sedimentary magnetism, environmental magnetism, and magnetostratigraphy. *Rev. Geophys.*, 29, 358-370.
- Kruiver, P.P., Dekkers, M.J., Heslop, D., 2001. Quantification of magnetic coercivity components by the analysis of acquisition curves of isothermal remanent magnetization. *Earth Planet. Sci. Lett.*, 189, 269-276.
- Lalmuankimi, C., Tiwari, R. P., Jauhri, A. K. and Ralte, V. Z. 2010. Foraminifera from the Bhuban Formation of Mizoram. *Jour. Pal. Soc. Ind.*, 55(1): 71 - 75.
- Lalnuntluanga, P., 2013. Magnetostratigraphic study of the Surma Group and Tipam Groups in Parts of The Kolasib District, Mizoram. *Unpubl. Ph.D Thesis. Mizoram University.*
- Lalnuntluanga, P., Malsawma, J., Lalremruatfela, C., Tiwari, R.P and Sangode, S.J. 2014. Correlation of Four Magnetostratigraphically Constrained Sections of Miocene Bhuban Formation of Surma Basin in Mizoram, India. Special publication of *Jour. Pal. Soc. Ind.*, 5: 87 – 100.
- La Touche., 1891. Note on the geology of Lushai Hills. *Rec. Geol. Surv. India.* 24(2): 83-141.
- Lepland, A. and Stevens, R.L. 1996. Mineral magnetic and textural interactions of sedimentation in the Skagerrak, eastern North Sea. *Mar. Geol.*, 135: 51-64.
- Lohmann, H. H., 1995. On the tectonics of Bangladesh. *Swiss Assoc. Pet. Geol. Eng. Bull.* **62 (140)** : 29-48.
- Lokho, K and Singh, B.P., 2013. Ichnofossils from the Miocene Middle Bhuban Formation, Mizoram, Northeast India and their Paleoenvironmental Significance. *Acta. Geol. Sin. Vol.* 87: 801-840.

- Maher, B. A. and Taylor, R. M., 1988. Formation of ultrafine-grained magnetite in soils. *Nature*, **336** : 368-370.
- Mahoney, J.J., Macdougall, J.D., Lugmair, G.W., Gopalan, K., and Krishnamurthy, P., 1985, Origin of contemporaneous tholeiitic and K-rich alkalic lavas: a case study from the northern Deccan Plateau, India: *Earth and Planetary Science letters*, v.72, p. 39-53.
- Malsawma, J., Lalnuntluanga, P., Badekar, A., Tiwari, R. P. and Sangode, S. J., 2010. Magnetic Polarity Stratigraphy of the Middle and Upper Bhuban Succession, Surma Group, Tripura-Mizoram Accretionary Belt, India. *Jour. Geol. Soc. India*, **76** : 119-133.
- Malsawma, J., 2011. Magnetostratigraphic study of the Bhuban Formation (Surma Group) around Aizawl, Mizoram. *Unpubl. Ph.D Thesis. Mizoram University*.
- Mandaokar, B.D .,2000. Palynology and paleoenvironment of the Bhuban Formation (Early Miocene) of Ramrikawn, near Aizawl, Mizoram, India. *Palaeobot.*, **49**: 317-324.
- Mannan, A., 2002. Stratigraphic Evolution and Geochemistry of the Neogene Surma Group, Surma Basin, Sylhet, Bangladesh. *Unpubl. M.Sc Dissertation Thesis. University of Oulu*.
- Mazumder, B. I., 2004. A Study of Miocene Invertebrates from the area around Kolasib, Mizoram. *Unpubl. Ph. D. Thesis of Nagaland University, Kohima*, 213p.
- McElhinny, M. W. and McFadden, P. L., 2000. Paleomagnetism: Continents and Oceans. *Academic Press*.
- Mehrotra, R. C., Mandaokar, B. D., Tiwari, R. P. and Rai, V., 2001. *Teredolites clavatus* from the Upper Bhuban Formation of Aizawl District, Mizoram, India. *Ichnos*, **8(I)**: 63-68.
- Mehrotra, R. C., Sukhla, M., Tiwari, R. P. 2002a. Occurance of Palaeophycus in Barail sediment of Mizoram, India. *Elsevier, Geosci.Jour.*,

- Mehrotra, R. C., Tiwari, R. P. and Mazumder, B. I., 2003. *Nypa* megafossils from the Tertiary sediments of Northeast India. *Elsevier, Geobios.*, **36** : 83-92.
- Mitchell, A. H. G., 1993. Cretaceous – Cenozoic tectonic events in the Western Myanmar (Burma)-Asia region. *J. Geol. Soc. London*, **150** : 1089-1102.
- Murphy, R. W. and Staff of BOGMC, 1988. Bangladesh enters the oil era. *Oil Gas J.*, 76– 82, Feb. 29, 1988.
- Nandy, D. R., Gupta, S. D., Sarkar, K. and Ganguly, A., 1983. Tectonic Evolution of Tripura-Mizoram Fold Belt, Surma Basin, North Eastern India. *Quart. Jour. Geol. Min. Met. Soc. India*, **55(4)** : 186-194.
- Nandy, D. R., Mukherjee, R.N. and Majumder, T. 1972. Geological Mapping and mineral survey in parts of Mizoram. *Geol. Survey of India, Progress report for FS 1971-72* (unpublished).
- O'Reilly, W., 1984. *Rock and Mineral Magnetism*, Glasgow: Blackie, pp220.
- Opdyke, N. D. and Channell, J. E. T., 1996. *Magnetic Stratigraphy*. *Academic Press*.
- Opdyke, N. D., Johnson, N. M., Johnson, G., Lindsay, E. and Tahirkheli, R. A. K., 1982. Palaeomagnetism of the Middle Siwalik formations of northern Pakistan and rotation of the Salt Range Decollement. *Paleogeogra., Palaeoclimatol., Palaeoecol.*, **37** : 1-15.
- Opdyke, N. D., Johnson, N., Johnson, G. D., Lindsay, E., Tahirkheli, R. A. K. and Mirza, M. A., 1979. Magnetic polarity stratigraphy and vertebrate paleontology of the upper Siwalik Subgroup of northern Pakistan. *Paleogeogra., Palaeoclimatol., Palaeoecol.*, **27** : 1-34.
- Pachau, R., 1994. *Geography of Mizoram* (1<sup>st</sup> ed.), *New Aizawl Press*, Chanmari, Aizawl, 54p.

- Patil, R. S., 1991. Palaeontology of the Bhuban Rocks of parts of Lunglei district, Mizoram. *Rec. Geol. Surv. India*, 124(IV) : 227.
- Patil, R. S., 1990. Palaeontology of the Upper Bhuban Formation of the Lunglei district, Mizoram. *Rec. Geol. Surv. India*, 123(IV) : 168-169.
- Raju, A. T. R., 1968. Geological evolution of Assam and Cambay/Basins of India. *Am. Assoc. Pet. Geol. Bull.*, **52** : 2422-2437.
- Rajkonwar, C., Tiwari, R. P. and Patel, S. J. 2013. *Arenicolites helixus* isp. nov. and associated ichno-species from the Bhuban Formation, Surma Group (Lower-Middle Miocene) of Aizawl, Mizoram, India. *Hima. Geol.* 34 (1)
- Rajkonwar, C., Fanai, L., Malsawma, J., Lalnuntluanga, P., Lalremruatfela, C. and Tiwari, R. P. 2014. Ichnofossil assemblage of Bhuban Formation, (Surma Group) from Zuangtui area, Aizawl, Mizoram. *Science vision*, 15: 164-177.
- Ralte, Victor Z., Lalchawimawii, Malsawma, J. and Tiwari, R. P., 2009. Decapod fossils from the Bhuban Formation, Surma Group, Aizawl, Mizoram. *e-Journal Earth Science India*, **2(3)** : 196-210.
- Ralte, Victor Z., Tiwari, R. P., Lalchawimawii and Malsawma, J., 2011. Selachian Fishes from Bhuban Formation, Surma Group, Aizawl, Mizoram. *Jour. Geol. Soc. of India.*, **77** : 328-348.
- Rahman, M. J. J., 1999, Sedimentology of the subsurface Neogene Surma Group of the Sylhet Trough, Bengal Basin, Bangladesh: [*Ph. D Thesis*], *University of Vienna*, Vienna, 173 p.
- Rai, J., Malsawma, J., Lalchhanhima, C., Lalnuntluanga, P., Ralte, Victor Z. and Tiwari, R.P. 2014. Nannofossil Biostratigraphy from Middle Bhuban Formation, Mizoram, Northeast India and its Paleoenvironmental Interpretations. Special publication of *Jour. Pal. Soc. Ind.*, 5: 121 – 134.
- Ranga Rao, A., 1983. Magnetic Polarity stratigraphy of Upper Siwalik of north western Himalayan foothills, *Current Sci.*, **64 (11 & 12)** : 863-873.

- Ranga Rao, A., Agarwal, R. P., Sharma, U. N., Bhalla, M. S. and Nanda, A. C., 1988. Magnetic polarity stratigraphy and vertebrate palaeontology of the Upper Siwalik Subgroup of the Jammu Hills, India. *Jour. Geol. Soc., India*, **31 (4)**: 361-385
- Reimann, K. U., 1993. Geology of Bangladesh. *Borntraeger*, Berlin, 160 pp.
- Rowley, D. B., 1996. Age of initiation of collision between India and Asia: A review of stratigraphic data. *Earth Planet. Sci. Lett.*, **145** : 1-13.
- Robertson, D.J., France, D.E., 1994. Discrimination of remanence-carrying minerals in mixtures using isothermal remanence magnetization acquisition curves. *Phys. Earth and Planet. Int.*, **82**, 223-234.
- Sangode, S. J., 1997. Magnetostratigraphy and sedimentation history of the Siwalik foreland basin in Dehra Dun Nahan sector, NW Himalaya, D. Phil. thesis, H.N.B. Garhwal University, India.
- Sangode, S. J. and Bloemendal, J., 2004. Pedogenic transformation of magnetic minerals in Pliocene-Pleistocene palaeosols of the Siwalik Group, NW Himalaya, India, *Palaeogeography, Palaeoclimatology, Palaeoecology*, **212** : 95-118
- Sangode, S. J., Kumar, R. and Ghosh, S. K., 2003. Magnetic polarity stratigraphy of Late Miocene Siwalik Group sediments from Kangra re-entrant, HP, India. *Jour. Himalayan Geology*, **24/1** : 47-61.
- Sangode, S. J., Kumar, R. and Ghosh, S. K., 1999. *Mem. Geol. Soc.India*, **44** : 221-248
- Sangode, S. J., Kumar, R. and Ghosh, S. K., 1996. Magnetic polarity stratigraphy of the Siwalik Sequence of Haripur area (H. P.), NW Himalaya: *Geological Society of India Journal*, **47** : 683-704.
- Sangode, S. J., Bloemendal, J., Ghosh, S. K. and Kumar, R., 2001. Plio-Pleistocene pedogenic changes in the Siwalik palaeosols: A rock magnetic approach. *Current Science*, **81 (4)** : 387-392.

- Sangode, S.J., Sinha, R., Phartiyal, B., Chauhan, O.S., Mazari, R.K., Bagati, T.N., Suresh, N., Mishra, S., Kumar, R., Bhattacharjee, P. (2007). Environmental magnetic studies on some Quaternary sediments of varied depositional setting in the Indian subcontinent. *Quaternary International*, 159 (1), 102-118.
- Sarkar, K. and Nandy, D. R. 1977. Structures and Tectonics of Tripura - Mizoram area, India. *Geol. Surv. India. Misc. Publ.*, **34(1)**: 141 - 148.
- Sengupta, S., 1966. Geological and geophysical studies in the western part of Bengal Basin, India. *Am. Assoc. Pet. Geol. Bull.* **50** : 1001-1017.
- Shamsuddin, A. H. M. and Abdullah, S. K. M., 1997. Geological evolution of the Bengal Basin and its implication in hydrocarbon exploration in Bangladesh. *Indian J. Geol.* **69** : 93–121.
- Sikder, A.M. and Alam, M.M., 2003. 2-D modelling of the anticlinal structures and structural development of the eastern fold belt of the Bengal basin, Bangladesh. *Sediment. Geol.*
- Sikder, A. M., 1998. Tectonic Evolution of Eastern Folded Belt of Bengal Basin. Unpubl. PhD Thesis, Dhaka Univ., Dhaka, 175pp.
- Singer, M. J. and Fine, P., 1989. Pedogenic factors affecting magnetic susceptibility of northern California soils. *Soil Sci. Soc. America Jour.*, **53** : 1119-1127.
- Sinha, N. K., Chatterjee, B. P. and Satsangi, P. P., 1982. Status of Palaeontological researches in the north-east states of India. *Rec. Geol. Surv. India*, **112(IV)** : 66-88.
- Srivastava D.K; Lalchawimawii and Tiwari 2008, R.P. Echinoids from the Bhuban Formation (Surma Group), Mizoram. *Jour. of The Pal. Soc. of India*, **52**: 221-226.
- Stacey, F. D. and Banerjee, S. K., 1974. *The Physical Principles of Rock Magnetism. Elsevier, Amsterdam*, **38** : 195p.



- Tandon, S. K., Kumar, R., Koyama, M. and Niitsuma, N., 1984. Magnetic polarity stratigraphy of the Upper Siwalik Subgroup, east of Chandigarh, Panjab Sub-Himalaya, India. *Jour. Geol. Soc. India*, **25(1)** : 45-55.
- Tauxe, L.S., Kent, D.V., Opdyke, N.D., 1980. Magnetic Components Contributing to the NRM of Middle Siwalik Red Beds. *Earth and Planet. Sci. Lett.*, **47**, 279-284.
- Tauxe, L. and Opdyke, N. D., 1982. A time framed work based on Magnetostratigraphy for the Siwalik sediments of the Khaur area, northern Pakistan. *Palaeogeography, Palaeoclimatology and Palaeoecology*, **37** : 43-61.
- Thellier, E. 1938. Sur l'aimantation des terres cuites et ses applications geophysiques. *Ann. Inst. Phys. Globe Univ. Paris*, **16**, 157-302. [61]
- Thompson, R. and Oldfield, F., 1986. Environmental Magnetism, *Allen and Unwin*, London, p 227.
- Tiwari, R. P., 2001. Neogene palaeontology of the Surma group, Mizoram, India. 1-The Arcoida (Mollusca : Bivalvia). *Jour. of The Pal. Soc. of India*, **46** : 147-160.
- Tiwari, R. P., Rajkonwar, C., Lalchawimawii, Lalnuntluanga, P., Malsawma, J., Ralte, V. Z. and Patel, S.J. 2011. Trace fossils from Bhuban Formation, Surma Group, (Lower to Middle Miocene) of Mizoram and their palaeoenvironmental significance. *J. Earth System Science*, **120** (6): 1127-1143
- Tiwari, R. P., 1992. Palaeontological and biostratigraphic studies of the Surma Group rocks around Aizawl and Lunglei, Mizoram, India. *Unpubl. Ph.D Thesis. Gauhati University*.

- Tiwari, R. P. and Bannikov, A. F., 2001. Early Miocene marine fishes from the Surma Group, Mizoram India. *Bollettino del Museo Cavico di Storia Naturate di Verona, Geologia Paleontologia Preistoria.*, **25** : 11-26.
- Tiwari, R. P. and Kachhara, R. P., 2003. Molluscan biostratigraphy of the tertiary sediments of Mizoram, India. *Jour. of the Pal. Soc. of India*, **48** : 65-88.
- Tiwari, R. P., and Kachhara, R. P., 2000. Two new species of Apolymetis (Bivalvia: tellinidae) from the Miocene of Mizoram, India, *Ter, Res*, **20(1-4)** : 79-84.
- Tiwari, R. P. and Mehrotra, R. C., 2002. Plant Impressions from the Barail Group of Champhai-Aizwal Road section, Mizoram, India. *Phytomorphology*, **52(1)** : 69-76.
- Tiwari, R. P. and Mehrotra, R. C., 2000. Study of fossil wood from the Tipam Group (Neogene) of Mizoram, India *Tertiary Research*, **20(1-4)** : 85-94.
- Tiwari, R. P., and Satsangi, P. P., 1988. Fossil crab from Mizoram, *Curr. Sci.*, **57(7)** : 956-958.
- Tiwari, R. P., Barman, G. and Satsangi, P. P., 1997. Miocene crabs from Mizoram, India. *Jour. Pal. Soc. India*, **42** : 127-132.
- Tiwari, R. P., Mishra, V.P. and Lyngdoh, B.C., 1998. Lower Miocene fish teeth from Mizoram of India. *Geoscience Journal*, **19** : 9-17.
- Tiwari R. P., Malsawma, J., Sangode, S. J. and Arora, B. R., 2007. Magnetostratigraphy of a Part of Middle Buhhan Sequence (Surma group), Aizawl, Mizoram. *Jour. Geol. Soc. of India*, **70** : 667-674.
- Uddin, A. and Lundberg, N., 1998. Unroofing history of the eastern Himalaya and the Indo–Burman ranges: heavy mineral study of the Cenozoic sediments from the Bengal basin, Bangladesh. *Journal of Sedimentary Research* **68**, 465– 472.
- Uddin, M. N. and Ahmed, Z., 1989. Palynology of the Kopili formation at GDH-31, Gaibandha District, Bangladesh. *Bangladesh J. Geol.* **8** : 31-42.

- Walden, J.F., Oldfield, F., Smith, J., 1999. Environmental magnetism: A Practical Guide, No.6. Quaternary Research Association, London, (243pp.)
- Verosub, K.L. and Roberts, A. P., 1995. Environmental magnetism: past, present, and future. *J. Geophys. Res.*, **100(b2)** : 2175-2192.
- Vine, F.J., and Matthews, D.H., 1963. Magnetic anomalies over oceanic ridges. *Nature*, 199, 947-949.
- Wilson, R.L. 1962c. An instrument for measuring vector magnetization at high temperatures. *Geophys. J. R. Astron. Soc*, 7, 125-130. [117]
- Worm, H. U., Ahmed, A. M. M., Ahmed, N. U., Islam, H. O., Hug, M. M., Hambach, U., Lietz, J., 1998. Large sedimentation rate in the Bengal Delta: Magnetostratigraphic dating of Cenozoic sediments from northeastern Bangladesh. *Geology*, 26(6) : 487-490.
- Zijderveld, J. D. A., 1967. A.C. demagnetization of rocks: Analysis of results, In: Collinson, D. W., Creer, K. M., Runcorn, S. K. (Eds.), *Methods in Paleomagnetism. Elsevier, Amsterdam*, 254-286.

**APPENDIX-A**

**CURRICULUM VITAE**

NAME OF THE CANDIDATE : C. LALREMRUATFELA

DEGREE : Ph.D

DEPARTMENT : DEPARTMENT OF GEOLOGY

TITLE OF RESEARCH : MAGNETOSTRATIGRAPHIC STUDY  
OF BARAIL GROUP IN CHAMPHAI  
DISTRICT, MIZORAM

DATE OF PAYMENT  
OF ADMISSION : 01.09.2011

APPROVAL OF RESEARCH  
PROPOSAL

1. BPGS : 14.05.2012

2. SCHOOL BOARD : 15.05.2012

UNIVERSITY REGISTRATION  
NO. AND DATE : 307 of 2006-2007

Ph.D REGISTRATION NO.  
AND DATE : MZU / Ph.D. / 461 of 15.05.2012

EXTENSION : 2 YEARS

ANY AWARD/FELLOWSHIP : NET (LS) CSIR-UGC

**HEAD**

**DEPARTMENT OF GEOLOGY**

### **BRIEF BIO-DATA OF THE CANDIDATE**

NAME : C. LALREMRUATFELA

FATHER'S NAME : C. LALTLANMAWIA

MOTHER'S NAME : LIANSILOVI

DATE OF BIRTH : 17.08.2019

NATIONALITY : INDIAN

TRIBE : SCHEDULED TRIBE

PERMANENT ADDRESS : H.No. C-130A, BIAKIN MUAL  
RAMHLUN NORTH  
AIZAWL: MIZORAM-796012

EMAIL : svenchhakchhuak@gmail.com

NUMBER OF PUBLICATION : 1 (ONE)

## **PARTICULARS OF THE CANDIDATE**

NAME OF THE CANDIDATE : C. LALREMRUATFELA

DEGREE : Ph.D.

DEPARTMENT : GEOLOGY

TITLE OF RESEARCH : MAGNETOSTRATIGRAPHIC STUDY  
OF BARAIL GROUP IN CHAMPHAI  
DISTRICT, MIZORAM.

DATE OF ADMISSION : 01.09.2011

APPROVAL OF RESEARCH PROPOSAL

1. B.O.S. : 14.05.2012

2. SCHOOL BOARD : 15.05.2012

Ph.D. REGISTRATION : MZU / Ph.D. / 461 of 15.05.2012

EXTENSION (IF ANY) : 2 YEARS (No.16-2/Adm-I(Acad)/15/55)

Dated 17<sup>th</sup> February 2017

Head

Department of Geology

